GATING AND PORE BLOCK OF THE HUMAN ETHER-À-GO-GO RELATED GENE (*hERG*) VOLTAGE-GATED POTASSIUM CHANNEL (K_V11.1)

by

Logan Campbell Alexander Macdonald

B.Sc., St. Francis Xavier University, 2013

A THESIS SUBMITTED IN PARTIAL FULFILLMENT OF

THE REQUIREMENTS FOR THE DEGREE OF

DOCTOR OF PHILOSOPHY

in

THE FACULTY OF GRADUATE AND POSTDOCTORAL STUDIES

(Pharmacology)

THE UNIVERSITY OF BRITISH COLUMBIA

(Vancouver)

June 2017

Abstract

Ion channels are integral membrane proteins that form an aqueous pore through the cell lipid bilayer, and allow ions to traverse the membrane at rates approaching limits set by diffusion. Selectivity and gating differences amongst members of this protein family enable complex physiological processes such as action potentials. The diversity in ion channel selectivity and gating is endowed through structural permutations of protein structure that slightly alter factors such as the rate at which a channel activates or the width of the pore region and thus the type of ions it interacts with. This thesis investigates structural bases for the anomalous gating and drug interaction behaviour exhibited by the human ether-à-go-go related gene (*hERG*) voltage-gated potassium channel (VGKC). The unique gating kinetics of *hERG* allow it to fulfill its role as the rapid delayed rectifier potassium current of the cardiac action potential and the unique susceptibility to drug block can compromise this function. Chapter 2 describes how slow deactivation of *hERG* can be largely attributed to cytosolic domain interaction with channel gating, an interaction that serves to establish a mode shift of the channel gating charge, shifting the deactivation gating pathway to more hyperpolarized potentials. Chapter 3 demonstrates that an interaction between an acidic residue at the bottom of the S1 and a basic residue at the bottom of the S4 stabilizes the closed state of the channel and slows activation. Through gating currents and fluorescence experiments, we propose a model of *hERG* gating in which this unique interaction stabilizes an early closed state of the channel. Chapter 4 investigates the role of cation-π interactions in *hERG* drug block, testing the importance of the two most significant residues for drug interaction, Y652 and F656. Using unnatural amino acid mutagenesis, this final study shows that cation-π interactions do not appear to play a major role in drug interaction with the *hERG* pore.

Lay Abstract

The function of a number of tissues in the body are highly regulated by the voltage across the cell membrane (ex. heart, brain tissues). The proteins chiefly responsible for coordinating the voltage across the cell membrane are ion channels, which are a family of proteins that form gated pores across the ion-impermeable lipid bilayer of the cell membrane. Ion channels are a diverse protein family whose individual members differ in gating means (stimuli to which they respond and open or close), drug interaction, cofactor interaction (how they are modulated by other physiological entities), selectivity (which ions are passed through them), and kinetics of gating (rates with which they open and close). The present thesis has used electrophysiological techniques to investigate the unusual gating kinetics and propensity to drug block of a voltage-gated potassium channel, the human ether-à-go-go related gene (hERG) voltage-gated potassium channel.

Preface

The work that follows was conducted in the laboratory of Dr. David Fedida and in collaboration with Dr. Ying Dou, Dr. Sam Goodchild, Robin Kim, Yue Wu, and Dr. Harley Kurata.

A version of Chapter 2 has been published [Goodchild SJ, Macdonald LC, Fedida D. Sequence of gating charge movement and pore gating in *hERG* activation and deactivation pathways. Biophys. J. 2015 Mar 24; 108(6): 1435–1447]. In this work, I was involved in experimental design, data acquisition, data analysis, and manuscript composition. Sam Goodchild was involved in project conception, experimental design, data acquisition, data analysis and manuscript composition. David Fedida was the supervisory author and was involved in project conception and manuscript composition.

In Chapter 3, I was involved in experimental design, data acquisition, data analysis, and manuscript composition. Ying Dou was involved in project conception, experimental design, data acquisition and data analysis. Yue Wu was involved in data acquisition and data analysis. David Fedida was the supervisory author and was involved in project conception and manuscript composition.

In Chapter 4, I was involved in project conception, experimental design, data acquisition, data analysis, and manuscript composition. Robin Kim was involved in project conception, experimental design, and data acquisition and manuscript composition. Harley Kurata was

involved in project conception and manuscript composition. David Fedida was the supervisory author and was involved in project conception and manuscript composition.

Table of Contents

List of Tables

List of Figures

List of Symbols and Abbreviations

A Amplitude

Å Angstrom

Ala, A Alanine

ANAP 3-(6-acetylnaphthalen-2-ylamino)-2-aminopropanoic acid

ANOVA Analysis of variance

Arg, R Arginine

Asn, N Asparagine

Asp, D Aspartic acid

C- terminus Carboxy- terminus of protein

$CaCl_2$ Calcium chloride

CaMES Calcium methanesulfonic acid

CsCl Cesium chloride

cDNA Complementary deoxyribose nucleic acid

CNBD Cyclic nucleotide binding domain

CNBhD Cyclic nucleotide binding homology domain

CNG Cyclic- nucleotide gated

COVG Cut-open Vaseline gap

cRNA Complementary ribonucleic acid

Cys, C Cysteine

eag Ether-à-go-go

F Faraday constant

F1 Singly fluorinated phenylalanine unnatural amino acid

F2 Doubly fluorinated phenylalanine unnatural amino acid

F3 Triply fluorinated phenylalanine

FV Fluorescence- voltage relationship

g Gram

GV Conductance- voltage relationship

Gln, Q Glutamine

Glu, E Glutamic acid

Gly, G Glycine

h Hours

h Hill coefficient

HCN Hyperpolarization- activated nucleotide- gated

hERG The human ether-à-go-go–related gene

HEPES 4-(2-hydroxyethyl)-1-piperazineethanesulfonic acid

His, H Histidine

Hz Hertz

IC_{50} Concentration of half- maximal inhibition

Ig_{OFF} Time integral of gating current

I_K Potassium current

I_{Kr} Rapid delayed rectifier potassium current

I_{Ks} Slow delayed rectifier potassium current

IK_{tail} Peak of ionic tail current

Ile, I Isovaline

J Joule

k Slope factor

K Kelvin

K^+ Potassium

K_A Ligand concentration which results in half-maximal block

KCl Potassium chloride

kHz Kilohertz

K_V Voltage-gated potassium channel

L Litre

Leu, L Leucine

Lys, K Lysine

LQTS Long QT syndrome

LQT2 Long QT syndrome type 2

M Molar

MΩ Megaohm

Met, M Methionine

MES Methanesulfonic acid

$MgCl_2$ Magnesium chloride

mg Milligram

mL Millilitre

mM Millimolar

ms Milliseconds

mV Millivolts

MTSET [2-(trimethylammonium)ethyl] methanethiosulfonate

N- terminus Amino- terminus of protein

nA Nanoamperes

NaCl Sodium chloride

NaMES Sodium methanesulfonic acid

NaOH Sodium hydroxide

ND96 Extracellular recording solution

ng Nanogram

nL Nanolitre

nm Nanometer

NMR Nuclear magnetic resonance spectroscopy

pANAP Vector containing DNA for the orthogonal tRNA as well as the DNA for the amino-acyl tRNA synthetase necessary to incorporate ANAP

PAS Per-Arnt-Sym

pCMBS p- chloromercuriphenylsulfonic acid

pdCpA An aminoacyl dinucleotide made up of cytosine and adenine

Phe, F Phenylalanine

Pro, P Proline

Q Charge

Q_{fast} Fast gating charge component

Q_{off} Gating charge after membrane repolarization

Q_{slow} Slow gating charge component

QA Quaternary ammonium ions

QSAR Quantitative structure- activity relationship

QV Gating charge-voltage relationship

R Ideal gas constant (8.314 J/mol K)

s Seconds

Ser, S Serine

t Time

T Temperature

τ Time constant

TEA-OH Tetraethyl ammonium-hydroxide

Thr, T Threonine

tRNA Transfer ribonucleic acid

Trp, W Tryptophan

Tyr, Y Tyrosine

TEVC Two-electrode voltage clamp

TMRM Tetramethyl rhodamine

μA Microamperes

μM Micromolar

UAA Unnatural amino acid

V Voltage

$V_{1/2}$ Potential of half- maximal activation

$V_{0.5}$ Potential of half- maximal activation

VCF Voltage clamp fluorometry

VGKC Voltage- gated potassium channel

VSD Voltage-sensing domain

WT	Wild-type
y/y_{max}	Normalized response
z	Equivalent charge
ΔN	N- terminal truncation
^{o}C	Degrees Celsius
β	Chemical rate constant
ΔG	Change in free energy
ΔG_0	Change in free energy at 0 mV

Acknowledgements

Thanks to Dr. David Fedida and the lab for their support over the past four years. In particular, I would like to thank Dr. Sam Goodchild for putting me through the electrophysiology equivalent of an apprenticeship in my first two years in the lab.

Thanks to the members of my committee for their help throughout this degree.

Thanks also to the members of the Kurata and Van Petegem labs with whom I enjoyed many discussions over lunch, pool, and badminton.

Thanks to UBC for funding through the 4YF program.

Lastly, many thanks to my family and friends. In particular, thanks to Amanda for being a wonderful partner to share this West coast adventure with.

Chapter 1: Introduction

1.1 Voltage-gated potassium channels

Voltage-gated potassium channels (VGKC) are a ubiquitously expressed and diverse family of transmembrane proteins. VGKCs selectively pass potassium ions through a pore whose open state probability is primarily dependent on the voltage across the membrane (Long *et al.*, 2007; Yellen, 2002). In a physiological system, upon opening of one of these proteins, the potassium ion electrochemical gradient directs a potassium efflux from the cell. In excitable cells, this outward potassium current regulates firing rates, maintains the resting membrane potential, and directs the shape and duration of action potentials (Hille, 2001).

Structurally, VGKCs are tetrameric (MacKinnon, 1991) with each subunit consisting of six transmembrane segments between two cytosolically located N- and C- termini (Gutman *et al.*, 2005; Long *et al.*, 2007). The first four transmembrane segments (S1-S4) comprise the voltage sensing domain (VSD). In response to changes in membrane potential, the VSD initiates conformational rearrangements of the protein that regulate the open state probability of the channel (Bezanilla, 2000; Cha *et al.*, 1999). This is largely thought to come in the form of a translational/rotational movement of the fourth transmembrane segment (S4) (Bezanilla, 2008; Bezanilla and Perozo, 2003; Long *et al.*, 2005). The S4 houses a high concentration of positively charged amino acids that are drawn extracellularly upon a depolarizing change in membrane potential and intracellularly upon a hyperpolarizing change in membrane potential (Bezanilla, 2000; Bezanilla and Perozo, 2003). The pore domain of the channel is composed of the fifth and sixth transmembrane segments, S5 & S6, from all four subunits coming together to delineate a central ion conducting pathway (Long *et al.*, 2007). For conventional VGKC, the movement of

the voltage sensor is thought to be translated to the pore domain primarily through a linker region between the fourth and fifth transmembrane segments, the S4-S5 linker (Ferrer *et al.*, 2006; Long *et al.*, 2007; Tristani-Firouzi *et al.*, 2002). When the S4 segment is in a deactivated position, as a result of negative membrane potentials, it pushes the S4-S5 linker against the bottom of the pore domain, effectively closing the pore. Upon depolarization, the S4 segment adopts an activated state, pulling the S4-S5 linker along with it, allowing the channel to open (Bezanilla, 2000).

The pore domain houses the highly conserved selectivity filter of the VGKC family. A series of amino acids, TXGYG, in the re-entrant P-loop between the S5 and S6 select for potassium ions with these amino acids' carbonyl atoms, which jut out along a 12 Å pathway through the pore (Doyle *et al.*, 1998; Jiang *et al.*, 2002). The oxygen atoms of the carbonyl groups are arranged at such a distance from one another so as to compensate for the loss of the hydration shell surrounding potassium ions (Zhou *et al.*, 2001). Smaller ions, such as sodium, are not of an appropriate size to trade their hydration shell for coordination by these backbone carbonyl oxygen atoms and thus would bind less favourably.

VGKCs play many different specific physiological roles and, over time, evolution has tailored their structures into a wide array of variations on the same VGKC theme (Gutman *et al.*, 2005). Structural differences between individual channels modify responses to voltage, temperature, pH, channel modulators, drug interaction, inactivation states of gating, etc. Detailing the structural features of specific VGKC channels that endow them with unique traits has preoccupied many biophysicists over the last few decades.

The following sections of this introductory chapter aim to provide an understanding of the structure and function of the *hERG* VGKC. The general focus is the work that has attempted to identify the structural features of the *hERG* channel that lead to its unique gating kinetics and promiscuous drug sensitivity.

1.2 The human ether-à-go-go related gene (*hERG*) voltage-gated potassium channel

1.2.1 *hERG* structure - The human ether-à-go-go related gene (*hERG*, KCNH2), encodes an α-subunit of a VGKC, K_v 11.1 (commonly referred to as *hERG*) (Warmke and Ganetzky, 1994). This VGKC is widely expressed throughout the body and regulates cell activity in both excitable and non-excitable cells (Wymore *et al.*, 1997). *hERG* was first cloned by Warmke and Ganetzky in a screen of human hippocampal cDNA and was noted to bear similarities to both plant inward-rectifier potassium channels and cyclic nucleotide-gated ion channels (Warmke and Ganetzky, 1994). In their assessment of the primary structure of the protein, they noted a hydrophobic core that housed 7 domains, which they proposed to be analogous to the S1-S6 α-helical domains and P-loop of the VGKC family. They also found that the *hERG* sequence had large cytosolic domains, which bore many similarities to those of cyclic nucleotide-gated channels.

Soon after the cloning of the *hERG* channel and expression in oocytes, it was recognized that *hERG* currents greatly resembled the I_{Kr} current of the cardiac action potential (Sanguinetti *et al.*, 1995). This potassium current had drawn some attention due to its unique gating kinetics and curious voltage-dependent rectification (Sanguinetti and Jurkiewicz, 1991; Shibasaki, 1987). Since the mid-1990s, many studies have set out in attempts to establish the structural features of the *hERG* channel that give rise to the atypical gating features of the channel (Al-Owais *et al.*,

2009; Cheng Y. M., 2012; de la Pena *et al.*, 2011; de la Pena *et al.*, 2013; Fernandez-Trillo *et al.*, 2011; Ferrer *et al.*, 2006; Ficker *et al.*, 2001; Gianulis *et al.*, 2013; Gustina and Trudeau, 2009, 2011, 2012, 2013; Ju *et al.*, 2009; Li *et al.*, 2014; Liu *et al.*, 2003; Morais Cabral *et al.*, 1998; Ng *et al.*, 2011; Ng *et al.*, 2012; Piper *et al.*, 2005; Smith and Yellen, 2002; Subbiah *et al.*, 2004; Subbiah *et al.*, 2005; Tan *et al.*, 2012; Thomson *et al.*, 2014; Thouta *et al.*, 2014; Tristani-Firouzi *et al.*, 2002; Tristani-Firouzi and Sanguinetti, 2003; Van Slyke *et al.*, 2010; Wu *et al.*, 2014; Zhang *et al.*, 2005; Zhang *et al.*, 2004).

Like other VGKCs, the voltage sensitivity of the *hERG* channel is predominantly influenced by the S1-S4 transmembrane domains. The S1, S2, and S3 transmembrane domains of VGKC house a number of negatively charged amino acids that are thought to act as counter-charges or means of stabilizing the high concentration of positively charged basic amino acids found in the S4 transmembrane domain (Chanda and Bezanilla, 2008). These acidic residues have also been suggested to play an important role in the initial folding of the channel in the endoplasmic reticulum (Tiwari-Woodruff *et al.*, 2000). As the transmembrane domains of *hERG* resemble those of the *eag* family member K_v 10.1 channels, it is reasonable to presume that the S4 segment's three dimensional structure is likely to be a 20 amino acid-long 3_{10} helix (Whicher and MacKinnon, 2016). The S4 of both *eag* and *hERG* channels contain 6 positively charged amino acids that are spaced throughout this alpha-helical transmembrane segment. The impetus for conformational changes of channel structure is thought to be the movement of the positively charged amino acids of the S4 as the electric field across the membrane exerts force upon them. The voltage sensing domain of *hERG* had previously been suggested to be coupled to the pore domain through the S4-S5 linker, which in *hERG* is much shorter than that of previously

determined potassium channel structures (Cheng and Claydon, 2012; Ferrer *et al.*, 2006; Hull *et al.*, 2014; Ng *et al.*, 2012; Tristani-Firouzi *et al.*, 2002; Van Slyke *et al.*, 2010). The interaction was thought to involve the S4-S5 region butting up against the bottom of the S6 to push the channel closed in the deactivated state of the voltage sensor, or to allow it to open in the activated state (Ferrer *et al.*, 2006; Long *et al.*, 2007; Ng *et al.*, 2016; Tristani-Firouzi *et al.*, 2002). Two recent studies have questioned whether this is the manner in which *hERG* voltage sensing is translated into changes in open state probability in the pore domain. The first, by Lorinczi *et al.*, detailed that *hERG* gating was relatively unaffected by disrupting covalent linkage between the voltage sensing domain and the pore domain (Lorinczi *et al.*, 2015). A year later, Whicher *et al.* published a structure of the closely related r*Eag*1 channel determined via cryo-electron microscopy (Whicher and MacKinnon, 2016). They detailed an alternate means of gating translation from the voltage sensing domain to the pore domain. They suggested that interaction of the bottom of the S4 with the C-linker region was responsible for pore opening and closing. In the deactivated state of the voltage sensor, the S4 would push down on the C-linker and introduce a kink in the bottom of the S6 region that would constrict the pore and not allow potassium ions to pass through. In the activated state of the voltage sensor, this pore constraint would be lifted and the channels would be able to pass current. Such involvement of the cytosolic domains in translation of voltage sensing to the pore region would be novel, but more functional work needs to be done in order to establish that this is the actual means by which VSD movement is translated to the pore region.

The S5, P-loop, and S6 of *hERG* form the pore domain and selectivity filter of *hERG*. This region is markedly different from the pore domain seen in other VGKC as it lacks a PVP motif in

the S6 segment that would narrow the pore region and this, in other channels, is suggested to orient the S6 to allow it to interact with the S4-S5 linker. The lack of this structure combined with the short S4-S5 supplements the idea that *eag* family channels may have unconventional means of gating (Lorinczi *et al.*, 2015; Thouta *et al.*, 2014; Van Slyke *et al.*, 2010; Whicher and MacKinnon, 2016). The lack of a PVP motif may also result in a larger inner vestibule area, which has been suggested to be of importance for *hERG* drug block (Mitcheson *et al.*, 2000b).

The cytosolic domains of *hERG* are of a unique size and structure. The 400 amino acid-long N-terminus houses a 110 amino acid Per-Arnt-Sym (PAS) domain in the ether-à-go-go region of the channel, a characteristic region of the KCNH family (Morais Cabral *et al.*, 1998; Vandenberg *et al.*, 2012). Immediately before this is the 25 amino acid PAS-cap region (Vandenberg *et al.*, 2012). PAS domains are known as signal sensors, and in other proteins have been shown to mediate responses to a range of stimuli, though in K_v 11.1 channels it is unknown if this region is modulated by any cofactors (Vandenberg *et al.*, 2012). The C-terminus of K_v 11.1 is highly homologous to those of HCN channels and CNG channels, but, unlike these channels, it does not functionally interact with cyclic nucleotides (Brelidze *et al.*, 2009; Vandenberg *et al.*, 2012). In place of the cyclic nucleotide binding domain seen in HCN and CNG channels, it has a cyclic nucleotide binding homology domain (Brelidze *et al.*, 2012; Whicher and MacKinnon, 2016). In this structure, an intrinsic ligand fills the pocket that would ordinarily bind cyclic nucleotides. The cytosolic domains of *hERG* have been shown to be involved in all facets of *hERG* gating (Morais-Cabral and Robertson, 2015). A description of studies that have detailed the role of these domains in *hERG* gating is found later in this chapter.

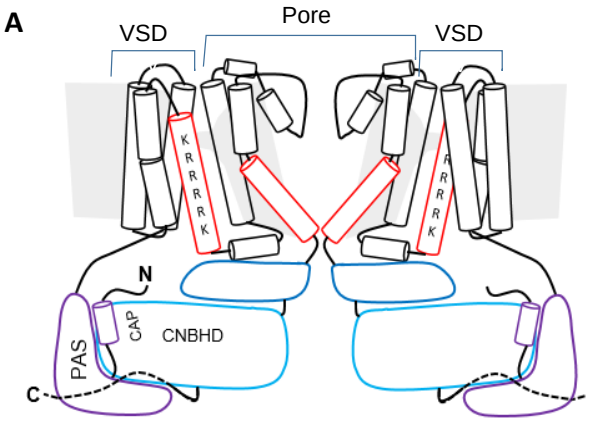

Figure 1.1 Cartoon structure of the hERG VGKC
Movements of the VSD, largely initiated by forces acting on the charged residues of the S4, lead to overall conformational changes in the channel that lead to the opening or closing of the intracellular gate in the pore region (activation and deactivation) or collapse and recovery from collapse of the selectivity filter (inactivation).

1.2.2 *hERG* activation gating - There are three general states that a *hERG* channel can assume: open, closed, and inactivated. These generalized states are each an ensemble of specific orientations of the channel that control currents through the channel. An open state of the channel comprises activated voltage sensors and an open pore region passing current. A closed state of the channel is one in which the voltage sensors are deactivated and the pore region is shut. An inactivated state is one in which the voltage sensors are activated, but the pore region is impermeable to ions. Transitioning between these states is chiefly coordinated through movement of the voltage-sensing domain of the channel in response to changes in transmembrane potential. The gating of *hERG* has received considerable attention over the past twenty years as it is unusual when compared to more conventional VGKC like the Shaker family of channels. Activation and deactivation of *hERG* are slow and are paired with fast and voltage-dependent inactivation (Wang *et al.*, 1997a) (Fig. 1.2). Many studies over the past twenty years have aimed to detail the structural basis of these unique attributes.

Less charge is moved overall in the voltage sensing process of *hERG* channels as compared to conventional VGKCs (Zhang *et al.*, 2004). This has been suggested to be a potential basis for the slow activation kinetics of the channel. Whereas *Shaker* channels have been shown to move between 12-13 equivalent charges in response to activation of the gating charge, *hERG* channels move only between 6-8 equivalent charges (Aggarwal and MacKinnon, 1996; Schoppa *et al.*, 1992; Zhang *et al.*, 2004). Considering the tetrameric nature of these proteins, this translates into approximately 1 less net charge moving across the gating charge transfer center in each subunit. The possible reasons for this are: the S4 of *hERG* not moving as far; gating charges at the top of the S4 being permanently affixed past the gating charge transfer center; a less focused electric field; or the gating charges of the *hERG* S4 being further down the transmembrane segment, resulting in a similar degree of translocation not moving as many charges. Early charge neutralization and accessibility studies of *hERG*, when compared to similar experiments done in *Shaker*, seemed to indicate that the *hERG* S4 segment may not translocate as far as the S4 of *Shaker* and that this could be the reason for the reduced gating charge. As the S4 of *hERG* does not share a large degree of homology with that of *Shaker*, it is difficult to determine where to begin the alignment of this region. Initial accessibility studies showed that K525 of the *hERG* S4 (the first charge in the *hERG* voltage sensor) becomes accessible to external MTSET upon activation of the channel, but R528C does not show a change in kinetics upon application of external MTSET (Subbiah *et al.*, 2004; Zhang *et al.*, 2004). This was interpreted as R528 being equivalent to the third charge in the *Shaker* S4, which is also inaccessible to external MTSET upon activation. This would mean that the S4 of *hERG* has its charged residues begin one helical turn down as compared to *Shaker*. However, later accessibility studies using external pCMBS

showed that R528 was accessible upon activation and noted that there was the potential for MTSET exposure to not affect residues to which it had attached (Elliott *et al.*, 2009). As a result, the general consensus in the field at present is that K525 of *hERG* aligns with the first charged residue of the *Shaker* S4. Accessibility experiments also noted that K525C was not able to interact with internal MTSET when the voltage sensor was in a deactivated position (Zhang *et al.*, 2004). There is therefore a possibility that K525 sits in the focused electric field in the deactivated state of the voltage sensor. As to *hERG* S4 translocation, a 2009 study by Elliott *et al.* argued that it was unlikely that *hERG* S4 translocation was much different than that noted for other K_v channels as the accessibility of S4 residues to a membrane impermeable chemical, pCMBS, that could be linked to an introduced cysteine was not overly different from that which was seen in other VGKC (Elliott *et al.*, 2009). A gating charge neutralization study by the Tseng lab found that neutralization of the first 3 gating charges of the S4 (K525, R528, and R531) reduced the number of gating charges associated with channel activation as estimated by limiting slope analysis, but that neutralization of the last 3 gating charges (R534, R537, and K538) had no effect on this parameter (Zhang *et al.*, 2004). They concluded that these first three charges of the S4 were those involved in the voltage sensing of the channel. It could be that the first and third residues do not fully cross the electric field: K525 may already reside within the electric field in the closed state and R531 may not fully cross the field in the open state of the channel. This has proven difficult to demonstrate experimentally.

The slow activation and deactivation seen in *hERG* ionic currents are in part due to the slow movement of the voltage sensor as described in voltage clamp fluorometry and gating current experiments (Es-Salah-Lamoureux *et al.*, 2010; Goodchild *et al.*, 2015; Piper *et al.*, 2005; Piper

et al., 2003; Thouta *et al.*, 2017; Yellen, 2002). In 2002, Smith and Yellen incorporated a fluorophore at several sites at the top of the *hERG* S4 and, using VCF, were able to show that movement of the voltage sensor of *hERG* followed a very similar time course to the ionic currents (Smith and Yellen, 2002). The fluorescence-voltage (FV) and conductance-voltage (GV) relationships obtained using a fluorophore at L520C overlay one another. They concluded that the movement of the voltage sensor itself was rate limiting in the activation of ionic current. They suggested that the fast fluorescence component observed in E518C and E519C constructs was the result of movements of the voltage sensor related to inactivation of the channel. The following year, Piper *et al.* published the first recordings of *hERG* gating currents in which they showed a slightly different picture of *hERG* gating charge movement (Piper *et al.*, 2003). They reported a charge-voltage (QV) relationship that was left-shifted from the GV relationship. Following studies looking at respective rates of activation in ionic and gating currents of *hERG* showed that the time constant of gating charge activation is much faster than that of the ionic current activation at physiological potentials (Goodchild and Fedida, 2014; Goodchild *et al.*, 2015; Wang *et al.*, 2013). This indicates that the movement of gating charge is not wholly rate limiting and that there is some intermediary step(s) between voltage sensor activation and opening of the pore region that slow *hERG* activation. Piper *et al.* also found that, similar to other VGKC, *hERG* gating currents exhibit two identifiable components: a fast gating charge movement (Q_{fast}) and a slower gating charge movement (Q_{slow}). Q_{fast} is a very brief initial burst of gating charge that is moved nearly instantaneously upon activation, representing a very small amount of gating charge that activates with a time constant of roughly 0.5 ms at +10 mV. Q_{slow} represents the movement of the majority of the gating charge and is much slower to activate, with a time constant of 53 ms at +10 mV (Piper *et al.*, 2003). The rapid kinetics of the fast

component is tempting to correlate with inactivation and whether or not this is the case has been assessed by several groups. The charge-voltage relationship of the fast component was found to be greatly right-shifted relative to the voltage dependence of inactivation, and therefore is not likely associated with this gating feature. Piper *et al.* suggest that the fast component of gating charge may be due to some sort of early transition between closed states of the channel. This conclusion was bolstered by the fact that the majority of the charge moved at early stages in the activation pathway was Q_{fast} (Piper *et al.*, 2003). However, this Q_{fast} component does not saturate until well after the majority of gating charge has moved. This early step in *hERG* gating has a voltage dependence greatly right-shifted to that of the overall charge voltage relationship (Piper *et al.*, 2003). The fast gating movement was also present in fluorophore reports from E519C and E518C which both exhibited a biphasic fluorescence signal (Es-Salah-Lamoureux *et al.*, 2010; Smith and Yellen, 2002). The exact structural basis of this fast movement of gating charge lacks a satisfactory explanation.

The voltage-dependent movement of gating charge and certain areas of the channel can be experimentally determined through measurement of gating current and voltage clamp fluorometry experiments. Figure 1.1 details isochronal voltage dependences of activation of conductance, charge movement, and a fluorescence report from the top of the S4. The far left shift of the FV relationship at E519ANAP relative to the GV relationship suggests that fluorophore incorporation at this site reports early movements in the VSD. The other included FV relationship, I521ANAP, overlays the GV relationship from that construct, suggesting a movement related to pore opening, or events immediately preceding or following pore opening.

The QV relationship of *hERG* is left-shifted to the GV. In *hERG*, this is thought to be a result of a prolonged translation of gating charge movement to pore opening.

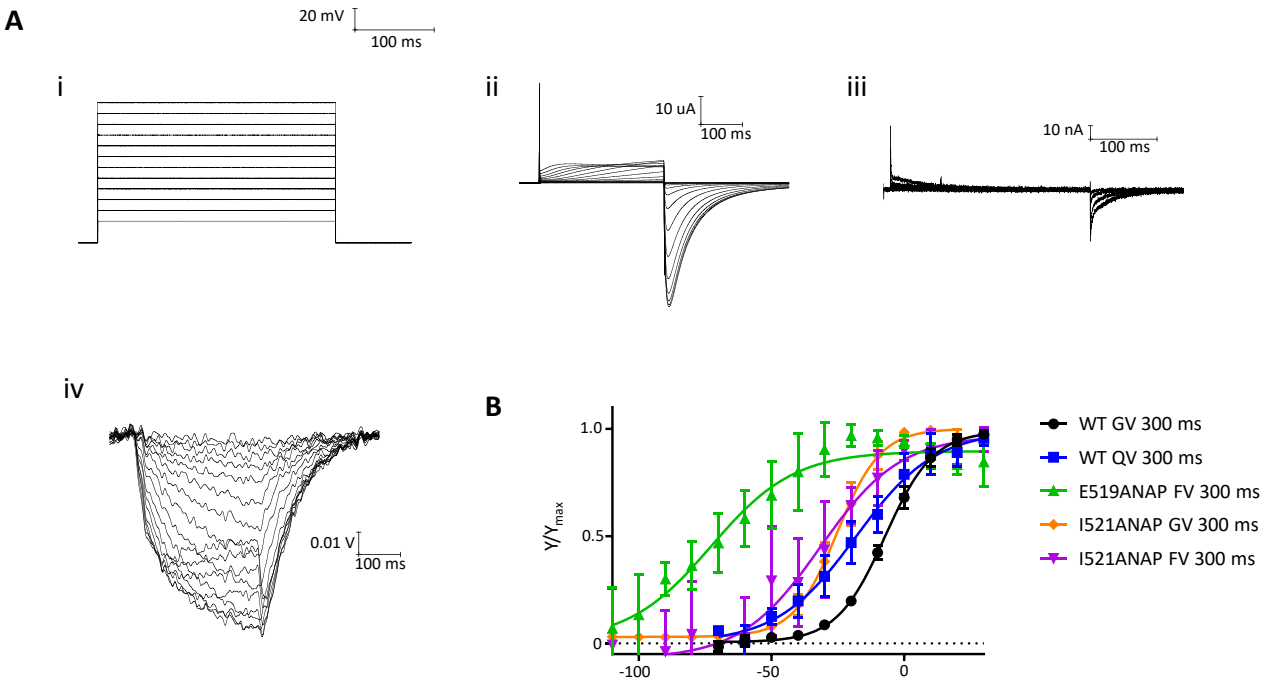

Figure 1.2 - Conductance-, charge- , and fluorescence-voltage dependence of activation relationships of *hERG*.
(A) (i) Protocol used to assess voltage dependence of activation. From a holding potential of -110 mV, cells are depolarized to a set potential and returned to holding potential. Each successive depolarization command is 10 mV higher than the last. In GV relationships, conductance of *hERG* assessed as peak current upon the repolarization to -110 mV. In QV relationships, gating charge moved is assessed as the charge returned upon repolarization to -110 mV. In FV relationships, the relative fluorophore movement is assessed as quenching levels upon repolarization to -110 mV. (ii) Ionic currents of WT *hERG* in response to protocol shown in (i). (iii) Gating currents of WT *hERG* in response to protocol shown in (i). (iv) Fluorescence signal from an unnatural amino acid fluorophore, ANAP, incorporated at E519 of the *hERG* S4 in response to the protocol shown in (i). **(B)** 300 ms GV and QV relationships for WT *hERG*, and 300 ms FV relationships for E519ANAP and I521ANAP. A 300 ms GV relationship for I521ANAP is also present.

Activation in *hERG* is uniquely slow and this has led to suggestion that there may be specific structural impediments to activation. In the S1-S3 segments of the voltage sensing domain, there are an extra three negatively charged acidic amino acids that are not found in *Shaker*-like

channels (Liu *et al.*, 2003). Conventional VGKC have 3 negatively charged residues in this part of the voltage sensing domain and their role has been well studied (Borjesson and Elinder, 2008; Chanda and Bezanilla, 2008; Seoh *et al.*, 1996). It is generally thought that these residues provide a means of stabilizing the charged residues of the S4 segment as they maneuver in response to the transmembrane potential. The extra charges in *hERG* are D411 in the S1, D460 in the S2, and D509 in the S3. Neutralization of D411 results in much faster rates of activation and deactivation. In double mutant cycle analysis experiments, this residue was suggested to interact with K538 of the *hERG* S4, stabilizing the closed state (Zhang *et al.*, 2005). Also in this study, K525 was suggested to interact with D456 to stabilize the closed state (Zhang *et al.*, 2005), which is equivalent to the R1-E283 interaction reported in *Shaker*. R528 was also suggested to interact with D456, stabilizing a partially activated state of the voltage sensor. Piper *et al.*, in a later charge neutralization study, proposed that R531 is coupled to all of the negatively charged residues in the *hERG* VSD (Piper *et al.*, 2008). This does not necessarily mean that they interact in an electrostatic manner, alternatively they could be stabilizing similar states of the channel. Overall, the most functionally impactful interaction known to influence *hERG* activation is the D411-K538 interaction (Zhang *et al.*, 2005), which appears to stabilize the closed state of the channel. Chapter 3 of this thesis closely examines this interaction and its effects on channel gating.

The gating charge transfer center is ‘an occluded site, conserved in voltage sensors, that catalyzes the transfer of positive charges across the membrane field in the process of voltage sensing’ (Tao *et al.*, 2010). In *Shaker*, the charged amino acids of the S4 going through this region are thought to interact with residue F290. Tao *et al.* showed that lysine residues seem to

interact with F290 more strongly than arginines when incorporated at the same site. The first charge in the S4 segment in Shaker is an arginine and upon mutation to lysine, the channel's activation becomes greatly slowed (Tao *et al.*, 2010). Conversely, in *hERG*, a lysine is the first charge of the S4 segment and the activation of *hERG* is already slow. Mutation of this lysine to an arginine results in a large left-shift of the conductance-voltage relationship (Cheng Y. M., 2012). This may be taken as an indication that a similar form of gating charge transfer to that seen in *Shaker* channels is also operating in *hERG*. It may also provide another potential explanation for the slow activation of the channel.

1.2.3 Voltage-dependent inactivation – *hERG* channels exhibit voltage-dependent inactivation that is anomalous among VGKC. Initial descriptions of *hERG* rectification took different approaches. Based on homology in the pore region with inward rectifier channels as well as similar interactions with metal ions, Trudeau *et al.* suggested that inactivation took the form of some sort of block by polyamine or divalent cations (Trudeau *et al.*, 1995). Sanguinetti *et al.* proposed voltage-dependent inactivation as a mechanism, similar to that seen in *Shaker* channels (Sanguinetti *et al.*, 1995). *Shaker* N-type inactivation, was ruled out when truncation of the N-terminus did not eliminate inactivation, but, surprisingly, increased rates of deactivation (Schonherr and Heinemann, 1996; Spector *et al.*, 1996b). Divalent cations were ruled out as the cause as well (Spector *et al.*, 1996b). *hERG* inactivation is currently attributed to a distinctive form of C-type inactivation that is voltage-dependent. C-type inactivation is believed to involve a temporary collapse of the selectivity filter of the channel that would constrict the pathway to ion permeation (Hoshi *et al.*, 1991). In *Shaker* channels this process has a slow onset and no observed voltage dependence (Hoshi *et al.*, 1991), but in *hERG* it is rapid and has a defined

voltage dependence (Schonherr and Heinemann, 1996; Spector *et al.*, 1996b). The voltage sensor for inactivation is widely presumed to be the S4 segment, though that has not been thoroughly defined in the literature. Several point mutations in the pore region (Ficker *et al.*, 1998; Smith *et al.*, 1996) eliminate inactivation in *hERG*. In addition, fast voltage-dependent inactivation can be introduced in the closely related *eag* channel through introduction of a small region of the *hERG* pore domain (Herzberg *et al.*, 1998). There is likely no simple explanation for the structural basis of *hERG* inactivation as it is a highly concerted process involving all subunits and one that features substantial intra-subunit interaction between several different areas of the channel (Perry *et al.*, 2015; Perry *et al.*, 2013; Wang *et al.*, 2011; Wu *et al.*, 2014). The mechanism by which voltage sensitivity is conferred to the inactivation process has not been fully determined. Several studies have shown that the voltage dependencies of activation and inactivation are very different (Chen *et al.*, 2002; Smith and Yellen, 2002; Wang *et al.*, 1997a; Zhang *et al.*, 2004) and that several mutations solely affect inactivation with minimal effects on activation gating or vice versa, but these findings alone do not rule out that inactivation draws its voltage sensitivity from the S4 segment. Further work will be required to determine a specific structural basis of inactivation.

1.2.4 Slow deactivation gating and role of the cytosolic domains of *hERG* - The uniquely large cytosolic domains of K_v 11.1 have been shown to play a large role in the gating of the channel and have been a focal point of *hERG* study over the last 20 years (Morais-Cabral and Robertson, 2015; Morais Cabral *et al.*, 1998; Schonherr and Heinemann, 1996; Wang *et al.*, 1998). The first to investigate the role of cytosolic domains in KCNH family channels were Schonherr & Heinemann who described the effects that truncation of the N-terminus had on

hERG channel kinetics (Schonherr and Heinemann, 1996). They showed that N-terminal truncation resulted in the abnormally slow deactivation rates of *hERG* increasing by over an order of magnitude at -80 mV (Schonherr and Heinemann, 1996). While previous studies had shown that potassium channel kinetics could be affected by alteration of the cytosolic domains (Hoshi *et al.*, 1990; VanDongen *et al.*, 1990), none had observed such a large change in deactivation kinetics. Crystallization of the N-terminal ether-à-go-go domain demonstrated that the three dimensional structure of the region embodied a PAS domain, and was the first evidence of such a domain in a eukaryote (Morais Cabral *et al.*, 1998). PAS domains essentially act as sensors for a variety of stimuli (Taylor and Zhulin, 1999), though no stimulus has been found that interacts with the *hERG* PAS domain (Sanguinetti and Tristani-Firouzi, 2006). The crystal structure also revealed a hydrophobic patch of residues along a face of the domain. This was proposed to be responsible for interacting with the body of the channel and the means by which the N-terminus somehow caused slow deactivation (Morais Cabral *et al.*, 1998). They further showed that the accelerated deactivation rate of the N-terminal truncation could be obtained by truncating just the first 25 amino acids. As these 25 amino acids were not a part of the PAS domain of the structure, nor a part of the hydrophobic patch found in the structure, that their truncation increased deactivation rates complicated the idea of how the N-terminal domain regulates deactivation gating. This study also found that upon introduction of the *eag* domain as a peptide into a cell expressing the truncated, fast deactivating mutant channel, the slow deactivation phenotype of WT *hERG* could be rescued. Also in 1998, Wang *et al.* showed that they could mimic this fast deactivation effect observed upon N-terminal truncation by covalently linking N-ethylmaleimide to an aphenotypic cysteine residue substituted to the S4-S5 linker region (Wang *et al.*, 1998). In this experiment they also found that the introduction of

aphenotypic cysteine residues to different sites in this region could speed up deactivation rates to similar rates seen in the ΔN truncation. Notably, disruptions to the S4-S5 linker resulted in very similar phenotypes as the ΔN truncation, suggesting that an interaction between the N-terminus, potentially the PAS-cap, and the S4-S5 linker was a mechanism for N-terminal effects on *hERG* channel gating. They also found that elevated levels of external potassium would increase the rate of deactivation in WT channels, which they concluded was the result of a disruption of whatever interaction the N-terminal domain was involved with in slowing deactivation, a 'knock-off' effect of the increased potassium flow. They also showed that a short deletion (Δ2-12) affected the deactivation rate just as much as a truncation of the entire N-terminal domain. An interpretation of this could be that the very initial bit of the N-terminal domain could be responsible for interaction with the S4-S5 linker. The same group later reported that the slow deactivation of *hERG* channels lacking an N-terminus could be rescued by introducing a short peptide of the first 16 residues of the *hERG* sequence (Wang *et al.*, 2000). This slowing was concentration-dependent manner and the Hill coefficient ($h = 2.2 \pm 0.1$) suggested at least 3 peptides per channel cooperate in this effect. A model was proposed in which the four amino terminal domains interact with binding sites that are uncovered during the activation process of the channel. This interaction of the N-termini with the binding site would stabilize the open state. This model would predict a state-dependent movement of the PAS-cap domain and did not involve the C-terminal domain.

A role of the C-terminus was reported the following year by Aydar *et al.*, who made a series of C-terminal deletions of varying lengths and found that deleting certain portions of the C-terminus resulted in a similar accelerated deactivation gating phenotype as the N-terminal

deletions (Aydar and Palmer, 2001). They further showed that constructs bearing deletions in both termini resulted in deactivation rates that were no faster than those of the single mutant constructs. This led to a competing theory of how the cytosolic domains regulate *hERG* deactivation: that the N-terminal domain interacts with the C-terminus in order to exert an effect on the rate of deactivation, though a mechanism for deactivation stabilization was not defined. In 2009, Al-Owais *et al.* constructed a *hERG* homology model of the cyclic nucleotide homology binding domain (CNBHD) of the C-terminus from a crystal structure of the HCN2 CNBD (Zagotta *et al.*, 2003) and made a series of lysine mutations along a hydrophobic patch observed along a face of the CNBHD (Al-Owais *et al.*, 2009). Lysine mutations disrupt domain-domain hydrophobic interactions (Sine *et al.*, 2002) and many of these lysine mutations increased the rate of deactivation similar to that seen in N-terminally disrupted mutants. This introduced further experimental evidence for an interaction between N- and C-termini. This potential interaction was further studied in 2011, when Gustina and Trudeau showed that a recombinant *eag* domain would only assemble with the channel to restore slow deactivation kinetics of *hERG* mutant channels if the CNBHD was intact (Gustina and Trudeau, 2011). They concluded that this demonstrated an interaction between the CNBHD and the PAS domain, which they suggested acted as a scaffold to orient the PAS-cap region to interact with the S4-S5 linker. A following study by the Trudeau group involving Forster resonance energy transfer experiments strayed from this hypothesis towards a theory that the main cause of slow deactivation was through N- and C- terminal interaction and that the S4-S5 linker was not of much importance for this phenomenon (Gianulis *et al.*, 2013). This hypothesis was put forth again in 2013, when Haitin *et al.* published a high resolution crystal structure of the *eag* domain and CNBHD of mouse *eag*1, which is highly homologous to *hERG* (Haitin *et al.*, 2013). It depicts a high degree

of interaction between faces of the CNBHD and *eag* domains, particularly along the previously described hydrophobic faces. Many LQTS2 mutations in these regions were found to lie along this interface. Unfortunately, the first 16 amino acids of the N-terminus were too disordered to be resolved in this study. Of the PAS-cap region that they did resolve, they found an interaction of the PAS-cap with the CNBHD region, which had been at odds with previous roles suggested by NMR studies (Li *et al.*, 2010; Muskett *et al.*, 2011). The study suggests that PAS-cap resides R4 and R5 interacting with the CNBHD at position E788 may be a means by which slow deactivation comes about.

In 2011, de la Pena *et al.* demonstrated physical proximity between the S4-S5 linker and PAS-cap through a cysteine cross-linking study. The cross-link was found between residues V3 of the PAS cap and Y542 of the S4-S5 linker. The cross-linking led to non-conducting channels and the rate of cross-linking was enhanced by holding the cell at hyperpolarized potentials. This seems to indicate that these sites interact with one another in the closed state and may not actually be involved in the slow deactivation process of the channel, but it is of interest to see that the end of the PAS-cap does interact with this region. A study in 2013 by de la Pena *et al.* showed that the PAS-cap can be cross-linked in a state dependent manner with both the C-linker portion of the C-terminus and the S4-S5 linker, suggesting that these regions are fairly close to one another and that there is mobility in the N-terminal domain. In 2014, Ng *et al.*, using mutant cycle analysis, looked for functional interactions between parts of the CNBHD and the PAS domain and found an interaction between R56 and D803 and a transient interaction between the N-terminal cap and the C-linker domain (Ng *et al.*, 2014). Together all of these findings seem to indicate that the PAS-cap region of the *hERG* N-terminus is able to interact with multiple areas of the channel

and that at least one of these interactions leads to the slow deactivation phenotype of the *hERG* channel.

From these studies of cytosolic domain regulation of *hERG* deactivation, two main theories have emerged as the basis for this phenomenon. The first is that the PAS domain region interacts with the CNBHD to allosterically modulate channel deactivation (Gustina and Trudeau, 2012; Haitin *et al.*, 2013; Muskett *et al.*, 2011) and the second is that the PAS domain interacts with the gating machinery of the channel to impede deactivation gating (Li *et al.*, 2010; Wang *et al.*, 1998). As it stands, neither of these hypotheses fully accounts for the manner in which these domains regulate *hERG* deactivation. Recently, however, the structure of the highly homologous *eag* channel was determined by the MacKinnon lab (Whicher and MacKinnon, 2016). This structure details an unprecedented involvement of the cytosolic domains in gating of the channel. The S4 appears to engage in a direct interaction with the bottom of the C-linker. In the deactivated state, the S4 would push the C-linker in a manner that would introduce a kink in its alpha helix shape and seal off the pore region to potassium ions. In the activated state, this constraint would be relieved and the pore would be able to pass ions. This study also notes the potential for many other interactions of the cytosolic domains with the rest of the channel. The PAS-cap region appears to hover around the S2-S3 linker region and could manipulate channel gating in some yet to be determined fashion. There is also extensive interaction noted between the PAS domain of the N-terminus and the CNBHD of the C-terminus, though this had already been detailed in Haitin *et al.* in 2013. The PAS-cap region in the *eag* structure is not shown to directly interact with any specific area of the channel, but it is in close proximity to the bottom of the voltage-sensing domain.

1.2.5 Role in the cardiac action potential - *hERG* is found in many tissues throughout the body, but is perhaps best known for its role in the cardiac action potential as the rapid delayed rectifier current, I_{Kr}, that aids in bringing an end to cardiac systole (Sanguinetti *et al.*, 1995; Trudeau *et al.*, 1995). I_{Kr}, along with the slow delayed rectifier current, I_{Ks} (encoded by K_v 7.1), are the primary means of cardiac action potential repolarization. These potassium currents were initially distinguished from one another in 1969 by Tsien and Noble. At the time, it was thought that the delayed rectifier current of the cardiac action potential came from one type of channel, but through assessing the activation kinetics of the potassium current of Purkinje fibres, Tsien and Noble were able to dissect the potassium current into two components: one an inward rectifier later found to be *hERG* and the other a much more slowly activating current later found to be K_v 7.1 (Noble and Tsien, 1969). Decades later, the kinetics of these two currents were able to be properly assessed when Sanguinetti and Jurkiewicz distinguished the two currents by blocking I_{Kr} with a drug, E-4031 (Sanguinetti and Jurkiewicz, 1990). Both of these currents are unusually slow to activate when compared to more conventional VGKCs. The result of this is a uniquely prolonged period of systole, the plateau phase of the cardiac action potential. The plateau phase allows enough time for sufficient calcium to be released from the sarcoplasmic reticulum in order to facilitate cardiac contraction. Along with slow activation, *hERG* is slow to deactivate, and rapid to inactivate and recover from voltage-dependent inactivation (Smith *et al.*, 1996; Spector *et al.*, 1996b). This results in little I_{Kr} being passed during the plateau phase of the cardiac action potential as *hERG* channels that open are quickly inactivated. Upon initial repolarization of the cardiac action potential, *hERG* channels begin to recover from inactivation and pass current. The slow deactivation kinetics of the channel allow it to pass a large amount of

current in the repolarizing phase of the cardiac action potential and also protects against ectopic beats (Lu *et al.*, 2001; Muskett *et al.*, 2011; Schonherr and Heinemann, 1996). Figure 1.2 shows how the gating of *hERG* shapes the ionic currents of the channel in response to a depolarization from -110 mV to 0 mV.

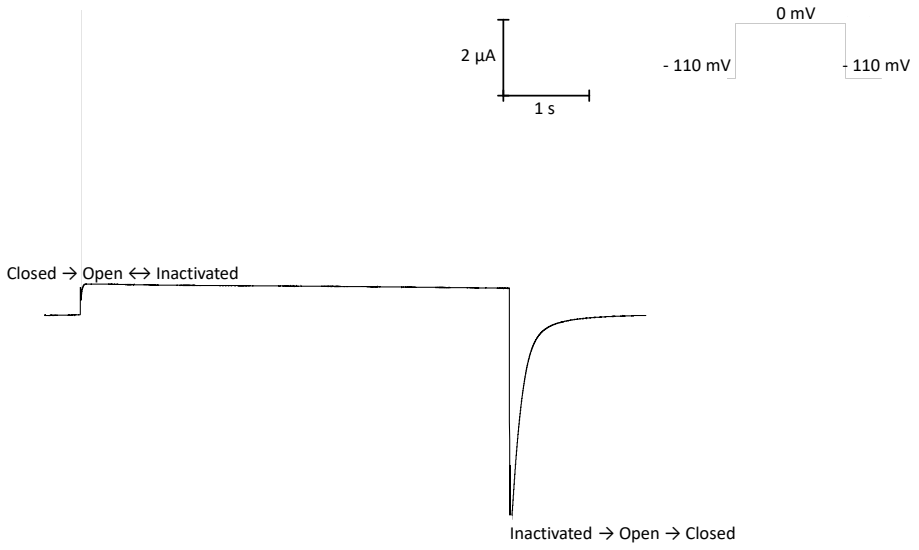

Figure 1.3 - *hERG* gating.
Upon depolarization, such as a voltage step from -110 mV to 0 mV (inset), *hERG* channels open slowly. Inactivation onsets quickly at depolarized potentials since it is a fast and voltage dependent process in *hERG*. As a result, throughout the breadth of a depolarizing stimulus, little *hERG* current is passed. Upon a hyperpolarizing stimulus, such as a voltage return to – 110 mV, inactivation is quickly relieved and, as the deactivation gating of *hERG* is quite slow, channels dwell in an open state for a substantial time before deactivating. These unique gating features produce the phenotypic hooked tail current of the *hERG* VGKC.

1.2.6 Genetic and acquired long QT syndrome type 2 (LQT2) - Long QT syndrome is the result of an impairment to cardiac electrical activity that prolongs the QT interval as seen on an

electrocardiogram. The QT interval itself is a reflection of the repolarization of ventricular myocytes. Prolonged QT intervals can cause tachycardia, which can lead to syncope or sudden death (Sanguinetti and Tristani-Firouzi, 2006). With respect to *hERG*, LQTS can manifest through either genetic mutation or drug block of the channel. Reduction of the *hERG* current, as it is a repolarizing current of the cardiac action potential, will increase the length of the QT interval. Roughly 40% of genetically related cases of LQTS can be accounted for by mutations in the KCNH2 gene that gives rise to the *hERG* channel, LQTS type 2 (Vandenberg *et al.*, 2012).

In 1995, one year after the *hERG* channel was discovered, *hERG* dysfunction was found to be the cause of LQT2 (Curran *et al.*, 1995; Sanguinetti *et al.*, 1995). The Keating group, through showing that several LQTS mutations localized to chromosome 7q35-336, mapping *hERG* to chromosome 7q35-36, showing strong *hERG* expression exists in the heart, and identifying *hERG* mutations that resulted in LQTS, provided strong evidence that *hERG* dysfunction caused LQT2. At the time, a function of the *hERG* gene had not been explicitly determined, but was suggested to be a VGKC based on sequence alignment with known VGKC (Warmke and Ganetzky, 1994). In the same year, two groups showed that the *hERG* gene provided the framework for a voltage-gated potassium channel that generates a delayed-rectifier current that highly resembled the rapid delayed rectifier current of the cardiac action potential (Sanguinetti *et al.*, 1995; Trudeau *et al.*, 1995). While in the 1995 study, Sanguinetti *et al.* found that drugs that typically block the I_{Kr} current in cardiac myocytes did not block the *hERG* channel in *Xenopus* oocytes, later studies showed that the *hERG* channels were indeed blocked by the same drugs that block the I_{Kr} current (Kiehn *et al.*, 1996; Roy *et al.*, 1996; Snyders and Chaudhary, 1996; Spector *et al.*, 1996a). These later studies made it clear that block of the *hERG* current by drugs was the cause of acquired long QT syndrome.

There are over 500 documented mutations of *hERG* that can result in LQT2 (Zhang *et al.*, 2010). Mutations can reduce *hERG* expression by introducing premature stop codons that cut short channel synthesis, causing gating defects that render *hERG* ineffective, reducing the single channel conductance of the channel, and, most commonly, reducing trafficking of the translated protein to the cell membrane (Anderson *et al.*, 2006; Anderson *et al.*, 2014). Reductions in trafficking can largely be attributed to misfolding of the protein, which vary in severity in the extent to which their channels are degraded/withheld by the endoplasmic reticulum. In situations in which membrane protein expression is hindered due to misfolding of the protein, pharmacological chaperones have been suggested as a means to aid the protein to reach the cell membrane. This has been suggested as a possible therapeutic target for LQT2 as well, however, the outcome of the drug intervention hinges on whether the mutant *hERG* protein will properly function should it make it to the membrane. A recent study from the Vandenberg lab addressed this question and found that in the majority of LQT2 mutations (79%), channel function upon rescue is still impaired due to gating defects (Perry *et al.*, 2016).

The vast majority of cases of long QT syndrome of any nature are not due to genetic factors, but are a result of drug block of the *hERG* channel (Roden, 2004; Vandenberg *et al.*, 2012). LQTS as a result of block of the *hERG* channel is commonly referred to as acquired long QT syndrome or drug induced long QT syndrome. The *hERG* channel has been found to be predisposed to block by a variety of chemical structures from a range of different drug classes. Block of *hERG* may result in many of the same symptoms seen in genetic LQTS; most notably syncope, *torsades de pointes* (a polymorphic ventricular tachycardia), and risk of sudden death. While syncope in

relation to quinidine use had been noted as early as 1920 and associations between drug use, QT prolongation, and *torsades de pointes* were made in the 1970-80s, it was not until the 1990s that acquired long QT syndrome began to impact drug development or clinical practice (Roden, 2016; Vandenberg *et al.*, 2012). At this time, it was determined that when an 'over-the-counter' antihistamine, terfenadine, was used in higher than recommended dosages or when used by a person with liver disease, it increased the QT interval of the cardiac action potential and that this increased the risk of torsades de pointes (Roden, 2016). Antiarrhythmic drugs that prolong the QT interval are found to cause *torsades de pointes* in 1-5% of exposed subjects (Abraham *et al.*, 2015). There are also many non-cardiovascular drugs, like astemizole, that can also result in *torsades de pointes*. The decision of whether or not a drug will be deemed acceptable for use or not is determined by comparing its potential for therapeutic benefit versus the risks associated with it at therapeutic dosages (Roden, 2004, 2016). Regulatory bodies suggest that the effect on QT interval be determined early in the drug development process (2005), but it is a fairly costly undertaking, and one that often is not completed until later in the development of a drug because of the requirement to define a therapeutic dose. *In silico* modeling is often used to assess the likelihood of block for different compounds at an earlier point in time of the drug development process. One of the most common reasons for a drug being withdrawn from the market or from clinical trials is because it extends the QT duration beyond a specified limit.

Pharmacophore models can identify specific chemical moieties that may lead a compound to be prone to interact with the channel pore. Having accurate models that will be able to very specifically determine which drug candidates are likely to block the channel is of high interest to those in the pharmaceutical industry. A high rate of false positives could lead to many potentially

helpful drugs never being pursued in earnest. While there is not a general consensus on a *hERG* pharmacophore model, there are several features common to the vast majority of models proposed: 1) a charged amine group increases drug potency; 2) increasing the number of phenyl rings increases drug potency; 3) areas of hydrophobicity increases drug potency; and 4) flexibility of the molecule increases drug potency (Vandenberg *et al.*, 2012).

It is not quite enough to measure whether or not a drug blocks *hERG* in order to determine if it will have a negative impact on patients. While the logic of blocking *hERG* leading to a prolonged QT interval which disrupts electrical activity of the heart, and predisposes an individual to arrhythmia seems fairly straightforward, the reality is not quite that simple. There are many drugs for which this is the case, but there are also many notable exceptions. These exceptions arise when a drug interacts with more than one factor that affects the electrical activity of the heart. For example, verapamil blocks both *hERG* and L-type calcium channels and the use of this drug does not prolong the QT interval (Fauchier *et al.*, 1999). There have also been concerns raised about whether the kinetics of drug block should be taken into account as the IC_{50} alone may provide too crude of an estimate for adverse cardiovascular events (Hill *et al.*, 2014). The determination of more exact markers for what will predispose patients to arrhythmic events is an ongoing discussion in the acquired LQTS community (Roden, 2016).

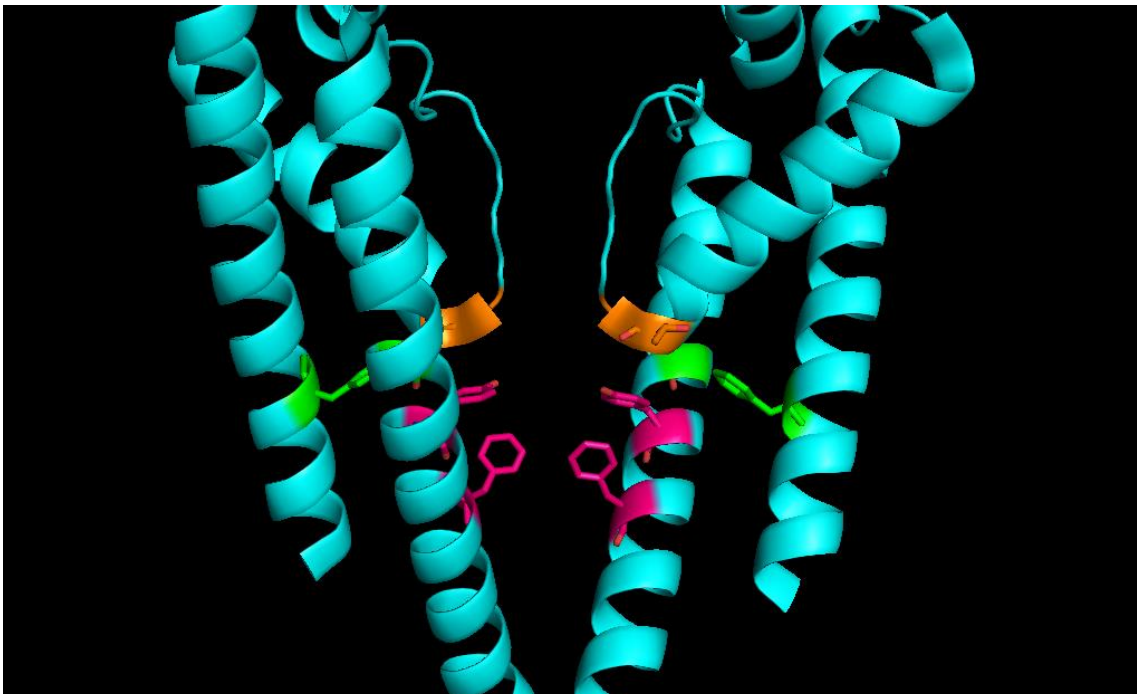

Figure 1.4 - Proposed sites of drug interaction in *hERG*.
View of the pore region of two subunits of the closely related *eag* voltage gated potassium channel (5K7L). Residues in pink are the residues homologous to Y652 and F656, two aromatic amino acids noted to interact with nearly all drugs that block the channel. Residues in green are residues homologous to G648 and F557. Alanine substitution at either of these sites has been found to impart a reduction in drug affinity. G648A is thought to allosterically modulate the S6 to reposition binding determinants of the channel in a manner unfavourable to drug interaction. F557 has recently been proposed as a *hERG* binding determinant, but it is unknown whether this is due to actual drug interaction or if mutation of the residue allosterically modulates position of other binding determinants. Residues in orange are the residues homologous to T623 and S624, two polar residues in the re-entrant P-loop. These residues have been shown to interact with many, but not all drugs that block *hERG*.

1.2.7 Molecular basis of *hERG* drug block - As it became apparent in the 1990s that *hERG* was an unusually common pharmaceutical antitarget, considerable interest developed in the pharmacology of the channel. The largest deviation in *hERG* drug block from that of conventional VGKCs is in the broad range of molecular structures that can lead to block of the channel, but the means by which *hERG* block occurs is fairly conventional.

Drug block of potassium ion channels was first described in depth by Armstrong in his series of papers detailing quaternary ammonium ion block of a delayed rectifier potassium channel. The main findings from this series of studies are: intracellular block of channels require activation and opening of the pore (Armstrong, 1971), onset of voltage-dependent block of the channel is seen as a reduction in I_K (Armstrong, 1966, 1971), and inward potassium currents aid in pushing the QA ions out of the pore region and relieving block of the channel (Armstrong, 1969). These findings suggested that there was a binding site that QA ions were able to access in the open state that was inaccessible in the closed state. Conformational changes of the protein's quaternary structure expose or occlude these sites of drug interaction. These experiments preceded those of Hille in the 1970s which established the premise of the modulated receptor hypothesis. Hille found that by manipulating constraints that affected the level of inactivation seen in sodium channels, there would be a response in the level of sodium channel block seen. He theorized that this was due to drugs exhibiting a preference for binding to the inactivated state of the channel and interact in a manner that stabilizes this non-conducting state (Hille, 1977).

The structural basis for *hERG* susceptibility to block from a diverse group of chemical moieties remains to be fully determined. While no study has been able to fully detail this phenomenon, a substantial amount of insight has been provided. The unique lack of a PVP motif in the S6 segment of the *eag* family of VGKC suggests that these channels have a larger inner vestibule volume than typical VGKC (Mitcheson *et al.*, 2000b). This could be important for 'drug trapping'. Experiments dealing with conventional VGKC found that channels blocked with larger QA ions were able to recover from block more quickly than channels blocked with smaller QA ions (Armstrong, 1971). This was attributed to the smaller ions allowing the channel pore to

close fully, trapping them in the inner vestibule area. The larger QA ions would be too big to allow the pore region shut around them and would have to exit the pore to allow the channel to shut. The lack of a PVP motif in *hERG* has led to the suggestion that the larger inner vestibule area would be able to accommodate larger molecules that would be slow to dissociate from the pore region as they would be able to reside in the pore region in the closed state of the channel. Several studies have noted channel block to be very slow to reverse (Kamiya *et al.*, 2006; Mitcheson *et al.*, 2000b; Perry *et al.*, 2004).

hERG is thought to be blocked by molecules that, while making several interactions in the inner vestibule of the channel, occlude the pore region and block the flow of potassium ions. An example of an alternate inhibitory mechanism could be that the 'blocking' agent interacts with the channel and allosterically stabilizes a closed or inactivated state of the channel. Much work has gone into detailing specific drug-interacting residues, whether it is the same residues for each drug, and what the molecular basis of these interactions may be. This area of investigation began with a group of papers performing mutagenesis experiments. In 2000, Lees-Miller *et al.* made a sequence alignment of *hERG* compared to other VGKC and made mutants of four *hERG* S6 residues that did not align with those of the other VGKC. Their most striking finding was that the mutation F656V weakened the IC_{50} of dofetilide by a factor of over 100 and quinidine by a factor of more than 30 (Lees-Miller *et al.*, 2000). This study was very shortly followed by a full alanine scan from the Sanguinetti lab that individually mutated each residue in the pore helix and inner helix of the pore (Mitcheson *et al.*, 2000a). This study identified several more residues that strongly reduced affinity for *hERG* block for the drug MK-499: T623, S624, and Y652. They also reported that G648 was notably important for a *hERG* drug block interaction, but as this

residue is strongly conserved amongst VGKC, it is unlikely to be the determining factor of *hERG* drug block. The polar residues of the pore helix T623 and S624 were later shown to have drug-dependent effects on drug potency (Perry *et al.*, 2004; Perry *et al.*, 2006), but Y652 and F656 have been shown to be extremely strong determinants of *hERG* drug block with nearly all *hERG* blockers (Chen *et al.*, 2002; Duncan *et al.*, 2006; El Harchi *et al.*, 2012; Kamiya *et al.*, 2008; Melgari *et al.*, 2015b; Milnes *et al.*, 2006; Sanguinetti *et al.*, 2005; Wu and Sanguinetti, 2016). In a study that systematically introduced all natural amino acids at Y652 and F656, Fernandez *et al.* showed that position Y652 required an aromatic amino acid and F656 required a hydrophobic amino acid in order to retain a high degree of drug affinity to cisapride and terfenadine (Fernandez *et al.*, 2004). This has led to the suggestion that the interaction taking place at Y652 has to do with the nature of the aromatic ring, i.e. a cation-π or π-stacking interaction (Fernandez *et al.*, 2004; Stansfeld *et al.*, 2007; Vandenberg *et al.*, 2012). Figure 1.3 displays a homology model of *hERG* based on the rat *eag* structure determined by Whicher *et al.* (2016). Highlighted are the amino acids mentioned in this section that have been shown to be important for drug block of the channel.

Y652 and F656 are not conserved amongst VGKC, but they are also present in the closely related K_v 10.1 channel. Interestingly, K_v 10.1 is not blocked by nearly as many drugs as the *hERG* channel despite possessing these two residues in homologous positions (Ficker *et al.*, 2001; Herzberg *et al.*, 1998). However, transfer of residues 612-650 from *hERG* channels to the equivalent positions in K_v 10.1 channels introduces not only a susceptibility to drug block, but also introduces the fast voltage-dependent inactivation seen in *hERG* channels (Herzberg *et al.*, 1998). This finding, paired with findings that *hERG* mutant channels with disrupted inactivation

are less sensitive to drug block (Ficker *et al.*, 1998; Lees-Miller *et al.*, 2000; Perrin *et al.*, 2008), seemed to indicate that drugs preferentially bind the inactivated state of the channel. Later studies found this to be true for some drugs, but not others (Perrin *et al.*, 2008). This suggests that the exact positioning of the aromatic residues Y652 and F656 is important to this drug block phenomenon in *hERG* and that in *eag* channels their orientation may be less prone to interact with drugs. A study that supports this idea is found in Chen *et al.* (2002) who showed that by repositioning Y652 and F656 one position down the S6 helix in K_v 10.1 channels, channels became sensitive to cisapride without introducing inactivation (Chen *et al.*, 2002). All of these studies taken together indicate that the exact positioning of these aromatic residues is highly important for the drug block phenomenon seen in *hERG*.

Another aromatic residue was recently determined to be involved in *hERG* drug block, F557 on the S5 segment (Saxena *et al.*, 2016). Saxena *et al.* showed through mutagenesis, two electrode voltage clamp, and molecular modeling experiments that F557 interacts with drugs that block the *hERG* channel. However, past studies have indicated that F557L, the mutant used in Saxena *et al.*, severely disrupts activation and inactivation kinetics of the channel (Ju *et al.*, 2009). The drug docking and molecular modeling in Saxena *et al.* suggests a direct interaction with drugs through π-stacking relationships (Saxena *et al.*, 2016). Further study is needed to determine whether F557 is involved in interaction with drugs or if the loss in drug potency can be attributed to allosteric changes in the channel.

Many studies have made attempts to visualize the exact positioning of aromatic residues by constructing homology models of *hERG*. Until very recently, homology models of *hERG* were

based on structures of VGKC that were not overly homologous with *hERG*: Kv1.2/2.1, MthK, and KcsA (Dempsey *et al.*, 2014; Durdagi *et al.*, 2012; Stansfeld *et al.*, 2007; Stary *et al.*, 2010). Even if it had been the case that these structures were fairly homologous with *hERG* and would be able to provide an accurate template, structures based on x-ray crystallography provide only a static picture of a single state of the channel, and one that may be subject to some unnatural constraints due to the crystallization process. Despite these limitations, several *hERG* models have been generated and many drugs have had their interactions assessed through drug docking studies in a defined pore area. A drug is given the opportunity in the computer model to reach its lowest possible energy state through interactions with different parts of the pore region. Unlike what had been suggested with the functional work done by Fernandez *et al.*, several molecular dynamics simulations fail to detect a cation-π interaction at either of the aromatic pore residues Y652 or F656 (Boukharta *et al.*, 2011; Dempsey *et al.*, 2014; Imai *et al.*, 2009; Stansfeld *et al.*, 2007). Instead, these studies suggest π-stacking and hydrophobic interactions of drugs with the pore region, and note that drugs do not often exhibit one single state of binding, but rather display a number of sites of interaction with the pore. Despite the lack of a cation-π interaction observed in the modeling work, it is worth noting that quantitative structure-analysis relationship models of *hERG* drug block have noted that a charged amine group correlates with higher affinity blockade of the channel (Vandenberg *et al.*, 2012).

1.3 Scope of the thesis

The aim of this thesis is to detail specific structural interactions that endow *hERG* with its unique gating and pharmacological properties. The unique gating of *hERG* allows it to fulfill its role as

the rapid delayed rectifier potassium current of the cardiac action potential and the unique susceptibility to drug block can compromise this function.

Chapter 2 aims to clarify the relationship between gating charge activation and pore opening. It begins with a general characterization of the relationship between charge movement and opening of the ionic pore in activation gating of the channel, details the voltage-independent transition of the gating charge, and studies the role of the cytosolic domains in the deactivation gating of the channel. This first study also shows that a stabilization of the *hERG* activated gating charge, referred to as a mode shift, is one that would be relevant on a physiological timescale.

Chapter 3 describes the origin of the biphasic movement of *hERG* gating charge as being a function of unique structural constraints in the *hERG* VSD that slow the movement of the majority of gating charge. An interaction between an acidic residue at the bottom of the S1 segment with residues at the bottom of the S4 stabilizes the closed state of the channel and slows activation. Through gating current and fluorescence experiments, we propose a model of *hERG* gating in which this unique interaction stabilizes an early closed state of the channel.

Chapter 4 investigates the role of cation-π interactions in the block of *hERG* channels. The aromaticity of the two most significant residues for drug interaction, Y652 and F656, has fueled the suggestion that they may interact with drugs by some manner specific to their aromaticity. Along with the many pharmacophore models that propose a protonated amine as beneficial for *hERG* block, this has led some groups to suggest that this interaction may take place via a cation-

π interaction. Through the use of unnatural amino acid mutagenesis, this final study shows that cation-π interactions do not appear to play a major role in drug interaction with the *hERG* pore.

Chapter 2: Sequence of gating charge movement and pore gating events in *hERG* channels' activation and deactivation pathways[1]

2.1 Introduction

The human ether-à-go-go related gene (*hERG*) potassium channel (K_V11.1, KCNH2) (Warmke and Ganetzky, 1994) is found throughout the body in a variety of excitable and non-excitable cells and serves many different functions (Wymore *et al.*, 1997). The most studied role of *hERG* channels is its activity during the repolarization phase of the cardiac action potential, as a rapid delayed rectifier potassium current (I_{Kr}) (Sanguinetti *et al.*, 1995; Trudeau *et al.*, 1995) critical to terminating cardiac systole. Suppression of *hERG* function can occur as a result of drug interactions (Yang *et al.*, 2002) or less commonly from inherited mutations. The result of either is a prolongation of the QT interval as seen on the electrocardiogram, referred to as acquired or congenital long QT-interval syndrome (*hERG* is LQT type 2) (Sanguinetti and Tristani-Firouzi, 2006). This can be associated with serious cardiac rhythm consequences such as *torsades de pointes* (a multifocal ventricular tachycardia) and sudden death (January *et al.*, 2000). Although *hERG* current in the heart is named I_{Kr}, where 'r' refers to 'rapid', this is mainly to distinguish it from I_{Ks} (slow), and in fact the activation and deactivation of *hERG* channels is surprisingly slow for a voltage-dependent potassium (K_V) channel, although entirely commensurate with its physiological role. Furthermore, since the slow kinetics of I_{Ks} arise from the association of the

[1] A version of this chapter has been published. Samuel J Goodchild, Logan C Macdonald, and David Fedida. (2015) Sequence of Gating Charge Movement and Pore Gating in *hERG* Activation and Deactivation Pathways. Biophysical Journal 108(6), 1435-1447

core pore-forming units with the accessory subunit, KCNE1 (Sanguinetti *et al.*, 1996), *hERG* channels are unique in that channel activation and deactivation rates determined by the alpha subunit properties alone are slow, at least an order of magnitude slower than K_V1-4 channels at potentials around 0 mV (Es-Salah-Lamoureux *et al.*, 2010; Goodchild and Fedida, 2014; Sanguinetti and Jurkiewicz, 1991). The reasons for slow activation and deactivation of the ionic current have focused on two linked aspects of channel function: intrinsic voltage sensor domain (VSD) movements; and VSD-pore coupling which causes the opening of the pore conduction gate.

The rise of the conductance-voltage relationship (GV) and the appearance of ionic currents mark the opening of the pore gate and a number of methodologies have been developed to follow dynamic VSD rearrangements in *hERG* channels in order to compare the voltage dependence and time course of the two sets of events. Direct measurement of gating currents is probably the best way to track VSD movement as it reflects a sum of all the charges moving, including those in S1-S3 as well as in S4. Earlier studies from Sanguinetti's laboratory using oocytes and the Cut-Open Vaseline Gap (COVG) technique established fast and slow components to the gating current that showed an overall hyperpolarized charge-voltage (QV) distribution compared with the GV (Piper *et al.*, 2005; Piper *et al.*, 2003). There was an initial spike of gating current that remains poorly understood, but the main body of gating current moved quite slowly, about 10 times slower than gating currents recorded from K_V1 channels in mammalian cells. The rates were not quantified in relation to the time course of pore opening (Piper *et al.*, 2003), but the authors concluded that slow gating charge movement was responsible for the overall slow ionic activation of *hERG* currents. Recently, we revisited *hERG* gating currents in measurements from

mammalian cells and confirmed a hyperpolarization of the QV compared with the GV, but found that bulk gating charge movement occurred several fold faster than *hERG* ionic current activation (Ferrer *et al.*, 2006; Goodchild and Fedida, 2014; Piper *et al.*, 2003; Wang *et al.*, 2013). We used a second methodology, namely MTS modification of I521C to confirm these two central findings. Our work suggested that activation steps downstream of VSD rearrangements provided the major delay to pore opening in *hERG* channels.

Due to the difficulties in measuring gating currents from *hERG* channels, most of the recent examination of VSD movement in *hERG* channels has been carried out by monitoring the environmental changes experienced by the amino acids in the S3-S4 linker using voltage-clamp fluorimetry (VCF). While it is an easier technique to use, it suffers from the disadvantage that it records environmental changes around the rather large fluorophores used to label the VSD, which may not directly report specific S4 displacement. Signals are also dependent on the type of fluorophore used, which highlights intrinsic photochromic properties that contribute to signal intensity, and the very nature of such measurements themselves cannot exclude the involvement of other adjacent moving elements of the channel structure. Data from labeling L520C in the S3-4 linker, or G516C has shown a quenching time- and voltage dependence that tracks channel pore opening, closely overlaying the GV relationship (Cheng *et al.*, 2013; Thouta *et al.*, 2014; Van Slyke *et al.*, 2010; Yellen, 2002), suggesting a tight coupling with essentially no kinetic separation of VSD movement and pore opening.

Throughout all this work on activation gating and its temporal relationship to pore opening, less attention has been paid to the process of deactivation, which, as pointed out above, is of great

physiological importance during the final repolarization of the cardiac action potential. Deactivation of *hERG* has previously been shown to be dependent upon N- and C-terminus interactions (Morais Cabral *et al.*, 1998; Schonherr and Heinemann, 1996; Tan *et al.*, 2012), but the question remains whether these domains interact with the voltage sensor directly through the pore domain, or via a coupling mechanism between the pore and VSD. Interestingly, activation of gating charges upon depolarization typically requires less applied voltage than that required to return the charge from a depolarized holding potential once channels are activated (Bezanilla, 2000; Fedida *et al.*, 1996; Goodchild *et al.*, 2012; Olcese *et al.*, 1997). This results in a hyperpolarized charge-voltage dependence of deactivation compared with activation, and is referred to as a mode-shift i.e. the gating charges move differently after they have entered into an activated mode (Blunck and Batulan, 2012; Haddad and Blunck, 2011; Hull *et al.*, 2014; Piper *et al.*, 2003; Tan *et al.*, 2012). VCF has been used to investigate a "mode-shift" of the *hERG* VSD after prolonged activation that appears to be independent of pore closing. Deletion of the amino terminal PAS domain of *hERG* accelerated ionic deactivation but did not cause a mode-shift of the VSD measured using fluorescence (Tan *et al.*, 2012). This led to the hypothesis that the VSD was intrinsically stabilized in the activated state and that coupling of the pore to the VSD was perturbed by the deletion or disruption of the PAS domain, particularly the positively charged residues in the PAS-cap R4 and R5.

In the present study we sought to address the sequence of gating events in *hERG* activation and deactivation using the COVG voltage clamp method to record ionic and gating currents from *hERG* WT and N-terminal mutant channels (R4AR5A, R56Q, and Δ2-135) that have previously been shown to greatly speed deactivation rates (Chen *et al.*, 1999; Muskett *et al.*, 2011;

Schonherr and Heinemann, 1996). Our quantitative analysis of the kinetics of *hERG* gating currents unequivocally demonstrates the existence of a critical coupling step between VSD charge movement and pore opening in activation. Slow VSD movement is definitely a feature of *hERG* VSD movement, but a slow coupling step to pore opening remains the key determinant of channel opening rate until very positive potentials are reached. We also found, as has been suggested from fluorescence measurements in *hERG*, that gating currents exhibit a mode-shift, which has a rapid and physiologically-relevant onset. Contrary to prior fluorescence results (Tan *et al.*, 2012), we found that gating currents are regulated by intracellular domain interactions coupling the pore state to the VSD state.

2.2 Materials and methods

2.2.1 Oocyte preparation and injection- Stage IV and V *Xenopus* oocytes were isolated following collagenase treatment to remove the follicular layer. cRNA was synthesized using the mMessage mMachine T7 transcription kit (Ambion). Oocytes were injected with 10-100 ng cRNA. *hERG*-injected oocytes were stored in ND96 (96 mM NaCl, 3 mM KCl, 2 mM $CaCl_2$, 1 mM $MgCl_2$, and 5 mM HEPES at pH 7.4) and incubated at 18 ^oC prior to use. Ionic current recordings were obtained 1-2 days following injection whereas gating current recordings were obtained 3-4 days following injection. There are literature reports that *hERG* can be regulated by accessory subunits, but the significance of these studies remains uncertain (Eldstrom and Fedida, 2011). We did not include other subunits in our experiments, so our findings can only reflect intrinsic alpha subunit properties and regulation.

2.2.2 COVG recording- A Dagan CA-1B COVG voltage clamp system (Minneapolis) was used to record all data (~20 ^{o}C). For ionic recordings, the external solution was composed of 96 mM NaCl, 3 mM KCl, 2 mM $CaCl_2$, 1 mM $MgCl_2$, and 5 mM HEPES (pH 7.4). The internal solution contained 120 mM Potassium-Glutamate and 10 mM HEPES (pH 7.0). For gating current recordings, the external solution was composed of 120 mM tetraethyl ammonium-hydroxide (TEA-OH), 120 mM methanesulfonic acid (MES), 10 mM HEPES, and 1 mM Ca-MES (pH 7.4). The internal solution contained 120 mM TEA-OH, 120 mM MES, and 10 mM HEPES (pH 7.4). All chemicals were obtained from Sigma-Aldrich Chemical Co. (Miss, ON). 20 µM terfenadine was added to both internal and external gating current solutions in a further effort to block any potential residual ionic current through the *hERG* pore. Terfenadine is an open channel blocker of *hERG* that binds to the inner pore cavity of the channel to prevent ion passage, and when channels close the terfenadine is trapped in the closed pore (Mitcheson *et al.*, 2000a). 0.3% saponin for 0.5 -2 minutes was used to make the interior of the oocytes electrically continuous with the internal solution. For gating current recordings the membrane was held at ~-10 mV for 20 min after breakthrough to ensure depletion of endogenous K+ ions from the oocyte cytosol. Electrodes had resistances ~0.5 MΩ with 3 M KCl for ionic and 3 M CsCl for gating current recordings. The COVG clamp was controlled with pClamp 10.2 (Molecular Devices). Data were analog low-pass filtered at 5 kHz and digitized at 25-50 kHz. The holding potential for all experiments was -110 mV. For gating currents, an online P/-6 or P/-8 leak subtraction protocol was employed. QV relationships for depolarizations > 1 s were not obtainable due to instability of the membrane patch over longer duration recordings.

2.2.3 Data analysis- The kinetics of *hERG* gating charge movement and ionic activation were measured using voltage protocols that depolarized the membrane to a given voltage for increasing durations. The peak tail current (IK_{tail}) for ionic currents and the time integral of gating current (Ig_{OFF}), to get gating charge (Q_{OFF}) after membrane repolarization, were then plotted against the duration of depolarization. The kinetic data were fit with single exponential functions of the form $y = y_0 + A\ e^{-t/\tau}$ where y is the normalized response, A is the amplitude, and τ is the time constant, or double exponential functions of the form $y = y_0 + A_1e^{-t/\tau1} + A_2\ e^{-t/\tau2}$ where A_1 and A_2 are the amplitudes of each component of the fit and $\tau1$ and $\tau2$ the accompanying time constants. For ionic deactivation currents at voltages where a double exponential gave the best fit, the fast component is quoted and accounted for >90% of the amplitude of the fit in each case. Isochronal Conductance-Voltage (GV) relationships were obtained by plotting peak tail currents, and isochronal Charge-Voltage (QV) relationships were obtained by plotting the Q_{OFF}, both as a function of the depolarizing pulse voltage. Isochronal deactivation GV relationships were assessed by depolarizing the membrane for 300 ms at +60 mV to open channels before repolarizing the membrane to potentials from -30 to -150 in 10 mV increments for 100 – 200 ms to allow channels to deactivate and then assessing the fraction of channels remaining open by measuring tail currents at -110 mV. Data points were normalized to their maximum values then fit with a Boltzmann function of the form $y/y_{max} = 1/(1+\exp(-zF/RT(V- V_{0.5})))$ where y/y_{max} is the normalized response, either G/G_{max} or Q/Q_{max}, $V_{0.5}$ is the potential of half-activation, and z is the equivalent charge. The voltage dependence of activation and deactivation kinetics were fit with a voltage-dependent exponential of the form $\tau = 1/(\beta_{(0\ mV)}\exp(zFV/RT)$ where $\beta_{(0\ mV)}$ is the chemical rate constant and z the equivalent charge. F and R have their usual thermodynamic meanings and T = 293.15 K. Statistical tests were made using

Graphpad Prism to perform one way ANOVA with a Dunnett post-test to compare WT with mutant channel values with significance level set at $P<0.05$.

2.3 Results

An established phenomenon of VSDs in a variety of channel types is the separation of the kinetics of charge movement and pore opening during voltage-dependent gating. Thus, we expect a displacement of the GV in a depolarized direction compared with the QV as energy is required to drive steps in pore opening that occur after voltage sensor displacement. But, this is not what is suggested for *hERG* channels where the delay in opening is directly attributed to the kinetics of the VSD movement, by both the other groups to have measured charge movement in *hERG* (Ferrer *et al.*, 2006; Goodchild and Fedida, 2014; Piper *et al.*, 2003; Wang *et al.*, 2013), and multiple VCF studies (Smith and Yellen, 2002; Tan *et al.*, 2012; Thouta *et al.*, 2014; Van Slyke *et al.*, 2010). As well, the kinetic properties of the mode-shift in *hERG* gating charge have not been investigated and the phenomenon has not been shown to operate on a physiologically relevant timescale.

2.3.1 Separation of the voltage dependence of the GV and the QV- To assess the voltage dependence of Ig_{ON}, the amount of charge that has moved at the end of 300 ms, a similar duration to the cardiac action potential in humans, at each voltage was measured by integrating Ig_{OFF} current upon repolarization as shown by the bracket on the representative traces in Fig. 2.1*A*. The resulting activation charge-voltage relationship ($Q_{ON}V$) is plotted as open circles in Fig. 2.1*C* with Boltzmann fit parameters of $V_{0.5}$ =-19.1 ± 1.9 mV, z=2.0 ± 0.3 (n=10). Ionic tail current activation, which indicates the proportion of channels that reached the open state was

assessed using the same voltage protocol (representative currents in the inset Fig.1*A*) and plotted as the GV in Fig. 2.1*C* (open squares) and fit with parameters $V_{0.5}$ = 4.1 ± 3.4 mV, z=2.3 ± 0.3 (n=4). The $Q_{ON}V$ relationship is hyperpolarized compared with pore opening, which suggests that the population of charges are sensing potential and moving over a more negative voltage range than that defining pore opening.

Equilibrium measurements require protocols with enough time for channels to fully relax into new state distributions after voltage jumps. This has been shown to take significant amounts of time for *hERG* at voltages close to the $V_{0.5}$ due to the exceedingly slow kinetics of activation and deactivation at those voltages (Schonherr *et al.*, 1999). To determine the proportion of channels that had reached the activated state up to and after 300 ms, where charge movement was initially measured, tail GVs were plotted from protocols with differing durations of depolarizations from 24 ms to 3 s from individual cells. Fig. 2.1*D* shows tail GV relationships normalized to the maximum tail current amplitude from a 3 s protocol and illustrates the hyperpolarizing shift in the GV as protocols were run for extended durations. After 300 ms it is apparent that ~80 % of the total population of channels have reached the fully activated and open state and that the $GV_{0.5}$ values of the Boltzmann fits are approaching saturating values that represent equilibrium (Fig. 2.1*E*). Across the range of durations tested the $QV_{0.5}$ values show a negative voltage dependence compared with the $GV_{0.5}$ indicating that, within the limits of our experimental durations, there is a prominent coupling step after movement of charge and the opening of the pore. This coupling step is more significant at shorter duration pulses that are relevant on the physiological timescale of cardiac action potentials, 200 – 400 ms.

2.3.2 *hERG* gating charges are stabilized in an activated state- To establish if gating charge in *hERG* is subject to a mode-shift after activation, we assessed the voltage dependence of deactivating charge movement. Channels were first depolarized to +60 mV for 300 ms to activate channels and then hyperpolarized to a range of different voltages as shown in Fig. 2.1*B*. The $Q_{OFF}V$ relationship that resulted from integrating currents displayed a $V_{0.5}$ of -85.9 ± 2.3 mV, z=2.1 ± 0.2 (n=7) (Filled circles, Fig. 2.1*C*), and indicated that more energy is required to return the charge from the activated position than to move charge into that position in the first place. The ionic deactivation G-V (inset of Fig. 2.1*B*) displayed a $V_{0.5,\ deact}$ of -78.1 ± 1.6 mV, z=2.7 ± 0.1 (n=4), shown in Fig. 2.1*C*. These observations established the presence of a mode-shift of *hERG* charge movement and pore deactivation.

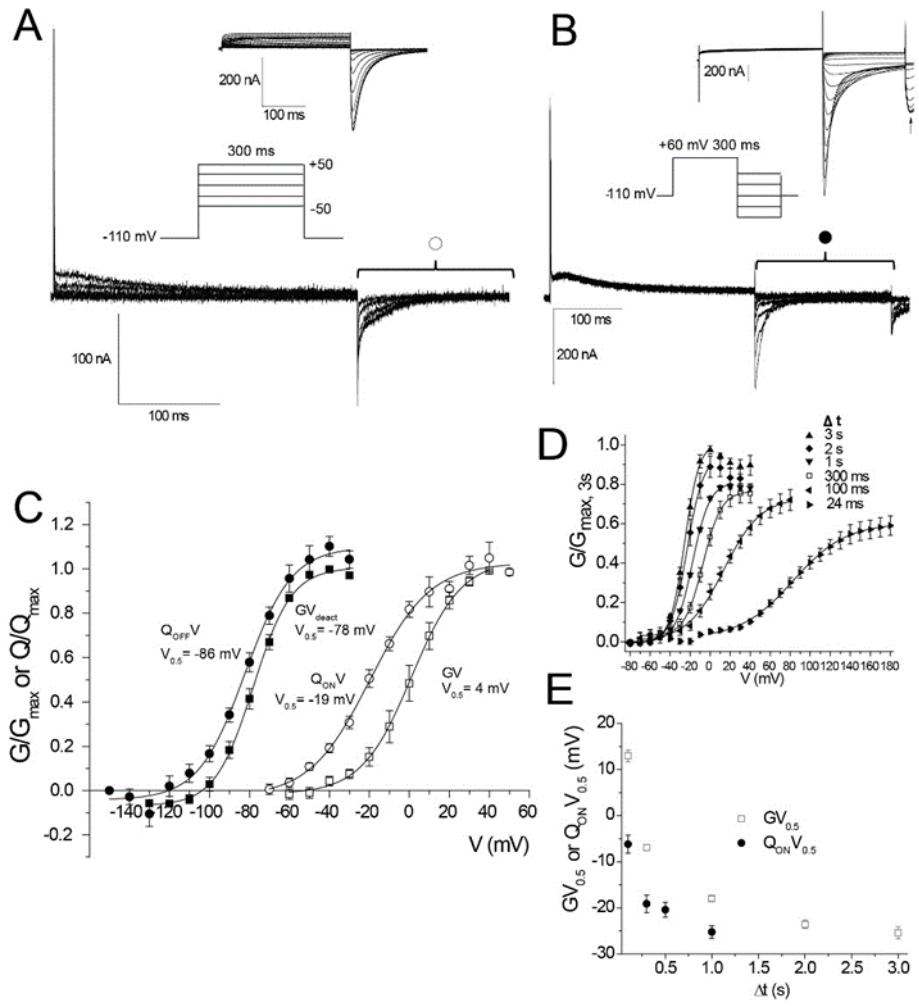

Figure 2.1 *hERG* gating charges are stabilized in the activated state.
(A) On-gating currents recorded during 300 ms depolarizing voltage pulses from -110 mV to +50 mV in 10 mV steps. Inset shows the voltage protocol and ionic currents for the same steps. Pulses were applied every 10 s. Open and filled circles indicate the integration period for the Q_{ON} and Q_{OFF} respectively. **(B)** Off-gating currents recorded during a range of repolarizing steps between 0 and -150 mV, after a 300 ms pulse to +60 mV to fully activate channels, as illustrated by the inset protocol. The GV_{deact} was generated from the normalized peak currents at the point indicated by the arrow in the ionic current inset. **(C)** Activation $Q_{ON}V$ relationship (open circles) measured by integrating Ig_{OFF} currents for 150 ms after 300 ms depolarizations, as shown by bracket in (A), the $V_{0.5}$ was -19.1 ± 1.9 mV, z=2.0 ± 0.3 (n=10). Return of charge from the activated state ($Q_{OFF}V$, filled circles) measured by integrating Ig_{OFF} for 100 ms, the $V_{0.5}$ was -85.9± 2.3 mV, z=2.1 ± 0.2 (n=7). GV relationship (open squares) measured from tail currents as in (A) inset, the $V_{0.5}$ was 4.1 ± 1.7 mV, z=2.3 ± 0.2 (n=4). GVdeact relationship (closed squares) measured from the fraction of channels that have closed after varying repolarizations from the open state as in (B) inset, the $V_{0.5}$ was -78.1 ± 1.6 (n=4). **(D)** Normalized GV relationships from a separate group of experiments in which GV's obtained by varying length of depolarizing pulses were recorded from the same cell. **(E)** Plot of the voltage dependence of $GV_{0.5}$ and $QV_{0.5}$ values from families of depolarizing pulses with increasing duration plotted for comparison. GV fit parameters were as follows: 24 ms $V_{0.5}$=-83.0 ± 3.3 mV, z=1.0 ± 0.02 (n=5), 100 ms $V_{0.5}$=-13.0 ± 1.3 mV, z=1.4 ± 0.05 (n=5), 300 ms $V_{0.5}$=4.1 ± 1.7 mV, z=2.3 ± 0.2 (n=4), 1 s $V_{0.5}$=-18.0 ± 0.5 mV, z=3.1 ± 0.1 (n=4), 2 s $V_{0.5}$=-23.3 ± 1.0 mV, z=3.4 ± 0.2 (n=5), 3 s $V_{0.5}$=-25.4 ± 1.3 mV, z=3.6 ± 0.2 (n=5). $Q_{ON}V$ fit parameters: 100 ms $V_{0.5}$=-6.2 ± 2.0 mV, z=1.5 ± 0.2 (n=5), 300 ms $V_{0.5}$=-19.1 ± 1.9 mV, z=2.0 ± 0.3 (n=10), 500 ms $V_{0.5}$ =-20.4 ± 1.6 mV, z= 2.5 ± 0.3 (n=6), 1 s $V_{0.5}$=-25.3 ± 1.4 mV, z=2.4 ± 0.3 (n=7).

2.3.3 The time course of gating charge movement is faster than pore opening - To examine the kinetics and sequence of the underlying voltage-dependent rearrangements that lead to pore opening we studied the rate at which gating charge moves versus the rate of pore opening at different voltages. In Fig. 2.2*A* the top panels illustrate a selection of representative gating current traces evoked by increasing duration depolarizing pulses to 0, +40 and +100 mV from a holding potential of -110 mV. As before, Q_{ON} during activation was assessed by integration of Ig_{OFF} for 150 ms after the end of the depolarizing pulses. This protocol allows for a more accurate measurement of the kinetics of charge movement than simply fitting the decay of Ig_{ON} currents (Fig. 2.1*A*), which have complex waveforms and can be very slow to decay at moderate depolarizations, and therefore difficult to resolve and fit. There are two obvious components to the return of charge on repolarization, which reflect the amount of charge moved in the prior depolarization, seen in Fig. 2.2*A*. There was an initial very large and brief spike of negative current followed by a slower decay of current to the zero current level. As the depolarization duration was increased, the initial negative spike amplitude declined and the slow phase of current decay became more prominent. Eventually, the size of each component stabilized, and the rate at which this occurred depended on the amplitude of the depolarization. At 0 mV this process did not appear to be complete after more than 300 ms, but at +40 and +100 mV the initial spike of current almost disappeared, and became absorbed into the slower component as that reached a stable maximum amplitude, more quickly at +100 than at +40 mV. The same protocol was repeated in ionic recording solutions on separate cells to obtain the ionic tail current data shown in the lower panels. As for gating charge, tail currents increased and tracked pore opening at a rate that is a function of the activating potential.

To quantify the rates of charge movement and pore opening, the normalized Q_{OFF} or peak tail current was plotted against the duration of the depolarizing pulse and fit with single exponential functions as shown in Fig. 2.2*B*. The kinetics of pore opening deviated from a single exponential at very early activation times due to the latency to opening indicating that several closed states must be traversed before reaching an open state. This is clearly revealed on the logarithmic time scale in Fig. 2.2*B*. To fit the activation of the ionic currents the fit was started from a point where opening could be accurately described with a single exponential. For 0 and +20 mV this was from 35 ms, for +40 and + 60 mV 20 ms and +80 and +100 mV from 15 ms. Plots of the data on a logarithmic scale clearly illustrate that the bulk of gating charge is moving prior to pore opening at moderate voltages, and that there is a prominent separation of the two relationships at 0 and +40 mV almost until the two processes reach equilibrium (not complete for 0 mV curves). This demonstrates a clear separation of pore opening from the bulk movement of charge. As depolarization is increased further, the time course of charge movement and pore opening become more closely associated and the two processes begin to overlap kinetically after about 30 ms at +100 mV. The voltage dependence of the time constants over a range of tested voltages for gating activation and pore opening is shown in Fig. 2.2*C*. There is a clear separation of charge movement and ionic activation in the physiological and supra-physiological voltage ranges, and both demonstrate single exponential voltage dependence. At +80 mV and above, the kinetics of charge movement and pore opening converge and appear to saturate at a similar rate, which suggests that opening speed is becoming limited by the maximum speed of movement of the VSD.

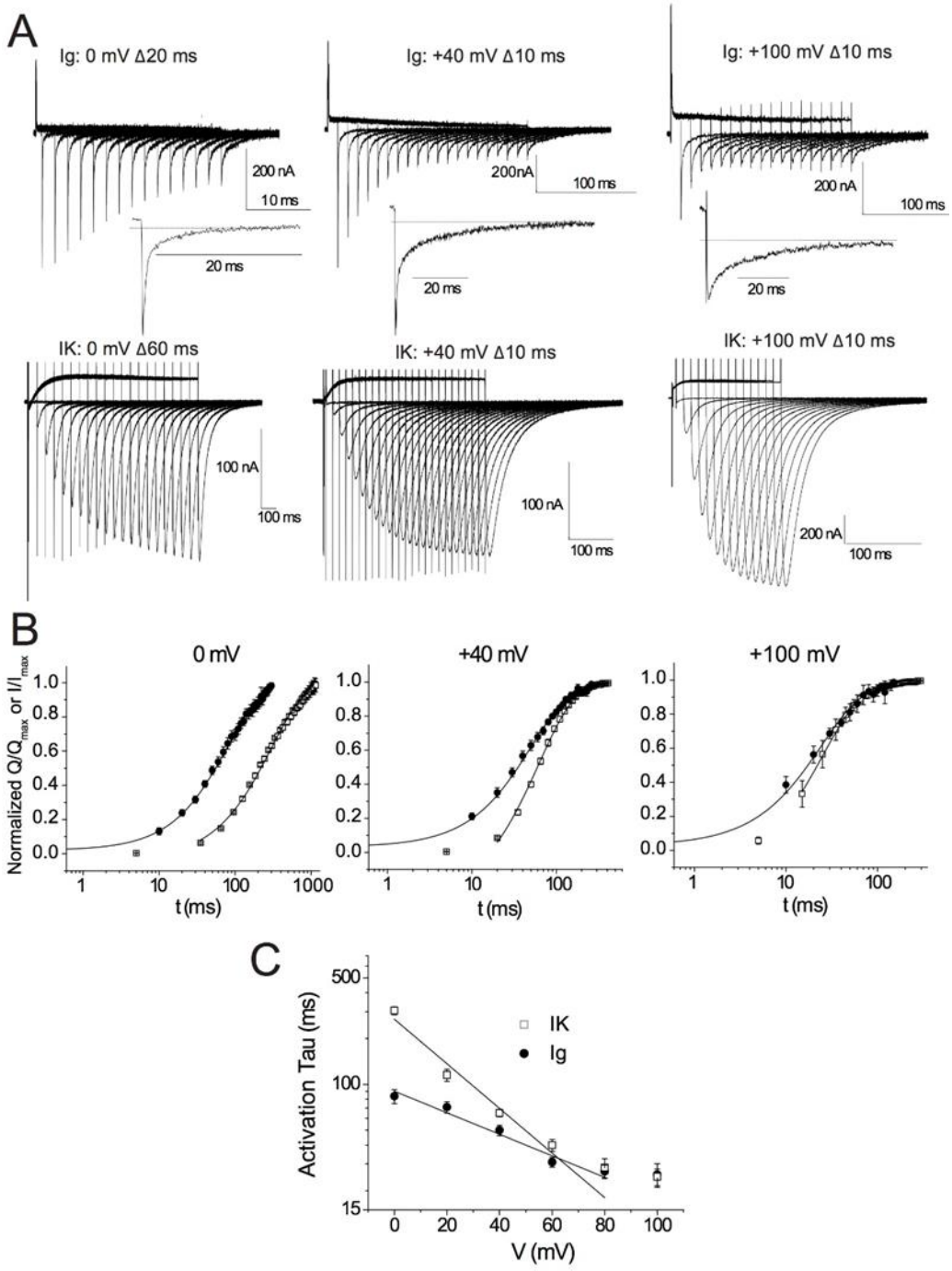

Figure 2.2 Time-course of activation of *hERG* reveals a separation between the charge movement and ionic current activation.

(A) Representative gating current (above) and ionic current (below) recordings during step depolarizations from a holding potential of -110 mV to 0 mV (left panels), +40 mV (middle panels), and +100 mV (right panels). The initial pulse duration was 10 ms for all gating current records, and was incremented by 10 ms for each subsequent cycle. To capture the activation time course in each case, the current recording initial pulse duration was 5 ms and then was incremented in 30 ms steps for 0 and +20 mV, and 10 ms for +40, +60, +80 and 100 mV. In the currents shown in (A) only selected traces are displayed for the increments stated. The pulse interval in (A) was 5 s for gating current and at least 1.5 s for ionic current records. **(B)** Normalized plots of conductance (squares, from peak tail currents) or integrals of Ig_{OFF} (Q_{off}, filled circles) from (A) vs. the duration of depolarizing steps (log scale). **(C)**

Time constants of single exponential fits to the Q/Q_{max} (circles) and G/G_{max} (squares) relations in (B). Data were as follows for gating charge (ms): 0 mV: 83.68 ± 9 (n=6), +20 mV: 70.9 ± 6.1 (n=7), +40 mV: 50.0 ± 3.9 (n=8), +60 mV: 30.9 ± 2.3 (n=8), +80 mV: 26.8 ± 2.7 (n=8), +100 mV: 25.6 ± 4.5 (n=6). For ionic activation current time constants from delayed single exponential fits were (ms): 0 mV: 305.5 ± 18.1 (n=5), +20 mV: 115.3 ± 10.4 (n=5), +40 mV: 64.8 ± 3.5 (n=5), +60 mV: 39.9 ± 3.6 (n=6), +80 mV: 28.4 ± 4.1 (n=5), +100 mV: 24.7 ± 3.1 (n=4). Straight lines through charge and current data points are single voltage dependent exponential fits between 0 and +60 mV.

2.3.4 Voltage-independent step precedes bulk of charge movement – In Fig. 2.2*C*, we see that the time constant of activation of both pore opening and charge movement saturates around 20 ms at potentials higher than +60 mV. Several past studies have noted this voltage independent step, though when input into a model, most groups have included this step as one happening after the majority of the charge has already moved. Our data, in showing that this voltage-independent transition is also reflected in the time constant of gating charge movement, show that the voltage-independent transition must occur before the bulk of gating charge movement in *hERG*. Fig. 2.3*A* shows a potential model for the movement of gating charge in *hERG*. This model details the transition of the voltage sensing domain through several closed states before reaching one which can couple to the pore region to increase the open state probability of the channel. Fig. 2.3*B* describes the first closed-closed state transition as one with a very small activation energy as well as a small amount of charge being moved. The next transition is described as the voltage- independent step, but at 0 mV it is not rate limiting in the activation pathway. The third transition involving the bulk of gating charge movement is rate-limiting at 0 mV. The coupling transition at 0 mV also has a large activation energy to overcome, thus the delay in coupling between VSD movement and pore opening. Fig. 2.3*C* provides an idea of what may happen to the energetic landscape with a greater upon a more severe depolarization, such as to +100 mV. The activation energies of all of the voltage-dependent transitions would be much

more easily overcome, but that of the voltage-independent step would become rate limiting. Further increases in the potential would not be expected to increase the rate of activation once the voltage-independent step becomes rate-limiting.

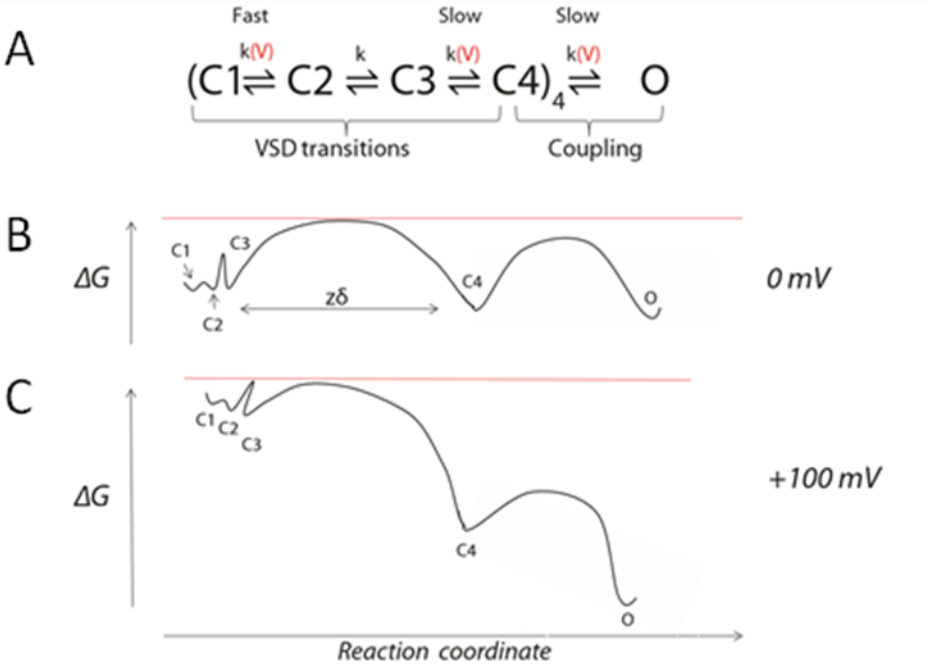

Figure 2.3 A model of the movement of *hERG* gating charge in the activation pathway.
(A) Voltage sensors traverse several closed states in *hERG*. A voltage – independent step early in the activation pathway appears to become rate limiting in charge movement and pore opening. **(B)** and **(C)** A visual representation of the energetic landscape at different voltages.

2.3.5 Charge becomes stabilized rapidly across activated states in *hERG* channels- In Fig. 2.1 we established a significant mode-shift of *hERG* gating charge after just 300 ms at +60 mV by showing that the $Q_{OFF}V$ was significantly hyperpolarized ($V_{0.5}$ = -85.9 mV) compared with the $Q_{ON}V$ ($V_{0.5}$ = -19.1 mV). Data in Fig. 2.4 extends this analysis to depolarizations of 100 and 300 ms at +20 mV (Fig. 2.4*A*) and 24 and 100 ms pulses at +60 mV (Fig. 2.4*B*). The Q_{OFF} at more hyperpolarized voltages was normalized to the maximum Q_{OFF} after 300 ms and plotted against voltage in Fig. 2.4*C* & Fig. 4*D*. A striking finding is that even after only 24 ms at +60 mV, although only ~40 % of the total charge has moved and ~20% of channels will be open (Fig. 2.1*D*), the charge is more resistant to return and displays a markedly hyperpolarized $Q_{OFF}V$ with a $V_{0.5}$ of -74.1 ± 5.0 mV, and z = 1.5 ± 0.2, (n=5). After 100 ms the charge return follows a similar voltage dependence to that seen after 300 ms at +60 mV with fit parameters of $V_{0.5}$ = -79.3 ± 2.4 mV, and z = 2.0 ± 0.1, (n=5). This is consistent with the time constant for the kinetics of charge movement at +60 mV of 31 ms (Fig. 2.2*C*) which indicates that after 100 ms ~90 % of the charge will have moved and that the moved charge has mode-shifted and is resistant to return from the activated state. This is despite the fact that only ~70% of channels have entered the open state (Fig. 2.1*D*). Similarly, at +20 mV after 100 ms the $Q_{OFF}V$ is hyperpolarized with a $V_{0.5}$ of -73.1 ± 4.0 mV, and z = 1.7 ± 0.1, (n=3), despite only ~40% of channels reaching the open state (Fig. 2.1*D*). After 300 ms the $V_{0.5}$ is -77.8 ± 0.8 mV, and z = 1.2 ± 0.1, (n=3). These data suggest that at physiologically relevant potentials such as +20 mV the mode-shift of charge movement is present and can occur over short periods of time.

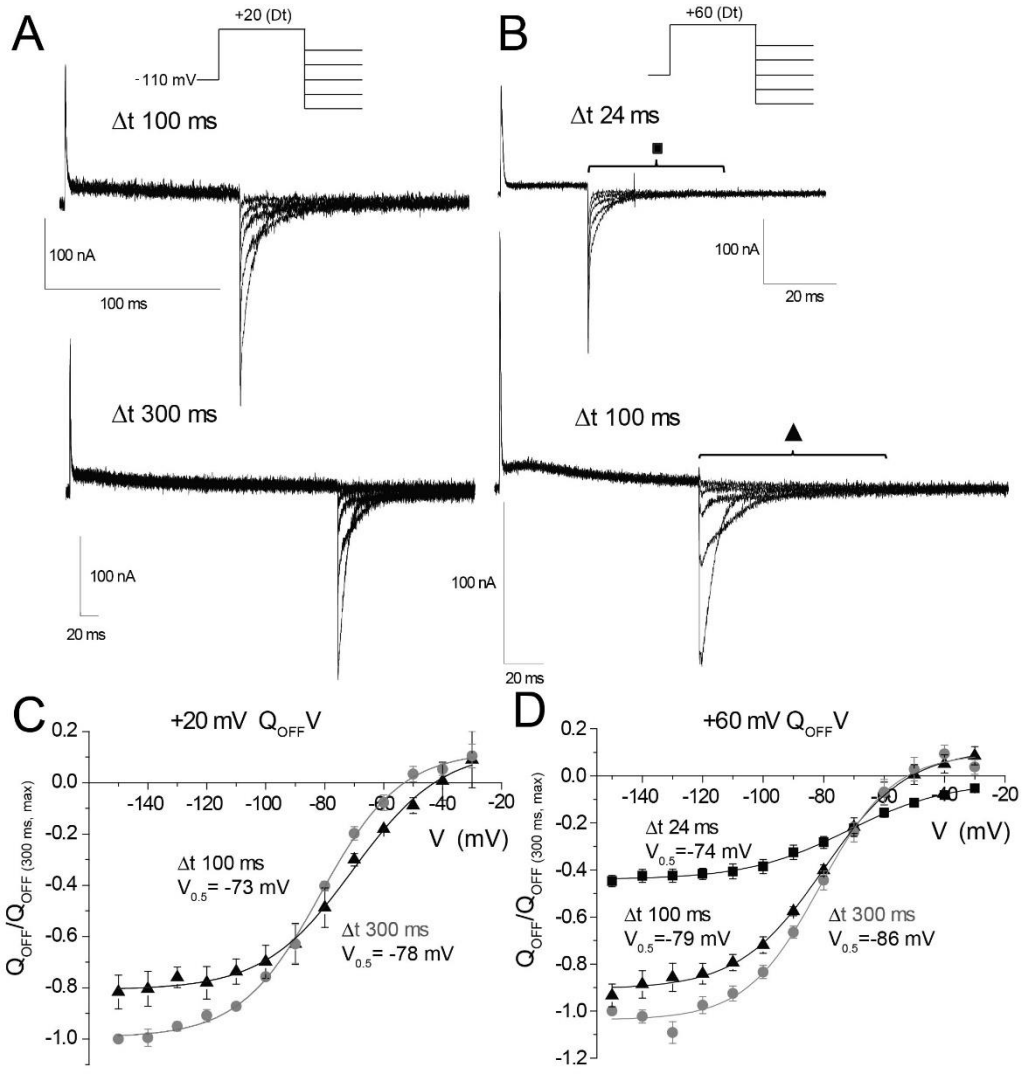

Figure 2.4 Voltage sensor mode-shift is established rapidly in *hERG*.
(A) Representative current traces and the voltage protocol used to assess the voltage dependence of gating charge return from the activated state after depolarizations of 100 ms and 300 ms to +20 mV, and in **(B)** 24 ms and 100 ms pulses to +60 mV. **(C)** Normalized $Q_{OFF}V$ relationships for charge return after depolarizations to +20 mV for 24, 100 and 300 ms. Ig_{OFF} was integrated for 100 ms to obtain $Q_{off}V$. After 100 ms at +20 mV the $V_{0.5}$ was -73.1 ± 4 mV, z = 1.7 ± 0.1 (n=3). At 300 ms the $V_{0.5}$ was -77.8 ± 0.8 mV, z = 1.2 ± 0.1 (n=3). **(D)** Normalized $Q_{OFF}V$ relationships for charge return after depolarizations to +60 mV for 24, 100 and 300 ms. Ig_{OFF} was integrated for 60 ms for the 24 ms depolarization, and 100 ms for 100 and 300 ms depolarizations. At 24 ms the $V_{0.5}$ was -74.1 ± 4.9 mV, z = 1.5 ± 0.2 (n=5). At 100 ms the $V_{0.5}$ was -79.3 ± 2.4 mV, z = 2.0± 0.1 (n=5). At 300 ms the $V_{0.5}$ was -85.9 ± 2.3 mV, z = 2.1 ± 0.2 (n=5).

2.3.6 Ionic current deactivation tracks charge return- The critical question in identifying the physiological role of the mode-shift is whether or not the stabilization of the voltage sensor in the activated state can directly rate-limit the gating of the channel as it closes. The delay between charge movement and pore opening shown in Fig. 2.2 along with the negatively placed QV relationship compared with the GV (Fig. 2.1E) implicates additional transitions in their coupling at most potentials, but it is uncertain how this influences the process of deactivation. A stabilized charge configuration in the activated state, if coupled tightly to the pore, would lead to a slow closure rate for the pore. To investigate this relationship we compared the voltage dependence of the rate of charge return with the rate of pore closure. The same protocols as used in Fig. 2.4 were implemented here to open the channels with a pulse to +20 mV or +60 mV for 24, 100, or 300 ms, and then to close the channels by repolarizing to a range of potentials (Fig. 2.5*A* and Fig. 2.5*B*). The decay phases of tail currents that represent channel pore closure at different repolarization voltages were fit with double or single exponential functions and the dominant time constants plotted in Fig. 2.5*C* (open symbols). Dominant time constants were defined as that which fit a proportionally larger segment of the deactivating charge. The rate of charge return was measured by the fit of exponential functions to the slower decaying phase of Ig_{OFF}, to avoid contaminating time constants with the very fast component of gating charge movement, and plotted (filled symbols) along with ionic data in Fig. 2.5*C*. It is clear that after 100 ms and 300 ms for either the +20 mV or +60 mV prepulse there is little distinguishable difference between the voltage-dependent rates of charge return and ionic current deactivation, which suggests a close coupling between these two events as the channels return to their resting states. After a 24 ms depolarization to +60 mV, charge returns more quickly than pore closing, and this is a lot less voltage-dependent. This charge represents about 40% of the total charge movement

(Fig. 2.4*D*), and it occurs at a time when only ~15% of channels would populate the open state (Fig. 2.1*D*). This separation suggests that a kinetic barrier to charge return is imposed as the population of channels reaching the open state increases.

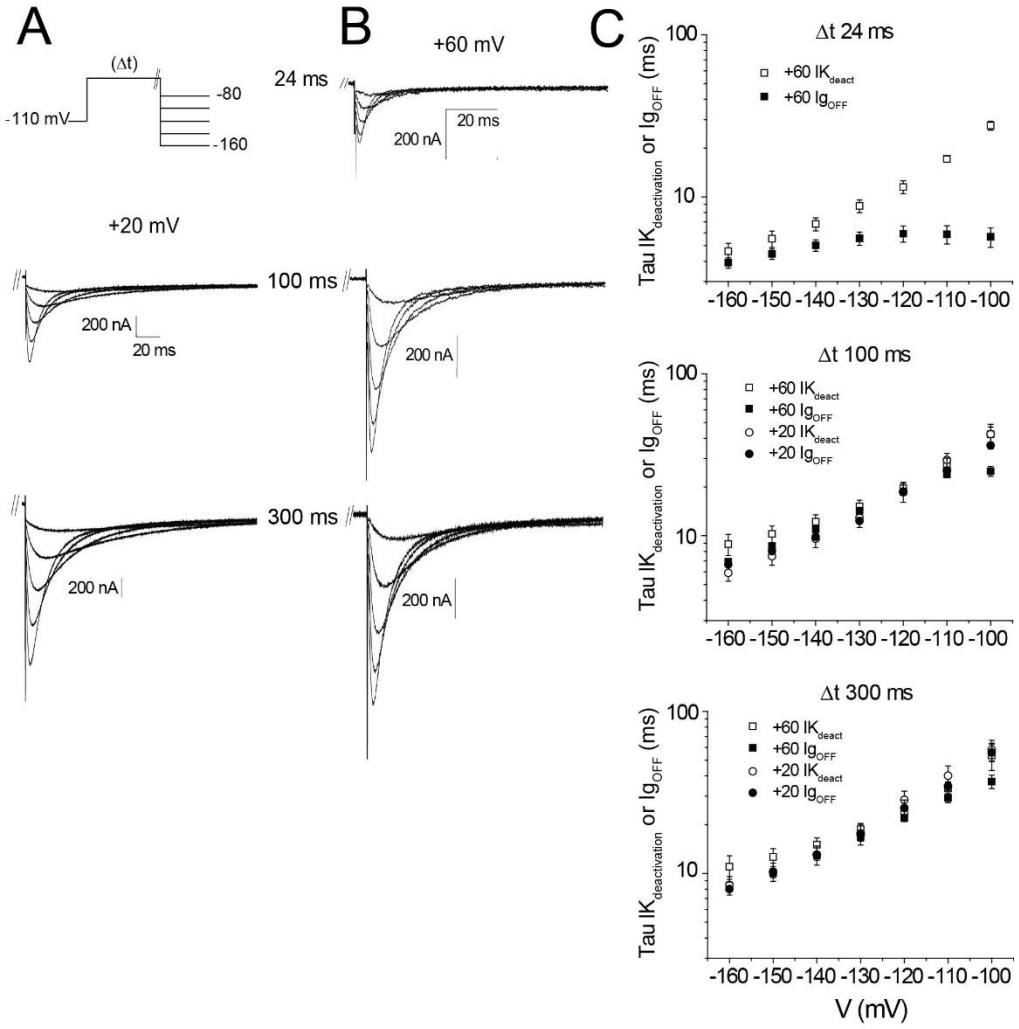

Figure 2.5 Comparison of the kinetics of ionic current deactivation with gating charge return.
(A) Voltage protocol and representative traces showing ionic current deactivation upon membrane repolarization from a potential of +20 mV after a period of 100 or 300 ms, and from +60 mV after depolarizations of 24, 100, and 300 ms. **(B)** Plot of time constants of single exponential fits to ionic (I_K, open symbols) and gating current decays (Ig_{OFF}, filled symbols) upon repolarization after 24, 100, and 300 ms pulses to +60 mV.

2.3.7 N- and C-terminal interactions regulate ionic deactivation and charge movement- The N- and C-termini of *hERG* play a pivotal role in the deactivation gating of the channel, with complete deletions of the PAS domain or the C-terminal CNBHD typically giving rise to a 3-4 fold increase in deactivation rates. This effect can be also be recapitulated by individual or combined mutations such as R4A and R5A or the LQT2-causing mutation R56Q that have been shown to cause similar increases in deactivation rate (Gustina and Trudeau, 2009; Thomson *et al.*, 2014). To assess whether the return of gating charge was affected by perturbations of N- and C-terminus interaction we tested 3 mutant channels: an N-terminal deletion of the entire PAS domain, a double mutation in the PAS cap (R4AR5A), and the LQT2 causing mutation R56Q. The structural interactions between the PAS domain and the CNBHD in *hERG* are not yet determined crystallographically, but are suggested to be similar to the homologous mouse *eag* channel domains recently resolved in complex (Haitin *et al.*, 2013) and supported by a recent NMR study of the *hERG* channel domains (Li *et al.*, 2014). Fig. 2.6*A* shows a homology model of the *hERG* cytosolic domain interaction with the PAS domain R56 residue highlighted, the location of R4A and R5A residues is not defined as the structure was only resolved from residue 16. The simplified cartoon in Fig. 2.6*B* depicts two adjacent subunits of the tetramer with a schematic of the cytosolic domain organization in relation to the transmembrane domain. The star symbols indicate the approximate location of the mutations R56 and R4AR5A in the PAS-cap that were tested.

To establish whether charge movement was altered in the mutant channels, we measured gating and ionic currents using the same protocols as for WT channels. Fig. 2.6*C* shows ionic activation and deactivation GV's for the mutants with WT for comparison, with the fitted parameters

summarized in Table 2.1. Representative traces for the voltage dependence of activation and deactivation of all mutants for ionic and gating currents are found in Fig. 2.7. The mutant activation GV's were similar to WT, but the mutant deactivation GV's were depolarized compared with WT, consistent with a destabilization of open states or a stabilization of closed states. The deactivation kinetics of the mutant channels shown in Fig. 2.6*D* display significantly accelerated kinetics across all voltages compared with WT ($P<0.05$), which suggests a destabilization of the open states. The voltage range for examining deactivation of -100 to -160 mV covers potentials at which the channel is closed and thus enables us to isolate the rate constant of the open to closed transition (β) with minimal contamination from closed to open transitions (α). The chemical rate constant and voltage dependence of this transition was determined by fitting the mean data with a voltage dependent single exponential function which gave values for WT of $\beta_0 = 1.3\ ms^{-1}$, z = -0.69; ΔN $\beta_0 = 11.4\ ms^{-1}$, z = -0.54; R4AR5A $\beta_0 = 7.65\ ms^{-1}$, z = -0.56; R56Q $\beta_0 = 5.2\ ms^{-1}$, z =-0.58. The acceleration of deactivation followed the order ΔN>R4AR5A>R56Q, which indicated that the total deletion had the most severe phenotype, followed by the PAS-cap neutralizations, and then the LQT2 mutation R56Q. The equivalent charge, z, remained similar across all the channels suggesting that the voltage dependence of the transition had not been perturbed by the mutations. In Fig. 2.6*E* the $Q_{ON}V$ and $Q_{OFF}V$ data are displayed for the mutant channels compared with WT. The $Q_{ON}V$ relationships were unchanged from WT suggesting that the mutations have little effect on the voltage-dependent movement of charge during activation (fitted parameters in Table 2.1). The mutant $Q_{OFF}V$ relationships were right shifted compared with WT, which indicates an attenuation of the mode-shift of the charge in these mutant channels, but importantly, the shifts were entirely commensurate with the changes in deactivation GVs (Fig. 6*C*).

Fig. 2.6*F* illustrates that the mutant channels had significantly accelerated rates of charge return across all voltages. The chemical rate constants and voltage dependence of these transitions for WT were: β_0 = 1.0 ms^{-1}, z = -0.8; for ΔN β_0 = 4.8 ms^{-1}, z = -0.7; for R4AR5A β_0 = 4.3 ms^{-1} , z = -0.7; and for R56Q β_0 = 3.5 ms^{-1}, z =-0.7. These data suggest that mutations that disrupt the N- and C-terminus interactions lead to the destabilization of the open state, and also to a destabilization of the activated state of the VSD as illustrated by the increased β_0 rates and right shifted $Q_{OFF}V$ for the mutants compared with the WT. In Fig. 2.6*G* the effects on the kinetics of Q_{OFF} are directly compared with ionic deactivation and show that charge return tracks pore closure closely although there is some divergence at voltages >-110 mV where the charge movement itself is intrinsically rate limited and becomes less tightly coupled to the pore.

	Activation GV			Deactivation GV			$Q_{ON}V$			$Q_{OFF}V$		
	$V_{0.5}$	z	N	$V_{0.5}$	z	N	$V_{0.5}$	z	N	$V_{0.5}$	z	N
WT	4.13 ± 3.36	2.30 ± 0.35	4	-78.11 ± 1.62	2.72 ± 0.11	4	-19.1 ± 1.92	1.98 ± 0.27	10	-85.88 ± 2.32	2.11 ± 0.2	7
ΔN	-2.26 ± 0.91	3.38 ± 0.09	7	-30.1 ± 1.85	3.41 ± 0.13	7	-21.18 ± 1.74	2.39 ± 0.25	7	-55.48 ± 2.01	2.31 ± 0.35	5
R4AR5A	5.77 ± 1.62	2.89 ± 0.1	10	-33.5 ± 1.79	3.16 ± 0.11	8	-16.93 ± 1.89	2.22 ± 0.32	9	-57.44 ± 3.10	2.86 ± 0.41	8
R56Q	-3.39 ± 0.39	3.09 ± 0.06	7	-44.2 ± 0.39	2.81 ± 0.08	6	-20.49 ± 1.89	1.80 ± 0.19	7	-60.86 ± 1.74	2.47 ± 0.24	7

Table 2.1 Activation and deactivation GV, $Q_{ON}V$ and $Q_{OFF}V$ Boltzmann fit parameters for WT and mutant channels.

The activation and deactivation GVs were collected using the protocols shown in Fig. 2.6C and the $Q_{ON}V$ and $Q_{OFF}V$ data using the protocols as for data in Fig. 2.6E.

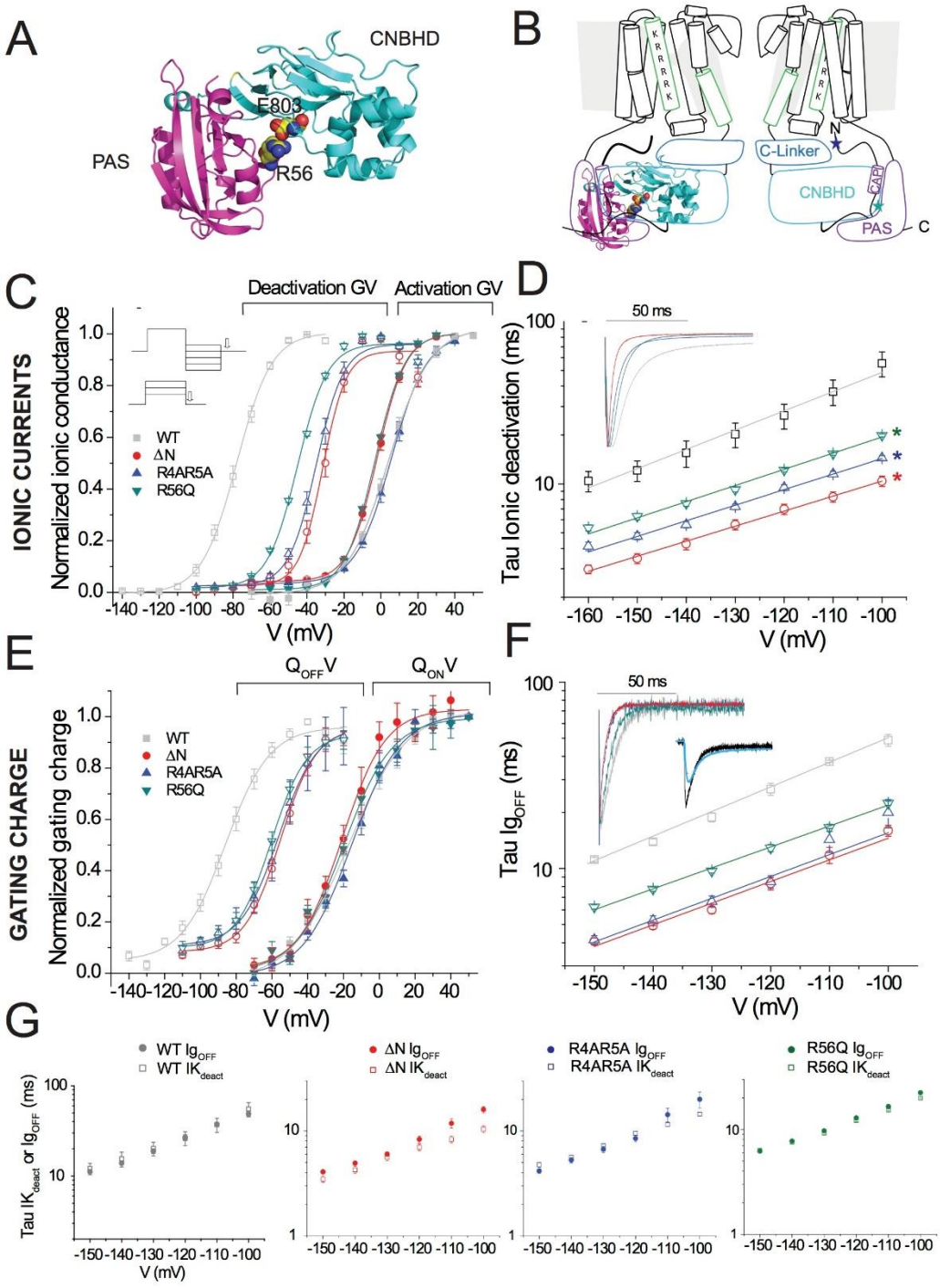

Figure 2.6 N-terminal mutations that accelerate deactivation reduce the mode-shift of gating charge.
(A) Homology model of *hERG* PAS and CNBHD regions based on the mouse *eag* ($K_V10.1$) with R56 residue highlighted and its putative interacting partner D803. **(B)** Cartoon schematic of two adjacent subunits of *hERG* with the cytosolic domains arranged beneath the channel illustrating the predicted topology including the C-linker that is situated between the bottom of S6 and the CNBHD. Stars represent the approximate locations of the mutations R56Q in the interacting surface between the Pas domain and the CNBHD and R4AR5A which are in a segment that

was not resolved in the crystal structure. **(C)** Normalized ionic current activation GV's (Filled symbols) obtained with 300 ms depolarizing pulses and deactivation GV's (open symbols) obtained with the same protocol used in Fig 2.1. **(D)** Time constants of ionic current deactivation from fits to tail currents after a 300 ms depolarization to +60 mV. Inset: normalized representative ionic current deactivation traces from hyperpolarizations to -150 mV. **(E)** Plot of normalized $Q_{ON}V$ (filled symbols) and $Q_{OFF}V$ (open symbols). **(F)** Voltage dependence of the time constants for gating charge return. Inset: normalized representative Ig_{OFF} traces at -150 mV for WT and mutant channels and separate traces showing gating at -150 mV (black) compared with ionic deactivation normalized to peak tail current adjusted for recovery from inactivation (turquoise). **(G)** Comparison of the voltage dependence of the time constants for gating charge return and ionic deactivation for each mutant channel.

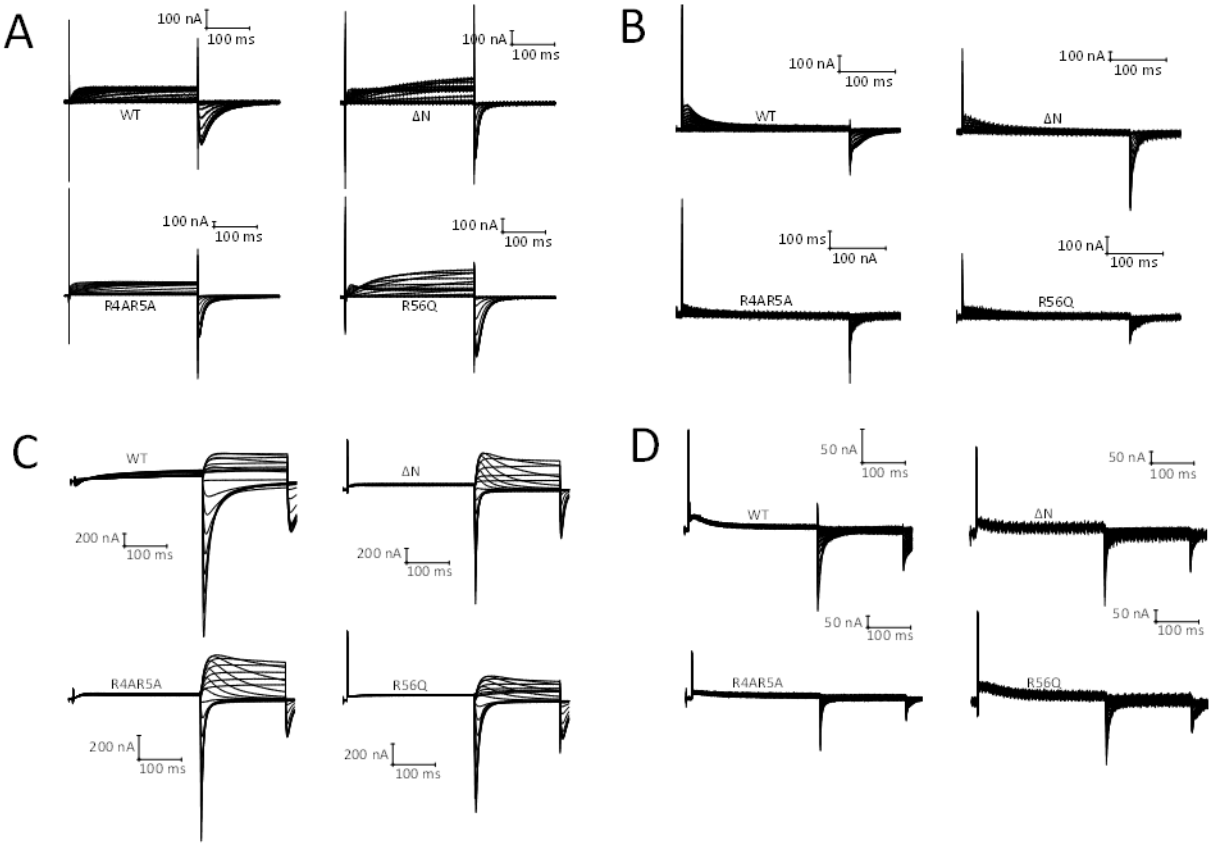

Figure 2.7 Representative traces of ionic and gating current recordings in response to protocols detailing voltage dependence of activation and deactivation.
(A) Ionic currents of all constructs in response to 300 ms depolarizations (-90 to +60) from a holding potential of -110 mV. **(B)** Gating currents of all constructs in response to 300 ms depolarizations (-90 to +60) from a holding potential of -110 mV. **(C)** Ionic currents of all constructs in response to an initial 300 ms depolarization to + 60 mV to activate all channels, followed by a second voltage command to potentials between -150 and 0 mV for 200 ms, and then a return to holding potential of -110 mV. **(D)** Gating currents of all constructs in response to an initial 300 ms depolarization to + 60 mV to activate all channels, followed by a second voltage command to potentials between -150 and 0 mV for 200 ms, and then a return to holding potential of -110 mV.

2.3.8 Coupling of activation of gating charge to pore region weaker for N –terminally disrupted mutants – The envelope of tails protocol employed in Fig. 2.2 to assess the WT time constants of activation of gating charge and pore opening was used to determine whether the disruptions to the N-terminus had an effect on channel activation. Fig. 2.8*A* shows representative ionic current traces for all constructs studied. More prolonged depolarizations result in the opening of more channels and this can be measured from the amplitudes of the peak tail currents

upon return to a potential of - 110 mV (which relieves channel inactivation and allows a proper characterization of the relative number of open channels). Representative gating current recordings of all constructs studied in response to the envelope of tails protocol are shown in Fig. 2.8*B*.In assessing the activation of gating charge, we integrated the first 150 ms of gating charge return upon repolarization to – 110 mV after each depolarizing pulse. The time constants of gating current activation (Fig. 2.8*D*) did not statistically differ amongst the constructs studied. Interestingly, the time constants of pore opening (Fig. 2.8*C*) for the mutant channels were only changed at more moderate voltages. ΔN displayed the most severe slowing of activation at +20 mV with a time constant of 385 ms, compared to 115 ms for the WT channel at the same potential. The R4AR5A and R56Q constructs also displayed a slowing of activation gating at moderate depolarizations, but not as severe as that of the ΔN construct. At +20 mV, the time constants of pore opening were 178 ms for R4AR5A and 180 ms for R56Q. As the time constants of gating charge activation were unchanged amongst the N- terminally disrupted mutants, and the time constants of ionic activation for N- terminally disrupted mutants were increased (slowed) at physiological potentials, it is reasonable to suggest that the mutant channels display a weaker coupling of the movement of the gating charge to the pore domain. This indicates a potential role of the cytosolic domains in the activation gating of *hERG*. Time constants of activation of gating charge and pore opening for all constructs for potentials 0 mV to +100 mV can be found in Table 2.2.

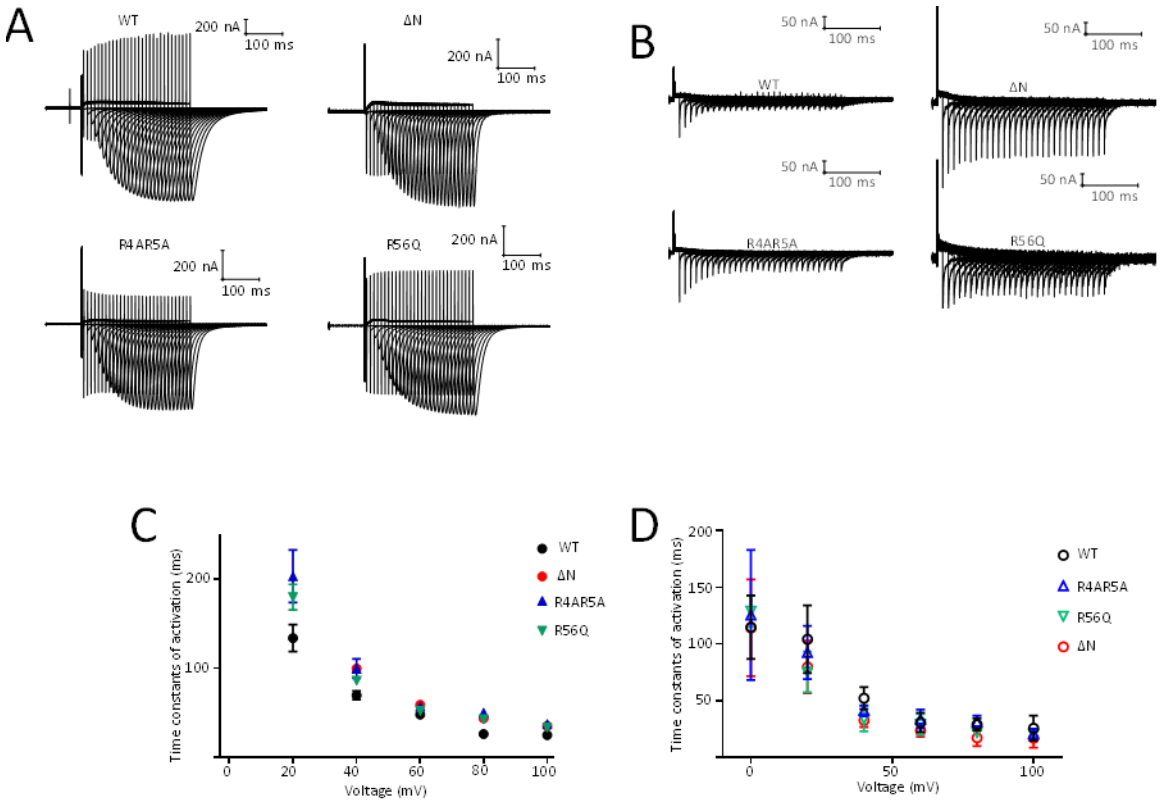

Figure 2.8 Time constants of activation for gating charge and pore opening unaffected by R4AR5A, R56Q, and ΔN mutations.

(A) Representative traces of WT, ΔN, R4AR5A, and R56Q ionic currents in response to envelope of tails protocol to assess time constants of activation. **(B)** Representative traces of WT, ΔN, R4AR5A, and R56Q gating currents in response to envelope of tails protocol to assess time constants of activation. **(C)** Time constants of activation for pore opening for WT, R4AR5A, R56Q, and ΔN. Values are found in Table 2.2. **(D)** Time constants of activation for gating charge for WT, R4AR5A, R56Q, and ΔN. Values are found in Table 2.2.

Construct	0 mV τ	+20 mV τ	+40 mV τ	+60 mV τ	+80 mV τ	+100 mV τ
Ionic - WT hERG	305 ± 18 ms (n=5)	115 ± 10 ms (n=5)	65 ± 3 ms (n=5)	52 ± 3 ms (n=6)	28 ± 4 ms (n=5)	25 ± 3 ms (n=4)
Ionic - R4AR5A	-	178 ± 38 ms (n=4)	99 ± 24 ms (n=5)	57 ± 11 ms (n=7)	50 ± 3 ms (n=3)	37 ± 3 ms (n=3)
Ionic- R56Q	-	180 ± 29 ms (n=4)	86 ± 10 ms (n=4)	52 ± 5 ms (n=4)	42 ± 5 ms (n=4)	33 ± 3 ms (n=4)
Ionic -ΔN	-	385 ± 30 ms (n=5)	100 ± 7 ms (n=5)	59 ± 3 ms (n=7)	43 ± 3 ms (n=5)	35 ± 3 ms (n=5)
Gating -WT hERG	115 ± 11 ms (n=6)	104 ± 11 ms (n=7)	52 ± 4 ms (n=7)	31 ± 3 ms (n=7)	29 ± 2 ms (n=7)	26 ± 4 ms (n=6)
Gating - R4AR5A	126 ± 22 ms (n=6)	93 ± 9 ms (n=7)	41 ± 2 ms (n=5)	34 ± 3 ms (n=7)	31 ± 2 ms (n=5)	21 ± 2 ms (n=4)
Gating - R56Q	129 ± 6 ms (n=6)	75 ± 8 ms (n=5)	34 ± 5 ms (n=6)	29 ± 3 ms (n=7)	22 ± 2 ms (n=5)	20 ± 2 ms (n=3)
Gating - ΔN	114 ± 19 ms (n=5)	80 ± 10 ms (n=5)	32 ± 3 ms (n=5)	24 ± 2 ms (n=7)	17 ± 3 ms (n=5)	17 ± 4 ms (n=4)

Table 2.2 Time constants of activation for all mutants: gating charge and pore opening.

2.4 Discussion

This study has established the temporal sequence of gating events in *hERG* activation and deactivation by quantitatively comparing the time course and voltage dependence of charge movement and pore gating using equivalent protocols.

2.4.1 Sequence of events during *hERG* activation and pore opening- The first important finding of our kinetic study on bulk gating charge movement during opening is that over physiological voltages and timescales the VSD movements and pore opening are significantly separated, by ~20 mV and an order of magnitude in time at 0 mV. Longer duration QV relationships of 500 ms and 1 s also displayed a hyperpolarized voltage dependence of charge movement to pore conductance indicating the continued presence of the coupling step pivotal to controlling the increase in channel open probability (Fig. 2.*1E*). The kinetic relationship between gating charge movements and pore activation over time on a logarithmic scale clearly illustrated the ionic current latency to opening indicative of the presence of several closed states which have

to be traversed before opening (Wang *et al.*, 1997a). However, the bulk of gating charge movement was well fit with a single exponential and started moving without a delay, which suggests that transitions through closed states that carry significant charge occurred prior to pore opening (Fig. 2.2*B*). This was reinforced by the large temporal separation of charge movement from pore opening at voltages below +80 mV that implicates a further downstream transition which is key to the opening of the channel, and may represent the specific electromechanical coupling of S4 rearrangements to the S6 pore gate in *hERG*.

Prior VCF studies with ionic currents have reported conflicting data on the kinetic separation between VSD movement and pore opening steps in activation that we have established here. Data from our lab from E518C did show kinetic separation (Es-Salah-Lamoureux *et al.*, 2010), whereas data from others using L520C, E518C and G516C did not (Smith and Yellen, 2002; Tan *et al.*, 2012; Thouta *et al.*, 2014; Van Slyke *et al.*, 2010). Possible issues include the incorporation of cysteine residues at sensitive sites on S3 or S4, and/or the detection of other events by the fluorophores than purely S4 movement. But, a more likely explanation of the differences is that comparisons are often made between non-equivalent and non-equilibrium GV and FV curves recorded from different pulse durations, which display close $V_{0.5}$ values and falsely lead to the conclusion that the kinetics of charge movement and pore opening are also similar. For example, in a recent study comparing VCF signals and gating currents the FV and QV data were found to have similar $V_{0.5}$ values but the protocols used were not isochronal and a longer duration FV protocol (2s) was compared with a short (100 ms) QV protocol (Thouta *et al.*, 2014). As we have demonstrated (Fig. *2.1E*) 100 ms is not sufficient to approach

equilibrium, and the QV curve shifts left if the duration is extended which would lead to a separation of the FV and QV relationships, consistent with our data.

The convergence of the kinetics of charge movement and pore opening to a saturating rate at potentials >+60 mV suggests the presence of a relatively weak or voltage independent step in the activation pathway becoming dominant (Fig. 2.2*C*). A voltage-independent step between closed states has been identified as required to represent *hERG* activation in a kinetic model (Wang *et al.*, 1997a), and here we demonstrate that charge movement also approaches a saturating rate. This may reflect two potential underlying mechanisms: a fundamental limit to the speed at which the voltage sensor can move during a certain transition (i.e. the charge cannot rearrange any quicker) or the presence of a voltage-independent transition upstream to the bulk of charge movement that becomes rate-limiting at positive potentials and prevents the subsequent charge movement from proceeding any faster.

2.4.2 Asymmetry of gating charge movement in *hERG*- We have also characterized an asymmetry in gating charge movement, also known as mode-shift, and found that the process occurs rapidly enough to be relevant on the time scale of cardiac action potentials. To examine the coupling between the voltage sensor and pore during deactivation we measured currents from channels harbouring N-terminal mutations that increase the deactivation rate of the channel and found that gating currents followed the increased rate of pore closure and reduced the magnitude of the mode-shift illustrated by a depolarizing shift of the $Q_{OFF}V$ (Fig. 2.6E). We propose that the mode-shift results at least in part from the stabilization of the open state of the channel imposed

by interactions between the N- and C-terminus of the channel and that the rate limiting step in channel deactivation at negative voltages may be attributed to the closure of the open pore.

A hyperpolarizing shift of the QV has previously been reported in *hERG* channels when charge movement was recorded from a holding potential of 0 mV (Piper *et al.*, 2003), which suggested the presence of a mode-shift. However, at that time, the concept of mode-shifting was not appreciated and due to the sustained holding potential it was not clear if the shift had occurred over an extended duration of seconds or minutes, representing a form of voltage sensor relaxation (Bezanilla *et al.*, 1982), or perhaps a shorter timescale that was relevant to the physiology of the channel. More recently, fluorescence reports of the voltage dependence of *hERG* deactivation from labelling residue E518C at the top of S4 have been reported to display a hyperpolarizing shift in the FV relationship compared with the voltage dependence of activation (Tan *et al.*, 2012). This lent further support to the hypothesis that *hERG* might mode-shift between activation and deactivation gating. Building on these observations, we first sought to establish if the gating charge in *hERG* underwent a mode-shift on timescales that more closely resembled that seen in the heart during systole (Fig. 2.1). After 300 ms, the $Q_{OFF}V$ was hyperpolarized by ~70 mV compared to the $Q_{ON}V$ relationship, which indicates the relative stabilization of the activated charges compared with the charges at rest, and is indicative of a mode-shift of *hERG* gating elements.

2.4.3 The mechanistic basis for the mode-shift and slow deactivation in *hERG* channels-

Several K_V1, NaV, and HCN channels, and even the poreless voltage-sensing phosphatase ciVSP (Arrigoni *et al.*, 2013; Villalba-Galea *et al.*, 2008; Wicks *et al.*, 2009) have been shown to

exhibit asymmetry in charge movement where movement of charge upon depolarization associated with activation requires less of an applied voltage gradient than that needed to return the charge from the activated state back to rest. The ubiquitous nature of this phenomenon in voltage-dependent transmembrane proteins suggests that it is a fundamental feature of voltage sensing domains, although the mechanism by which the effect is induced shows considerable diversity. Proposed mechanisms for the relative stabilization of the activated charge include an increased open pore stability that slows voltage sensor return, which may result from both intrinsic and allosteric effects of intracellular ions in the cavity (Chen *et al.*, 1997; French and Finol-Urdaneta, 2012; Goodchild and Fedida, 2012; Goodchild *et al.*, 2012; Melishchuk and Armstrong, 2001) or N-type inactivation particles (Perozo *et al.*, 1992), C-type inactivation that induces a pore structural rearrangement stabilizing the activated voltage sensor (Fedida *et al.*, 1996; Olcese *et al.*, 1997), and finally a fundamental structural reconfiguration of the voltage sensor that causes it to relax in the activated state (Priest *et al.*, 2013; Villalba-Galea *et al.*, 2008). Mode-shifts have been observed to occur over a broad range of timescales, which track either opening of the pore (milliseconds), entry into an inactivated state (hundreds of milliseconds) or intrinsic voltage sensor relaxation (seconds). *hERG* inactivates rapidly and is voltage dependent, which raises the question of whether inactivation is causing the mode-shift. However, TEA-containing external solutions are known to inhibit *hERG* channel inactivation (Smith *et al.*, 1996), making that possibility less likely in our experiments. Additional support for the proposition that inactivation is not required for the mode-shift in *hERG* comes from a non-inactivating mutant, S620T, which also displays a hyperpolarized QV from a holding potential of 0 mV (Piper *et al.*, 2003). It is, however, possible that both of these mechanisms of inhibiting

inactivation may only be affecting a late step in inactivation and not perturb an earlier conformational change associated with inactivation that induces a mode-shift.

2.4.4 Effects of crosstalk between the pore and VSD on the mode-shift- The effects of the pore structure on the VSD during our gating current measurements must be considered, as the two systems are coupled and canonical sequential gating models of K_V channel gating assert that the voltage sensors do not return to rest while the open pore holds the sensors in an activated position (Varga *et al.*, 2002). The pore can be stabilized extrinsically by intracellular ions (Goodchild and Fedida, 2012) as well as intrinsically by structural interactions exclusive to the open state, but in *hERG* channels it has not yet been established whether either of these mechanisms affect VSD movement. The use of TEA-containing internal solutions raises the possibility that TEA ions might be interacting with the inner pore to stabilize the open state, a phenomenon that is established in K_V1 channels (Goodchild *et al.*, 2012). In *hERG* this is unlikely because deactivation of ionic current in *hERG* tracks gating charge return after sufficient time to open the majority of channels (100 and 300 ms, Fig. 2.5*B*), in the absence of TEA. If the pore was propped open by TEA via a 'foot in the door' mechanism we would expect to see a slower rate of gating charge return than ionic deactivation in these experiments.

The question then arises whether the slow deactivation of *hERG* current is determined by the intrinsic voltage sensor kinetics, or if the open pore state is structurally stabilized to slow charge return. In contrast to longer pulses, we found that after a 24 ms depolarization the bulk of charge return was faster than ionic current deactivation (Fig. 2.5*B*), even though the charge had undergone a mode-shift (Fig. 2.4*B*). This indicates an intrinsic property to the voltage sensor in

transitions between closed states that contributes to the mode-shift but does not lead to the full slowing effect on deactivation seen with longer pulses of 100 ms or longer where synchronization of charge return and ionic deactivation rates occurs. This can be explained by the majority of channels not having transitioned out of deeper closed states at 24 ms such that a significant portion of the charge can return more rapidly than after transitioning into later pre-open closed states and open states.

2.4.5 N- and C-terminus interactions contribute significantly to charge mode-shift- Loads might be placed upon the sensor from other structurally coupled elements, given several large differences in *hERG* channel topology compared with K_V1 channels, which result from *hERG*'s closer relationship with *eag* and CNG channels. The N- terminus *eag* domain contains a PAS domain and PAS-cap structure, which in other proteins has been shown to act as a signal sensor for a variety of stimuli (Gustina and Trudeau, 2012). The C-terminus contains a CNBHD connected to the base of S6 through a C-linker region, and a recent crystal structure of the mouse *eag* N- and C-termini in complex indicates that the PAS and CNBHD domains are structurally interacting to regulate channel gating kinetics (Haitin *et al.*, 2013). It has previously been reported, using VCF to track S4 rearrangements, that deletion of the PAS domain accelerated ionic deactivation, but did not cause a mode-shift of the FV. This led to the hypothesis that the VSD was intrinsically stabilized in the activated state and that coupling of the pore to the VSD was perturbed by the deletion or disruption of the PAS domain, particularly the positively charged residues in the PAS-cap R4 and R5 (Tan *et al.*, 2012). Our studies, directly recording the movement of gating charges in the membrane on the comparable mutant channel R4AR5A as well as the LQT2 mutant R56Q, do not support the VCF studies. The gating current recordings

from PAS domain deleted or the mutant R4AR5A and R56Q channels displayed an attenuated mode-shift, indicated by the right shift of the $Q_{OFF}V$ relationship of the mutant compared with WT (Fig. 2.6). In the mutant channels the kinetics of gating charge return was accelerated to a similar degree as ionic deactivation across the voltage range tested. This suggests that these mutations all have the effect of destabilizing the activated charge as well as the open pore. This suggests that pore closure is rate limiting the return of the charge at negative potentials. Interestingly, at potentials >-110 mV the gating charge return starts to lag behind the pore closure in the mutant channels, particularly ΔN (Fig. 2.6*G*) which suggests that there is some decoupling of the pore gate from the charge movement in the mutants at moderate potentials. These findings suggest that the pore state contributes to the mode-shift of charge and support the notion that N- and C-terminus interactions stabilize the open pore and place a load on the VSD through the pore.

Our disruptions to the N- terminal domain only noticeably affected the deactivation gating of the mutant channels (Fig. 2.6). The time constant of activation of these constructs noted no significant changes amongst time constants of activation (Fig. 2.8).

Several structural interactions have been proposed to couple the N- and C-terminus and are therefore potential molecular determinants of the mode-shift. The PAS domain interacts with the CNBHD with high affinity, and the mutation R56Q leads to a weakening of the non-covalent interaction binding the domains together and has the effect of increasing deactivation rates (Gustina and Trudeau, 2011; Haitin *et al.*, 2013). A recent mutant cycle analysis of putative interacting residues between these regions confirms the structural studies indication that R56

forms a salt bridge with E803 (Ng *et al.*, 2014). In addition, this study also suggested that R4 and R5 in the PAS-cap form transient interactions with residues E698 and E699 in the C-linker which provides a possible mechanism by which the tight interaction of the PAS and CNBHD couples to S6 where the pore gate is located. Experiments using concatenated *hERG* subunits demonstrate that the slow deactivation can be disrupted by R56Q or R4AR5A mutations in a single subunit to the same degree as in all subunits suggesting that the stabilization of the open pore by these structures is controlled by a concerted fully cooperative interaction (Thomson *et al.*, 2014). FRET experiments have established that tetrameric arrangement of the PAS and CNBHD exhibit a domain swapped arrangement where the PAS from one subunit interacts with the CNBHD from the neighbouring subunit (Gianulis *et al.*, 2013) and it has been proposed that these domains might interact to form a gating ring reminiscent of the homologous HCN channel (Haitin *et al.*, 2013). Considering these studies leads to a model in which the strong interactions between PAS/CNBHD in the gating ring are coupled via the R4R5 PAS-cap domain residues to the C-Linker which would stabilize the open pore and thus allosterically stabilize the activated voltage sensor.

In summary, our data have uncovered several new features of the coupling mechanism of voltage sensing to pore opening in *hERG* that enable slow gating. We first showed definitively that the rate of activation of *hERG* at physiological voltages is not controlled exclusively by the slower rearrangement of the bulk of gating charge, but a further delay is imposed by a coupling step that increases the time to pore opening. Furthermore, we demonstrated that the mode-shift of charge, previously thought to be a property intrinsic to the VSD, is actually regulated by cytosolic domain interactions unique to *hERG* channels that control open state stability. These results

suggest that, in *hERG* channels, VSD function involves interactions with disparate structural elements that confer the necessary kinetic properties for its role in repolarization.

Chapter 3: The fast component of hERG gating charge activation: an interaction between K538 and D411

3.1 Introduction

The human ether-à-go-go related gene (KCNH2) encodes the alpha subunit of the K_v11.1 voltage gated potassium channel (VGKC) (Warmke and Ganetzky, 1994), also referred to as *hERG*. K_v11.1 is best known for its role in the cardiac action potential where it underlies the rapid delayed rectifier current, I_{Kr}, which aids in bringing an end to cardiac systole (Sanguinetti *et al.*, 1995; Trudeau *et al.*, 1995). Disruption of K_v11.1 channel function, through either drug block or genetic mutation, can result in long QT syndrome (Sanguinetti *et al.*, 1995; Sanguinetti and Tristani-Firouzi, 2006) (LQTS; disruption to K_v 11.1 is type 2), the consequences of which can include torsades de pointes and sudden death (Hancox *et al.*, 2008; January *et al.*, 2000).

hERG displays voltage-dependent gating behaviour that deviates strongly from the more canonical VGKC (Piper *et al.*, 2003; Sanguinetti and Tristani-Firouzi, 2006; Smith and Yellen, 2002) in that the rates of activation and deactivation are slower than for other K_v channel alpha subunits by about an order of magnitude (Es-Salah-Lamoureux *et al.*, 2010; Goodchild and Fedida, 2014; Goodchild *et al.*, 2015; Sanguinetti *et al.*, 1995; Smith and Yellen, 2002). The slow activation and deactivation is paired with a fast and voltage-dependent inactivation (Smith *et al.*, 1996; Spector *et al.*, 1996b) and tailors the *hERG* channel to its particular role during the cardiac action potential (Vandenberg *et al.*, 2012).

hERG shares the general structure of a VGKC, that of a tetrameric protein with four six-transmembrane segment subunits that come together to delineate a central ion conducting pore region (Long *et al.*, 2007; MacKinnon, 1991; Whicher and MacKinnon, 2016). The first four transmembrane segments make up the voltage-sensing domain (VSD) of the channel, with the fourth transmembrane segment containing a high concentration of positively charged residues that initiate conformational changes in the protein upon alterations in membrane potential (Bezanilla, 2000). Due to poor conservation of alignment between *Shaker* and *hERG*, it is difficult to directly compare *hERG* with *Shaker*, in which most gating biophysics has historically been done - as the distribution of charged residues in the *hERG* VSD is different in two aspects. First, although it is still suggested that the outer 3 residues (K525, R528, and R531) transfer most of the gating charge upon depolarization (Zhang *et al.*, 2004), overall, the S4 segment of *hERG* has approximately one less equivalent gating charge cross the electric field per subunit than most K_v channels based on limiting slope estimations. Second, *hERG* has three acidic residues (D411, D460, and D509) in addition to the widely conserved acidic residues in other Kv channels (D456, D466, and D501) (Liu *et al.*, 2003). Charge neutralization studies of S4 in *hERG* indicate that K525 and K538 are involved in stabilizing the closed state or destabilizing the open state (Cheng *et al.*, 2013; Piper *et al.*, 2005; Subbiah *et al.*, 2004; Subbiah *et al.*, 2005; Zhang *et al.*, 2005). Further, from double mutant cycle analysis, it is suggested that K525 and K538 stabilize closed states via interaction with the acid charges on D456 and D411, respectively (Zhang *et al.*, 2005). Thus, it has been suggested that the relatively slower activation of *hERG* S4 than *Shaker* channels could be influenced by interactions between these extra acidic residues and positive charges in S4 (Liu *et al.*, 2003; Zhang *et al.*, 2005). Additional causes for slow channel activation may also include factors such as a delayed coupling of the voltage sensing domain

movement to the pore domain that occurs much later in the activation pathway (Goodchild *et al.*, 2015; Piper *et al.*, 2003).

Many studies have relied on ionic current measurements as indirect indicators of activation gating, while *hERG* gating currents, which are direct measures of net charge displacement during VSD movement have been less commonly recorded, at least partly due to the difficulty of recording them. However, it is known that *hERG* gating currents have radically different properties than gating currents recorded from other Kv channels. Piper *et al.* (2003) described two readily separable components of charge movement in *hERG*: Q_{fast} and Q_{slow}. Q_{fast} is a poorly understood fast movement of a small amount of gating charge (< 10% of the total charge moved) that has an extremely broad voltage-dependent activation (Goodchild and Fedida, 2014; Goodchild *et al.*, 2015; Piper *et al.*, 2005; Piper *et al.*, 2003). Q_{slow}, which comprises >90% of the total gating charge movement, is a much larger but slower-moving component often lasting hundreds of milliseconds, whose more voltage-dependent charge–voltage (Q-V) relationship is hyperpolarized to that of the conductance–voltage (G-V) relationship (Goodchild *et al.*, 2015; Piper *et al.*, 2003). While the significance of Q_{slow} is fairly well understood, that of Q_{fast} largely remains to be determined.

In this study, we have investigated the hypothesis that Q_{fast} in *hERG* reflects dynamic charge displacement of the voltage sensor domain as the bonds between D411 (in S1) and K538 (in S4) are broken. We build on prior ionic current work, described above, that D411-K538 interactions stabilize *hERG* closed states and provide a limiting barrier to activation speed. Through the use of the cut-open Vaseline gap voltage clamp technique (COVG), we crucially show that mutations

to both D411 and several residues at the bottom of the S4 segment can change the qualitative nature of *hERG* gating currents by eliminating Q_{fast}. Fluorescence studies support the loss of a displacement step in S4 in constructs that lack the Q_{fast} component. In a double mutant cycle gating current analysis of D411 with the residues at the bottom of the S4, we find evidence of a functional interaction of D411 with residues of the bottom of the S4 and suggest that the energy required to disrupt this interaction both slows the overall gating charge movement and stabilizes early closed states of the channel.

3.2 Materials and methods

3.2.1 Molecular biology – The *hERG* plasmid was subcloned into the pBluescript SK+ expression vector. All mutations were generated using the QuikChange II site-directed mutagenesis kit (Stratagene, La Jolla, CA) and were confirmed with DNA sequencing by Macrogen (Maryland, USA). For RNA transcription, cDNA was linearized with NotI and cRNA was synthesized from this linearized cDNA using the mMessage mMachine T7 Ultra transcription kit (Ambion, Austin TX). A WT *hERG* or extracellular C-less background construct, *hERG* C445V:C449V, and/or additional E519C or I521C constructs were used for all gating current and fluorescence experiments. The *hERG* C445V:C449V:I521C was generally used as a Control in S1 and S4 mutant experiments and is denoted as such. The general gating properties of the WT, C-less mutant and C-less I521C Controls are described in Fig. S1 and Fig. 3.2, and the latter has previously been characterized by Es-Salah-Lamoureux *et al.*, 2010 (Es-Salah-Lamoureux *et al.*, 2010).

3.2.2 *Xenopus* oocyte preparation and expression - Experiments carried out in this study were approved by the University of British Columbia animal care guidelines, established by the Canadian Council of Animal Care (CCAC). *Xenopus laevis* frogs were anesthetized in 2 mg/mL tricaine methanesulphonate (Sigma-Aldrich, Canada). Oocytes were obtained and partially defolliculated by a solution containing 2 mg/mL type 1a collagenase (Sigma) in OR2 buffer (in mM: 82.5 NaCl, 2.5 KCl, 1 $MgCl_2$, and 5 HEPES) for about 1 hr to 1.5 hr with orbital shaking at room temperature (20 to 22 ℃). Oocytes were then washed several times with OR2 buffer to completely remove the collagenase solution. Defolliculated oocytes were initially rocked in an 18 ℃ incubator for approximately 1 hr in a modified oocyte Ringer solution, containing 500 ml Leibovitz's L-15 medium (in mM: 15 HEPES, 0.52 gentamicin, and L-glutamine, adjusted to pH 7.6 with NaOH). Selected stage V-VI oocytes were injected using a Drummond microdispensor with 50-100 ng of cRNA and incubated for 24-72 hr before experiments (Dou *et al.*, 2013; Goodchild *et al.*, 2015).

3.2.3 Cut-open Vaseline gap (COVG) recording - Gating current recordings were performed with a Cut-open Vaseline gap configuration (CA-1; Dagan Inc) and Dagan CA-1B COVG amplifier (Dagan, Minneapolis) at room temperature (20 to 22^{o}C)(Stefani and Bezanilla, 1998). The external solution in the top and guard pools consisted of (in mM): 120 tetraethylammonium hydroxide (TEA-OH), 120 methanesulfonic acid (MES), 10 HEPES, 1 CaMES, pH 7.4. The internal solution in the bottom pool was composed of (in mM): 120 TEA-OH, 120 MES, 10 HEPES, pH 7.4. Both solutions contained 20 µM terfenadine to further block ionic currents through *hERG* open channels. A 0.3% saponin solution was applied to the bottom pool for 0.5–2 min to make the interior of the oocytes electrically continuous with the internal solution. Each

agar bridge housed a fine platinum wire in a 1 M NaMES/agar solution. Low-resistance (0.1 to 0.5 MΩ) glass micropipettes were filled with 3M CsCl. To deplete endogenous K^+ ions in the oocytes for *hERG* gating current recording, the membrane potential was held at 0 mV for 10 to 20 min at the beginning of each experiment. Records were acquired at a sampling rate of 25 to 50 kHz with a 5 kHz low-pass filter. P/6 to P/8 protocols from a holding voltage (a range of -80 mV to -110 mV) were used to subtract linear leakage and capacitive currents.

3.2.4 Voltage clamp fluorometry - Channels expressed in oocytes were labelled with tetramethyl rhodamine maleimide 5 μM (TMRM) in oocyte depolarizing solution (in mM: 150 KCl, 5 $CaCl_2$, 5 $MgCl_2$, and 10 HEPES pH 7.5) and then incubated for 20-30 min at 10 ^oC. The labelled oocytes were transferred to ND96 solution (in mM: 96 NaCl, 3 KCl, 2 $CaCl_2$, 1 $MgCl_2$, and 5 HEPES at pH 7.4) to rinse away excess TMRM molecules that were not bound to the channel. Fluorometry was performed simultaneously with two-electrode voltage clamp as we have described previously (Es-Salah-Lamoureux *et al.*, 2010).

Voltage signals from the PMT, a function of the intensity of fluorescence emission, were digitized using an Axon Digidata 1440A analog to digital converter (Molecular Devices) and these signals were sent to a computer running pClamp10 software (Molecular Devices). Both fluorescent and ionic signals were sampled at a rate of 10 kHz and were filtered offline at 200 – 1000 Hz. To correct for photo-bleaching of the fluorophore over the course of each sweep, control fluorescence data were recorded in the absence of any change in voltage, and subtracted from the voltage-dependent signal.

3.2.5 Homology model - A published structure of the rat Eag1 voltage-gated potassium channel (5K7L) was used as a template for a *hERG* homology model (Whicher and MacKinnon, 2016). We used Swiss model to build a basic *hERG* homology model to visualize potential sites of interaction for residue D411. Sequence identity was found to be 44%.

3.2.6 Markov model - To compare our gating currents to modeled currents, we used the Piper 2003 Markov model as a template (Piper *et al.*, 2003). A Markov state model was constructed using IonChannelLab (San Luis Potosí, Mexico) (Santiago-Castillo *et al.*, 2010). Forward rates were generated as $\alpha = \alpha_0 \cdot \exp(z_\alpha \cdot VF/RT)$ and reverse rates were generated as $\beta = \beta_0 \cdot \exp(-z_\beta \cdot VF/RT)$. Values for α_0, z_α, β_0, and z_β were obtained from the Piper 2003 Markov model and any deviations are described in Tables S3 and S4. Cooperativity and statistical factors from the Piper 2003 model were also employed.

3.2.7 Data analysis - The kinetics of *hERG* gating charge movement were measured using voltage protocols that depolarized the membrane to a given voltage for increasing durations. The time integral of gating current (Ig_{OFF}), to measure gating charge (Q_{OFF}) after membrane repolarization were then plotted against the duration of depolarization. The kinetic data were fit with single exponential functions of the form $y = y_0 + A\, e^{-t/\tau}$ where y is the normalized response, y_0 is a constant, A is the amplitude, and τ is the time constant. QV relationships were obtained by plotting the first 150 ms of Q_{OFF} as a function of the depolarizing pulse voltage. Data points were normalized to their maximum values then fit with a Boltzmann function of the form $Q/Q_{max} = 1/(1+\exp(-zF/RT(V-V_{0.5}))$, where $V_{0.5}$ is the potential of half-activation, z is the equivalent charge, F is Faraday's constant, and R is the universal gas constant.

Fluorescence quenching responses were fit with either single or double exponential functions of the form $y = y_0 + A_1 e^{-t/\tau 1} + A_2 e^{-t/\tau 2}$, where A_1 and A_2 are the amplitudes of each component of the fit and $\tau 1$ and $\tau 2$ the associated time constants.

By simplifying gating to a two-state system (ie. activated vs deactivated), estimations of the change in free energy, ΔG_0, between these two states at 0 mV were calculated (Yifrach and MacKinnon, 2002). ΔG_0 was calculated as $-zFV_{0.5}$, where F is Faraday's constant 96485 C/mol, z is the equivalent charge, and $V_{0.5}$ is the potential of half–activation. The coupling energy (non-additivity) of the two mutations was calculated as $|\Delta\Delta G_o|_{coupling} = (\Delta G_{WTo} + \Delta G_{M1M2o}) - (\Delta G_{M1o} + \Delta G_{M2o})$. The standard error value for non-additivity was calculated as the square root of the sum of the square of standard errors of each of the ΔG_o values.

Statistical tests were made using Graphpad Prism to perform one-way analysis of variance with a Dunnett post-test to compare control with mutant channel values with a significance level set at $P < 0.05$.

3.3 Results

3.3.1 *eag* structure shows D221 (equivalent to D411 in *hERG*) to fold close to the bottom of S4 - Fig. 3.1*A* shows one subunit of a *hERG* homology model, based on the rat *eag* structure (5K7L) determined by Whicher and MacKinnon (2016). D411, highlighted in orange, is an acidic residue at the bottom of S1. Past studies involving D411 have noted that charge reversal and neutralization at this position increase the rate of ionic current activation and hyperpolarize the G-V (Liu *et al.*, 2003; Zhang *et al.*, 2005). D411, in this homology model, appears to be in close proximity to the bottom half of the S4 transmembrane domain, including charged residues

highlighted in cyan such as R537, K538, and less so, D540 in the S4-S5 linker. It is unknown how D411 stabilizes the closed state of *hERG*, though the proximity and role in gating of positive charges in the lower S4 segment make them prime candidates for interaction.

3.3.2 *hERG* gating currents reveal two distinct phases of charge movement: Q_{fast} and Q_{slow} - Gating current measurements are a powerful tool to understand charge movement arising from the S4, and a typical example of gating current at +30 mV illustrating the basic properties of Q_{fast} and Q_{slow} in comparison with the ionic current time course is shown in Fig. 3.1*B*. Clearly, the transient Q_{fast} component of gating current decays very early during ionic current activation, even though the apparent ionic activation time course is increased by concomitant inactivation. An inset showing a non-leak subtracted trace of *hERG* gating current details Q_{fast} on an expanded time base and illustrates that peak gating current (arrow) can be separated from linear capacitive transients using the (COVG) technique. The Q_{slow} component of gating current is sustained and lasts beyond the 300 ms pulse duration used in this protocol.

$Q_{fast}V$ was initially assessed by integration of the first 2 ms of the 300 ms QV protocol, as shown in Fig. 3.1*B*, but at +30 mV the fast component had still not saturated and more extreme depolarizations were required to complete the QV. WT *hERG* gating currents were therefore recorded during 1.5 ms depolarizations to potentials ranging from -100 mV to +160 mV. Integration of the off-gating currents at -110 mV was used to generate the $Q_{fast}V$ relationship. The isolated $Q_{fast}V$ relationship is shown in Fig. 3.1*C* along with the fast component of the total QV relationship. It confirms the broad voltage dependence and shallow slope of this relationship ($V_{0.5}$ = 34.1 ± 3.5 mV, z = 0.79 ± 0.03 e_0) first described by Piper *et al.* (2003). The hyperpolarizing displacement of the fast component of the total QV relationship obtained from

the 300 ms protocol is due to normalization of the data to a maximum value that had not reached saturation at +30 mV.

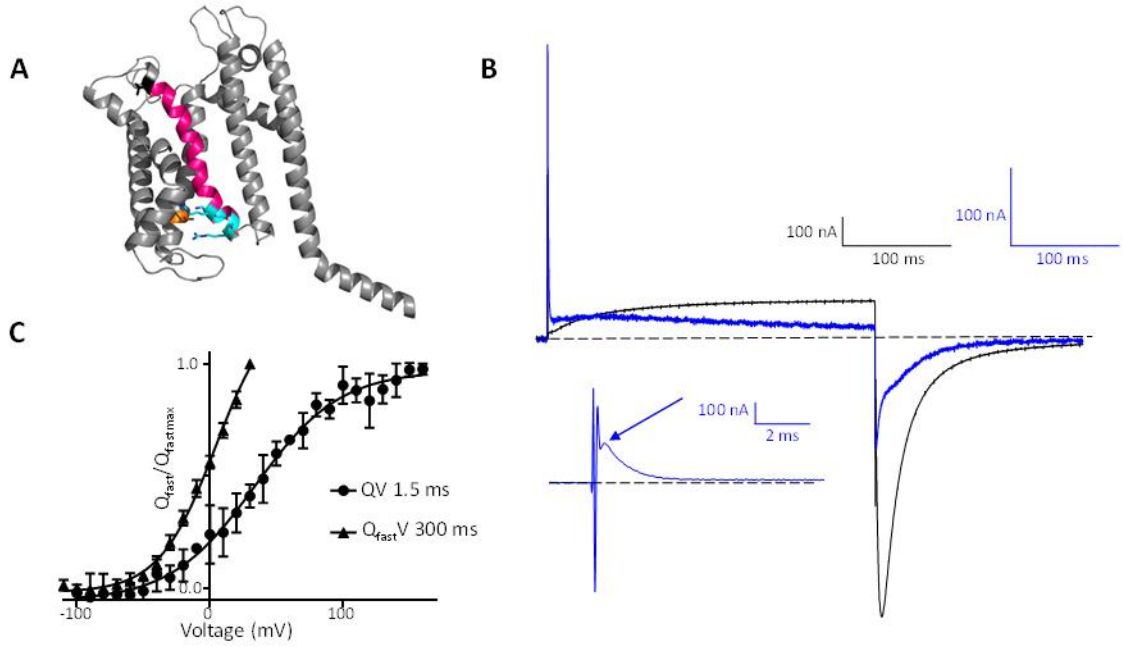

Figure 3.1 Weak voltage-dependence of fast component of *hERG* gating charge make it difficult to evaluate. **(A)** Lateral view of a *hERG* subunit with an activated voltage sensor. Homology model based on the rat eag channel (5K7L). Residue D411 in the S1 segment (pink) may interact with the bottom of the S4 (cyan). **(B)** WT gating (blue) and ionic (black) currents recorded during a 300 ms depolarization to 0 mV from a holding potential of – 110 mV. Inset is the first 15 ms of gating charge movement. Separation of peak fast gating charge movement from leak remaining capacitive transient is indicated by the arrow. **(C)** Voltage dependence of activation of the fast component, $Q_{fast}/Q_{fastmax}$ of WT *hERG* gating charge from a QV 1.5 ms protocol and as measured from a QV 300 ms protocol. For the QV 1.5 ms protocol $V_{0.5}$ = 34.1 ± 3.5 mV, z = 0.79 ± 0.03 (n = 3). The fast component as measured from the QV 300 ms protocol does not saturate and could not be fit with a Boltzmann function.

3.3.3 D411 and S4 positive charge neutralization changes the qualitative nature of *hERG* gating currents - To investigate the effect of D411, and residues in the lower part of S4 on the Q_{fast} component's role in *hERG* gating, our initial experiments involved comparing the gating currents of WT *hERG*, Control, and C-less *hERG* with a D411 construct mutated to an

asparagine to neutralize charge (D411N, Fig. 3.2*A*). Interestingly, the qualitative nature of the on-gating current of the D411N mutant was radically different from control. During 24 ms depolarizations to a range of potentials, the control record shows a very fast current spike followed by a much slower charge movement throughout the depolarization. Q_{fast}, however, is almost absent in the D411N record, and the Q_{slow} component appears to move much more

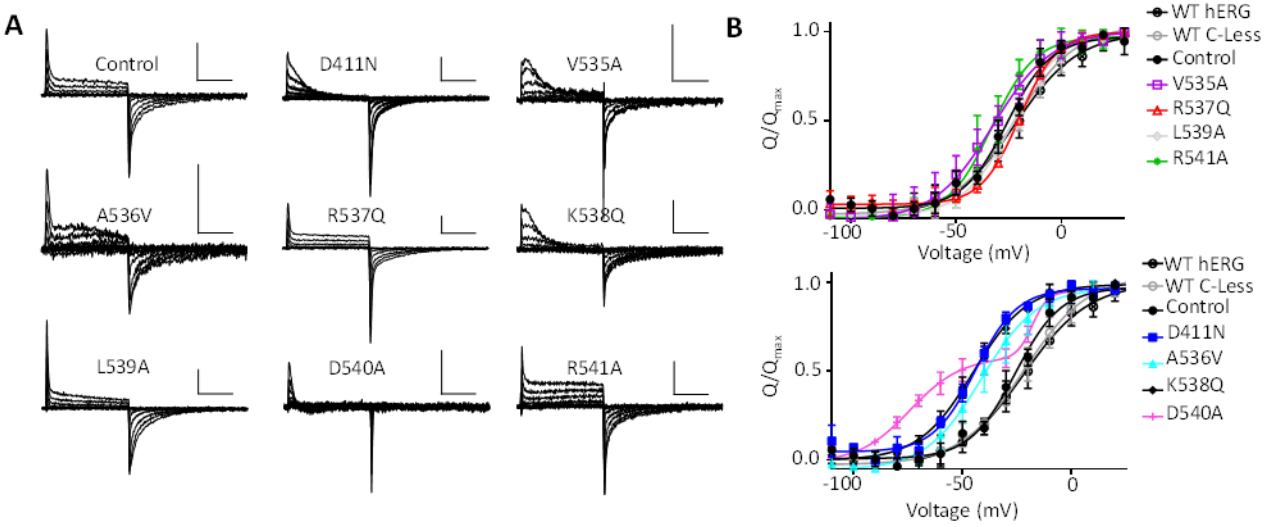

quickly, with charge movement complete within 20 ms. The elimination of the fast component of gating charge movement in D411N and increased rate of Q_{slow} activation, prompted us to record gating currents from mutated constructs that might have an electrostatic or steric relationship with D411N (Fig. 3.1*A*).

Figure 3.2 Mutation of residues D411, V535, K538, and D540 alter both fast and slow components of *hERG* gating charge movement.
(A) Gating currents of WT *hERG* and mutant channels recorded during 24 ms depolarizing voltage pulses from −110 mV to +30 mV in 20 mV steps. Pulses were applied every 10 s. All scale bars indicate 10 ms along the x-axis and 50 nA along the y-axis. **(B)** Charge-voltage relationships from WT, WT C-Less, Control, D411N, V535A, A536V, R537Q, K538Q, L539A, and R541A constructs during 300 ms depolarizing voltage pulses from -110 mV to +30 mV in 10 mV steps. QV fit parameters and *n* values for these constructs are found in Table 3.1. The D540A charge-voltage relationship is from 100 ms depolarizing voltage pulses from -110 mV to +30 mV in 10 mV steps. The holding potential in all experiments was – 110 mV. Off-gating charge movement was measured by integrating the first 150 ms of gating charge return following the depolarizing pulses.

3.3.4 Some S4 mutations also reduce or abolish Q_{fast}, and speed up Q_{slow} charge components - We performed a short alanine scan of the bottom half of the S4 and beginning of the S4-S5 linker and recorded voltage-dependent gating currents using the COVG. Expression was poor for R537A and K538A mutants, so we introduced glutamine residues at these positions, which produced more robust currents. Traces of each construct in response to a 24 ms depolarization are shown in Fig. 3.2*A*. Strikingly, V535A, K538Q, and D540A show an obvious reduction in the amplitude of Q_{fast} relative to Q_{slow} and an overall acceleration of the bulk of charge movement such that little sustained gating current remains after 24 ms. Constructs A536V, R537Q, L539A, and R541A all retained a gating current phenotype similar to WT. Total charge–voltage (QV) relationships during 300 ms depolarizations were obtained for WT *hERG*, I521C, the D411N mutant, and the lower S4 mutants (Fig. 3.2*B*). The upper panel of Fig. 3.2*B* depicts mutants with a ~10 mV shift or less from WT *hERG*, while the lower panel depicts mutants that show a greater shift (Table 3.1). A536V, K538Q, and D411N showed a significantly more hyperpolarized voltage dependence of charge movement compared to the WT and I521C constructs. D540A showed an unusual biphasic QV. Previous reports had noted similar properties arising in mutants at this position (Piper *et al.*, 2005) and shown that this channel can re–enter an open state at strongly hyperpolarized potentials (Sanguinetti and Xu, 1999). All three mutants, A536V, K538Q, and D411N showed a >20 mV hyperpolarization of the $QV_{0.5}$ compared with WT, with little change in the effective valence, *z* (Table 3.1). It is interesting that V535A, which exhibits a loss of Q_{fast}, shows steady-state QV kinetics relatively unchanged from WT, while A536V shows a QV hyperpolarization.

For comparison, the conductance–voltage (GV) relationships of WT *hERG*, Control, D411N and S4 mutants are shown in Fig. S1. Here, we observed that the $GV_{0.5}$ for both Control ($GV_{0.5}$ = -23.0 ± 0.4 mV) and D411N ($GV_{0.5}$ = -14.5 ± 0.9 mV) were quite similar (unlike the difference in QV relationships between these constructs in Fig. 3.2), with that of D411N being slightly depolarized to that of Control. The same is true for D540A, but not for mutants V535A and K538Q which have lost Q_{fast}, and whose $GV_{0.5}$ are significantly more hyperpolarized relative to the Control $GV_{0.5}$ than their $QV_{0.5}$ values. These results suggest two things: they are further confirmation of the previously noted poor coupling between the movement of the VSD and the pore domain (Goodchild *et al.*, 2015), and also demonstrate that the use of GV relationships to understand the movements of the VSD and gating charge during activation is fraught with problems, likely due to the important steps that occur between VSD activation and actual pore opening. In this study we rely on direct measurements of VSD charge movement and displacement to understand how the relationship between S1 and S4 changes during activation of the VSD.

3.3.5 Q_{fast}/Q_{total} reduced for mutants D411N, V535A, K538Q, and D540A - We next looked to quantify Q_{fast} in relation to the total charge moved. A previous study has defined Q_{fast} as any charge that is moved within the first 2 ms of a depolarization (Piper *et al.*, 2003). As a simple way to separate the two components, we defined Q_{fast} as the envelope of current that peaked above the slower moving gating charge in the first 2 ms after a depolarizing stimulus. An example of this region used for integration purposes is shown in Fig. 3.3*A* for Control and for V535A which lacks Q_{fast}. Complete sets of gating current tracings between -60 and +30 mV are shown from Control, D411N, and the S4 mutants in Fig. 3.3*B* and illustrate the clear increase in

Q_{fast} in WT channels as the potential is increased from -50 mV, where it first appears, up to +30 mV. The same is true in other Control-like mutants (A536V, R537Q, L359A, and R541A), but not in D411N, V535A, or K538Q, in which Q_{fast} is reduced or abolished. D540A gating currents are more difficult to interpret as overall charge movement is so fast that Q_{fast} and Q_{slow} cannot easily be separated.

The QV relationships for Q_{fast} and total charge (Q_{total}) are shown in Fig. 3.3*C* for Control and D411N, with just the Q_{fast} components for all mutant constructs plotted in Fig. 3.3*D*. The Control Q_{fast} can be seen to be a small proportion, about 5% of total charge, and shows a relatively linear voltage dependence, or at least a lack of saturation at +30 mV. At depolarizations of -10 mV and greater, D411N, V535A, K538Q, and D540A were all found to have significantly reduced Q_{fast} components compared to Control. The Q_{fast} component of constructs A536V, R537Q, L539A, and R541A were not found to differ significantly from Control.

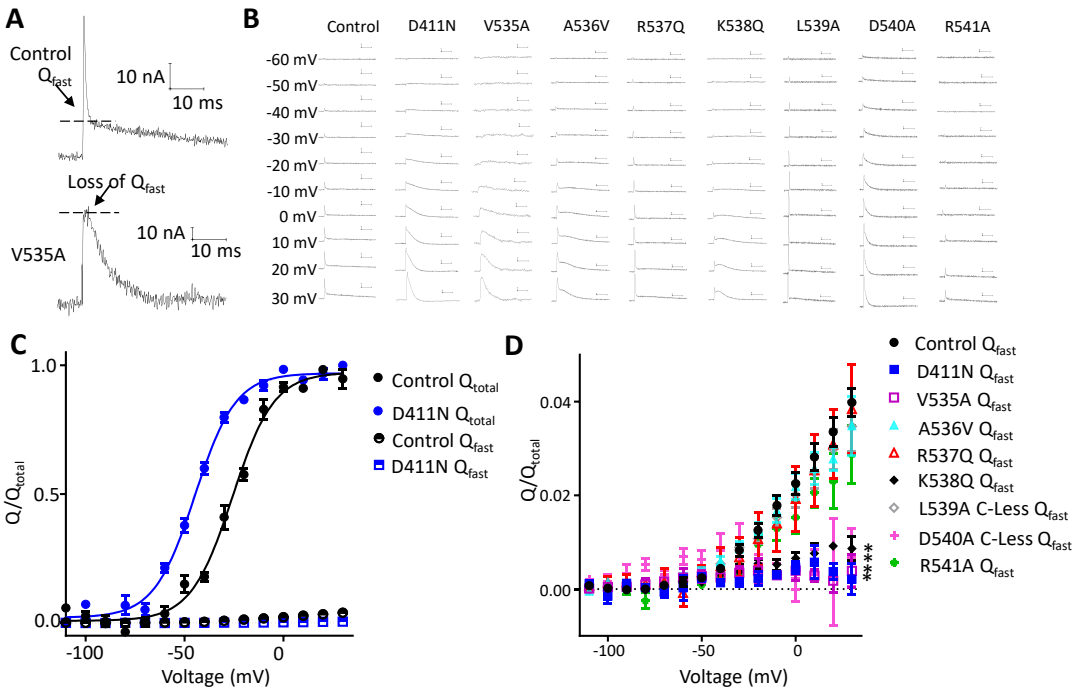

Figure 3.3 D411N, V535A, K538Q, and D540A mutants have reduced Q_{fast} during activation.
(A) Initial 50 ms of gating current traces of WT *hERG* and V535A during a depolarization to +30 mV from a holding potential of – 110 mV. Q_{fast} was defined as charge moving within 2 ms of a change in potential and peaks above the slower charge movement. **(B)** Gating currents from 50 ms depolarizations to potentials between -60 mV and +30 mV from a holding potential of – 110 mV for Control, D411N, V535A, A536V, R537Q, K538Q, L539A, D540A, and R541A constructs. All scale bars indicate 10 ms (x-axis) and 10 nA (y-axis). **(C)** Relationships of Q_{total} and Q_{fast} to voltage during 300 ms depolarizations to potentials from -110 mV to +30 mV in 10 mV steps. **(D)** Q_{fast} relative to Q_{total} for all constructs. D411N, V535A, K538Q, and D540A all show significantly reduced Q_{fast} at potentials greater than -10 mV, *P<0.05. Values of Q_{fast}/Q_{total} for all constructs are found in Table S1.

3.3.6 Time constants of activation of gating charge faster for D411N, V535A, K538Q, and D540A - To quantify the faster activation of total gating charge in the mutant channels, we employed an envelope of tails protocol to examine gating charge activation. Data in Fig. 3.4*A* show representative traces of WT *hERG* and D411N in response to successively longer depolarizations to +40 mV and 0 mV, respectively, from the holding potential of -110 mV. Shown below, the charge moved during each depolarization was assessed through integration of

the first 100-150 ms of gating charge return at a holding potential of -110 mV and the relationship between total charge moved and length of depolarizing stimulus to 0 mV for D411N and +40 mV for WT *hERG* was well fit with a single exponential, as shown in Fig. 3.4*B*. The time constant is clearly faster in D411N, even at a more negative potential than WT and this is borne out over a range of test potentials between -40 and +60 mV (in 20 mV steps), and in select S4 mutants as well as D411N (Fig. 3.4*C*). Some constructs had time constants of gating charge activation that were too slow to be measured at the lower depolarizations. Still, several of the mutant constructs had significantly faster time constants of activation than WT: D411N, V535A, K538Q, and D540A. A536V also seemed faster than WT, but when A536V's hyperpolarized QV relationship is accounted for (see Fig. 3.2), the faster kinetics are no longer apparent.

The same constructs with an absent or reduced Q_{fast} component of gating charge also had a faster rate of activation of gating charge. Figure 3.4*D* shows a linear regression of the time constants of charge activation and Q_{fast}/Q_{total} for all constructs at +20 mV, a potential at which all mutants show near complete charge movement during a 300 ms depolarization. Due to the hyperpolarized QV of mutants A536V, D411N, D540A, and K538Q, the time constants of charge activation and Q_{fast}/Q_{total} were taken from measurements at 0 mV. The linear regression showed an R^2 value of 0.81 when fit through the means, suggesting a good correlation between the loss in fast component of gating charge movement and the speed of activation of total gating charge in the channel.

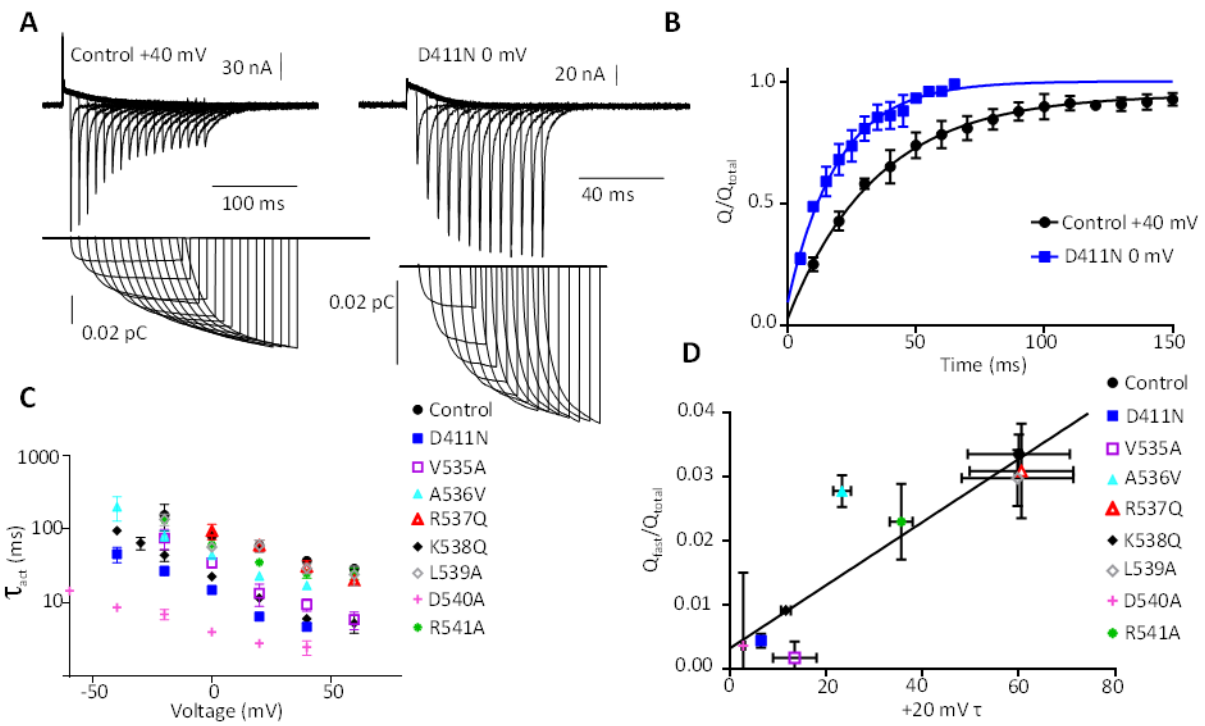

Figure 3.4 Loss of fast gating charge component is correlated with increased rate of gating charge activation. **(A)** Representative gating currents from WT and D411N recordings during step depolarizations to 0 mV (D411N) and +40 mV (Control) from a holding potential of −110 mV. The initial pulse duration was 10 ms for all gating current records, and was increased by 10 ms for each successive cycle. The amount of off-gating charge moved was measured by integration of the return of first 150 ms of gating charge during a repolarization to – 110 mV. **(B)** Plot of normalized integrals of gating charge return vs time of depolarizing steps for Control at +40 mV and D411N at 0 mV. **(C)** Time constants of activation calculated using single exponential fits of the Q/Q_{max} relations. Time constants of activation are displayed in Table S2. **(D)** Relationship between relative amount of fast gating charge during a 300 ms +20 mV depolarization from a holding potential of – 110 mV and time constants of activation at +20 mV.

3.3.7 Fluorescence recordings demonstrate loss of a fast fluorescence component for D411N, V535A, K538Q, and D540A - Several studies of *hERG* gating have used voltage clamp fluorometry (VCF) (Es-Salah-Lamoureux *et al.*, 2010; Smith and Yellen, 2002; Van Slyke *et al.*, 2010) to directly monitor movements of different parts of the VSD, mainly S4. Covalent attachment of a fluorophore to residues in the S3-S4 linker between E518 and I521 has allowed a variety of signals to be obtained that reflect aspects of the activation process. Labeling of E519C gives rise to a fluorescence signal with a very rapid fast fluorescence quenching and a slower

fluorescence quenching component (Es-Salah-Lamoureux *et al.*, 2010), analogous in some ways to the Q_{fast} and Q_{slow} components of gating charge that we have characterized above. After introduction of the mutation E519C to our *hERG* constructs and covalent attachment of the fluorophore tetramethyl rhodamine maleimide (TMRM) to E519C, VCF experiments were performed to test the idea that fast components of fluorescence quenching might track the physical displacement of the VSD underlying the initial Q_{fast} charge movement.

Representative TMRM fluorescence recordings from Control, D411N, V535A, R537A, K538Q, and D540A constructs in response to a step to -30 mV from a holding potential of -110 mV are shown in Fig. 3.5*A*. Of these constructs, only R537A remained similar to Control in the relative amount of fast fluorescence quenching. V535A retained a small amount of the fast fluorescence quenching, while D411N and K538Q retained none of the fast fluorescence quenching. In contrast, D540A showed only a rapid component and no slow fluorescence component. We attribute the D540A result to acceleration of total VSD movement, in agreement with our gating charge data (Fig. 3.2, Fig. 3.3*B*). The two mutants, D411N and D540A, were found to have only a single component of fluorescence quenching after exponential fitting of mean data, while K538Q retained a small fast component. Mean data for Fast fluorescence component amplitude as a proportion of the total quenching are shown in Fig. 3.5*B*. All constructs studied, with the exception of R537A, showed a highly significant reduction in the fast fluorescence quenching during depolarization when compared to Control.

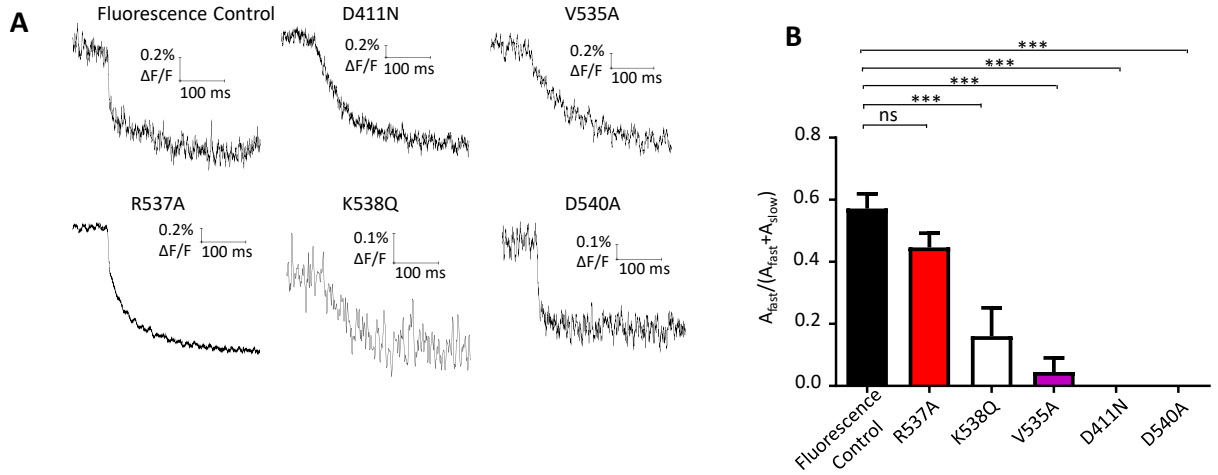

Figure 3.5 Loss of fast gating charge component also reflected in TMRM fluorescence quenching.
(A) VCF representative traces during depolarizing pulses to -30 mV from a holding potential of -110 mV for fluorescence control, D411N, V535A, R537A, K538Q, and D540A mutants. Quenching of the fluorescent signal was fit with either a single or double exponential function. **(B)** Proportion of fluorescent signal that reflects a fast quenching event. The proportions of fast quenching to total fluorescent quenching are as follows: WT: $A_{fast}/(A_{fast}+A_{slow})$ = 0.58 ± 0.05 (n=3); D411N: $A_{fast}/(A_{fast}+A_{slow})$ = 0 ± 0 (n=3); V535A: $A_{fast}/(A_{fast}+A_{slow})$ = 0.05 ± 0.09 (n=4); R537Q: $A_{fast}/(A_{fast}+A_{slow})$ = 0.45 ± 0.05 (n=4); K538Q: $A_{fast}/(A_{fast}+A_{slow})$ = 0.16 ± 0.09 (n=3); D540A: $A_{fast}/(A_{fast}+A_{slow})$ = 0 ± 0 (n=3).

3.3.8 Double mutant cycle analysis reveals functional interaction between D411 and S4 residues V535 and K538 - To establish whether a functional interaction was taking place between D411 and the residues at the cytoplasmic end of the S4 and beginning of S4-S5 linker, double mutant constructs were made with D411N and an additional one of the different S4 mutants of interest. Gating currents were obtained from the double mutants using a 300 ms depolarization protocol, and charge measurements from integration of these gating currents upon repolarization have been normalized and plotted in Fig. 3.6 for all single and double mutants. The change in free energy of activation of the double mutant channels was compared to that of the single mutant and WT channel constructs (see Methods for more detail). Boltzmann fit data from 300 ms QV protocols, $V_{0.5}$, z, and ΔG_{act} values for all constructs are found in Table 3.1.

Past studies using this type of analysis in voltage gated ion channels have suggested that double mutants with a $\Delta\Delta G_{act}$ greater than 4.2 kJ/mol indicate a significant interaction between the two sites (Cheng *et al.*, 2013; Yifrach and MacKinnon, 2002; Zhang *et al.*, 2005). We adopted the same threshold as an indication of an interaction between residues. Fig. 3.6*B* shows the values of $\Delta\Delta G_{act}$ obtained for all mutants. Both D411N/V535A and D411N/K538Q were found to have a $\Delta\Delta G_{act}$ greater than 4.2 kJ/mol. This, along with the proximity of D411 to K538 support past suggestion of an electrostatic interaction of these two residues (Cheng *et al.*, 2013). We were unsuccessful in obtaining gating currents from the construct D411N/D540A.

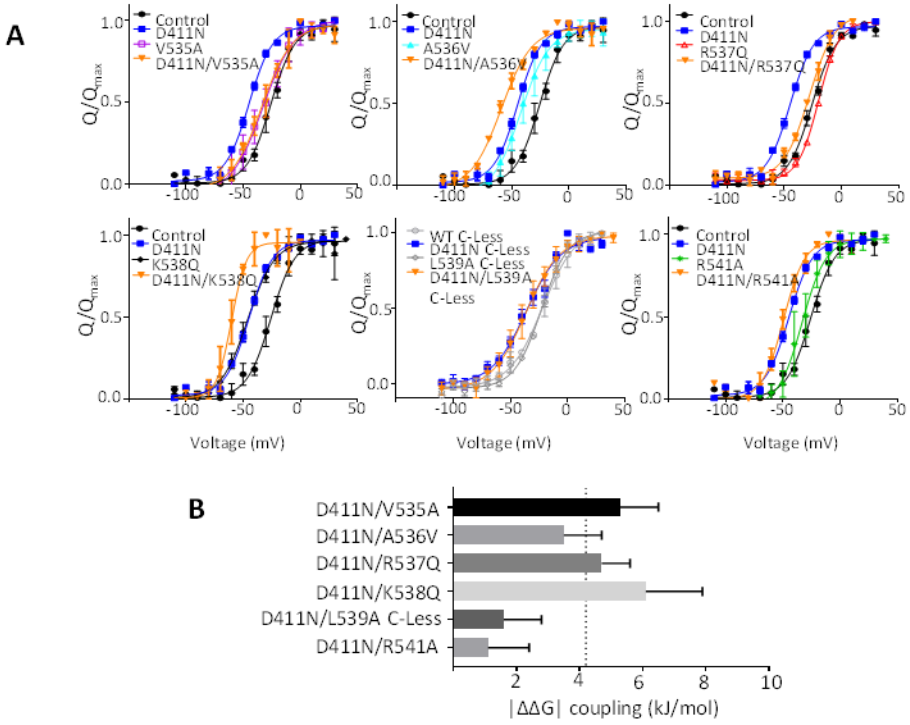

Figure 3.6 Double mutant cycle analysis reveals functional interaction between D411 on S1 and the bottom of S4.

(A) QV relationships of Control, V535A, A536V, R537Q, K538Q, L539A, R541A, D411N, D411N/V535A, D411N/A536V, D411N/R537Q, D411N/K538Q, D411N/L539A, and D411N/R541A. QV relationships were obtained from 300 ms activation pulses from a holding potential of -110 mV. The amount of gating charge moved after each sweep was assessed by integrating the first 150 ms of the return of gating charge. $V_{0.5}$ & z values can be found in Table 3.1. **(B)** $\Delta\Delta G_0$ relationships for D411N/V535A, D411N/A536V, D411N/R537Q, D411N/K538Q, D411N/L539A, and D411N/R541A. $\Delta\Delta G_0$ calculated described in Methods. Values are presented in Table 3.1.

Construct	*QV* 1/2 (mV)	*z*	ΔG_0 (kJmol^{-1})	$\lvert\Delta\Delta G_0\rvert$ *coupling* (kJmol^{-1})	n
WT hERG	-22.0 ± 1.6	1.8 ± 0.1	3.8 ± 0.4	N/A	5
Control (I521C)	-25.9 ± 1.7	2.3 ± 0.1	5.8 ± 0.5	N/A	4
WT C-less	-20.6 ± 2.8	1.7 ± 0.2	3.4 ± 0.6	N/A	3
D411N	-46.3 ± 0.3 *	2.5 ± 0.1	11.3 ± 0.5	N/A	3
D411N (C-less)	-36.7 ± 2.6 *	1.7 ± 0.0 *	6.1 ± 0.5	N/A	4
V535A	-32.4 ± 1.5	2.0 ± 0.3	6.2 ± 0.8	N/A	3
A536V	-40.2 ± 2.5 *	2.4 ± 0.1	9.2 ± 0.6	N/A	5
R537Q	-20.0 ± 0.4	2.8 ± 0.1	5.3 ± 0.2	N/A	3
K538Q	-45.2 ± 1.9 *	2.0 ± 0.1	8.9 ± 0.6	N/A	4
L539A (C-less)	-22.7 ± 1.2	2.2 ± 0.1	4.7 ± 0.3	N/A	5
R541A	-30.4 ± 1.8	2.7 ± 0.1	8.0 ± 0.5	N/A	4
D411N/V535A	-33.6 ± 1.5	2.0 ± 0.2	6.3 ± 0.6	5.3 ± 1.2	4
D411N/A536V	-58.4 ± 2.5 *	2.0 ± 0.1	11.2 ± 0.7	3.5 ± 1.2	3
D411N/R537Q	-28.7 ± 1.7	2.2 ± 0.2	6.1 ± 0.6	4.7 ± 0.9	3
D411N/K538Q	-58.7 ± 2.5 *	3.6 ± 0.2 *	20.4 ± 1.6	6.1 ±1.8	4
D411N/L539A (C-less)	-35.9 ± 5.0 *	1.7 ± 0.1	5.8 ± 0.9	1.6 ± 1.2	4
D411N/R541A	-49.1 ±0.9 *	2.6 ± 0.2	12.3 ± 1.0	1.1 ± 1.3	4

Table 3.1 $QV_{0.5}$, z, ΔG_0 values for all constructs involved in double mutant cycle analysis.

3.3.9 Modeling a disruption of early closed states of *hERG* - The experiments in this study suggest that D411-S4 interactions stabilize early closed states of the channel. Disruption of these interactions result in a loss of the fast component of gating charge as well as an increase in the rate of channel activation. In a 2003 paper describing the first measurements of *hERG* gating currents, Piper *et al.* constructed a Markov model of *hERG* gating. In Fig. 3.7, we have taken advantage of this model to describe the gating effects that occur upon destabilizations of early closed states of the *hERG* activation pathway. Fig. 3.7*A* shows the different variations of the Markov model shown in the subsequent panels. Fig. 3.7*A* (i) details the full Markov scheme as

constructed by Piper *et al.*, (ii) details the Markov scheme missing the first closed state in the Piper *et al.* model, and (iii) details the Markov scheme missing the first two closed states of the Piper *et al.* model. Transitions between early closed states of the channel are thought to give rise to the Q_{fast} charge movement. With the aim of modeling destabilizations of early closed states, we have presented variations of the Piper *et al.* model that lack early closed states and we have also modified the rates of each initial transitions to model the voltage-dependence seen experimentally. Any changes from the Piper *et al.* model are indicated in Tables S3 and S4. Fig. 3.7*B* (top) shows the gating currents obtained from (i) Control, (ii) D411N, and (iii) D411N/K538Q constructs. Fig. 3.7*B* (bottom) shows the modeled gating currents from (i) a complete Piper *et al.* Markov model, (ii) a Piper *et al.* model lacking the first closed state, and (iii) a Piper *et al.* model lacking the first two closed states. The modeled currents reveal an increase in the rate of slow gating charge activation upon removal of the early closed states. Removal of the first closed state results in a slight increase in the rate of charge activation and removal of both the first and second closed states results in a clear increase in the rate of charge activation. Both (ii) and (iii) note the loss of the Q_{fast} component of gating charge movement. Experimentally, we observed that upon disruption of the D411-S4 interaction, the time constants of activation become faster than the voltage-independent transition that had been noted to be a facet of *hERG* gating. As such, the rate of the voltage independent transition in both (ii) and (iii) Markov schemes was increased substantially. Fig. 3.7*C* shows the voltage dependence of activation relationships for Control, D411N, K538Q, D411N/K538Q, as well as all of the variations of the Piper *et al.* model. $V_{0.5}$ and z values are noted in Fig. 3.7. The QV relationships of D411N and K538Q overlay the (ii) Markov scheme quite well, as did the D411N/K538Q QV relationships with that of the (iii) Markov scheme. It appears that transitions between early

closed states of *hERG* may limit the later movement of gating charge. Experimental evidence has indicated that fast gating charge movement is only weakly voltage-dependent and is right-shifted to overall gating charge movement. In a modeled system, this has the effect of acting as a limit on the rate of activation charge movement as individual channels take time to traverse through these many weakly voltage-dependent transitions. Disruption of these early closed states, as we suggest is occurring in our experiments through disruption of D411-S4 interactions, therefore increases the rate of activation by removing this limit on charge movement.

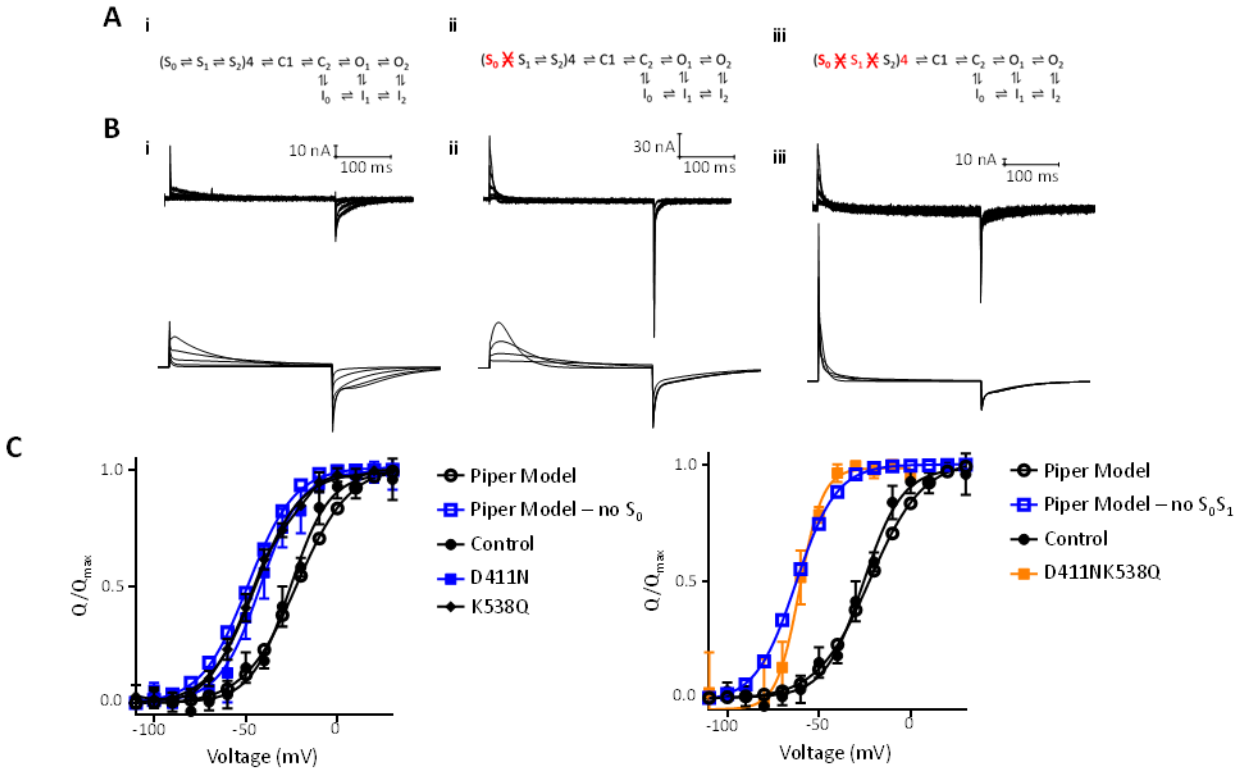

Figure 3.7 D411 and S4 interaction stabilizes an early closed state of the *hERG* channel.
(A) Schematic of the Piper model of *hERG* gating (i) full model (ii) model lacking the S_0 state (iii) model lacking the S_0 and S_1 states. **(B)** Experimental and modeled gating currents of 300 ms depolarizations to -40, -20, 0, +20 mV from a holding potential of – 110 mV. (i) Control *hERG* (top) and Piper model (bottom) gating currents. (ii) D411N (top) and Piper model lacking the S_0 state (bottom) gating currents (iii) D411N/K538Q (top) and Piper model lacking the S_0 and S_1 states. **(C)** 300 ms QV relationships from a holding potential of -110 mV for Control ($V_{0.5}$ = -25.9 ± 1.7 mV , z = 2.3 ± 0.1, n= 4) D411N ($V_{0.5}$ = -46.3 ± 0.3 mV, z= 2.5 ± 0.1 n= 3), K538Q ($V_{0.5}$ = -45.2 ± 1.9 mV, z= 2.0 ± 0.1 , n= 4), D411N/K538Q ($V_{0.5}$ = -58.7 ± 2.5 mV, z= 3.6 ± 0.2 n= 4), Piper Model ($V_{0.5}$ = -23 mV, z = 1.8), Piper Model – no S_0 ($V_{0.5}$ = - 51 mV , z = 2.1), and Piper Model – no S_0S_1 ($V_{0.5}$ = - 63 mV , z = 2.3).

3.4 Discussion

Experiments presented in this study indicate that an interaction between S1 charge D411 and K538 of the S4 is involved in stabilizing early closed states of *hERG*. Disruption of this interaction results in a loss of the fast component of gating charge, a charge movement thought to reflect transitions through early closed states (Cheng and Claydon, 2012; Piper *et al.*, 2003; Wang *et al.*, 2013). Additionally, destabilization of this interaction results in *hERG* channels that activate much more quickly, potentially as a result of channels residing in resting states further along the activation pathway. These increased rates of activation are similar to those of conventional VGKC such as *Shaker* (Schoppa and Sigworth, 1998). The data presented here suggest that the closed state stabilization of the D411-K538 interaction may underlie the basis for the unusually slow activation kinetics of *hERG*.

3.4.1 Basis of *hERG* slow activation gating - Determining the basis for the slow activation of *hERG* has been the subject of numerous studies (Liu *et al.*, 2003; Piper *et al.*, 2005; Subbiah *et al.*, 2004; Subbiah *et al.*, 2005; Van Slyke *et al.*, 2010; Zhang *et al.*, 2005; Zhang *et al.*, 2004). A recurring finding is that the flanking charges of the S4, K525 and K538, are involved in interactions that stabilize the closed state of the channel (Cheng *et al.*, 2013; Piper *et al.*, 2005; Subbiah *et al.*, 2004; Subbiah *et al.*, 2005; Zhang *et al.*, 2005). K525 has been suggested to interact with F463, D466 (Cheng *et al.*, 2013) and D456 (Zhang *et al.*, 2005) through interactions that are not likely to be electrostatic in nature as changes in voltage dependence due to mutations at this site are not charge-dependent (Cheng *et al.*, 2013; Subbiah *et al.*, 2004). K538 has been suggested to interact with D411 in the closed state (Zhang *et al.*, 2005) through an electrostatic interaction (Cheng *et al.*, 2013). Disruption of any of these interactions has the effect of

increasing the rate of activation and left-shifting the voltage dependence of activation, presumably through disrupting early closed states of the channel.

The present study investigated a proposed interaction between S1 charge D411 and the bottom of the S4, as well as the role of this interaction in the fast gating charge movement of *hERG*. Mutation to sites in both the S4 and S1 (D411N, V535A, K538Q, and D540A) resulting in similar changes to gating and fluorescence phenotypes (Figs. 3.2, 3.3, 3.5) and increases in activation rates (Figs. 3.4) supports previous findings of an interaction between these two sites (Zhang *et al.*, 2005). Additionally, double mutant cycle analysis experiments using gating currents from our mutant constructs were used to define S4 interaction partners with D411 (Fig. 3.6). The use of double mutant cycle analysis in the study of ion channels involves simplifying gating to a two-state system (Yifrach and MacKinnon, 2002). Determination of a functional interaction between D411 and the residues at the bottom of the S4 was estimated by comparing the free energy change between activated and deactivated charge, as estimated by the parameters obtained (z and $V_{0.5}$) from a Boltzmann fit of charge movement from a 300 ms QV protocol, of double mutant channels, single mutant channels, and Control. Should there be no interaction between two sites, then the change in free energy of the double mutant should equal the sum of the change in free energy of the single mutants. A large amount of non-additivity in these experiments is an indication of interaction (Yifrach and MacKinnon, 2002). Our findings suggest an interaction of D411 with the bottom of the S4 segment, but not the S4-S5 linker. There are indications of non-additivity with both D411N/V535A and D411N/K538Q, and to a lesser extent D411N/A536V and D411N/R537Q. These data indicate that D411 interacts with the bottom of the S4 segment, supporting previous work (Zhang *et al.*, 2005). This form of analysis does not

necessarily define direct physical interaction between specified residues, but rather suggests that 'interacting' residues both contribute to stabilization of a particular state (Horovitz, 1996; Yifrach and MacKinnon, 2002). However, as it has been shown that an electrostatic interaction is likely at K538 (Cheng *et al.*, 2013), the equivalent residues of K538 and D411 in the eag channel are in close proximity (Whicher and MacKinnon, 2016), neutralization of either K538 or D411 results in similar effects, and mutation of either K538 or D411 results in similar gating phenotypes, it is reasonable to suggest that an electrostatic interaction between these two residues contributes to a stabilization of an early closed state of the channel. Mutation to V535, A536, R537, and D540 may alter the steric environment in a way that destabilizes the D411-K538 interaction. The double mutant construct D411N/D540A had an extremely hyperpolarized voltage dependence of activation that caused challenges with quantification of the voltage-dependence of activation. We were therefore unable to apply double mutant cycle analysis to query an interaction between D540 and D411.

3.4.2 Q_{fast} - Previous studies detailing *hERG* gating have suggested that Q_{fast} results from rapid transitions through early closed states of the channel (Es-Salah-Lamoureux *et al.*, 2010; Goodchild and Fedida, 2014; Piper *et al.*, 2003; Wang *et al.*, 2013). Initial study of *hERG* gating currents found a curious biphasic response to depolarizing stimuli (Piper *et al.*, 2003). This study described a fast component, Q_{fast}, with a QV that was depolarized with respect to overall charge movement, had a shallow voltage dependence, extremely rapid activation and deactivation kinetics, but yet constituted less than 10% of the total charge movement (Piper *et al.*, 2003). As a result, Q_{fast} appears at more negative potentials than the majority of gating charge, but saturates at more positive potentials than Q_{slow} upon depolarization. As discussed above, K538 has been

previously suggested to stabilize a closed state of *hERG* (Cheng *et al.*, 2013; Subbiah *et al.*, 2005; Zhang *et al.*, 2005) through an electrostatic interaction with D411 (Zhang *et al.*, 2005). This early state stabilization appears to also be connected to the presence of the fast component of *hERG* activation gating charge movement. Our data suggest that disruption of this D411-K538 interaction results in such a destabilization of early closed states that, even at hyperpolarized potentials, such as -110 mV, channels no longer reside in these early closed states and thus have no need to transition from them during activation events. This would be reflected experimentally by an apparent loss of Q_{fast} and an increase in the rate of activation.

Past fluorescence studies have noted the presence of a fast component of fluorescence during *hERG* activation (Es-Salah-Lamoureux *et al.*, 2010; Smith and Yellen, 2002). Smith and Yellen suggested that this fast component of fluorescence was reporting on movements related to the inactivation pathway, whereas Es-Salah-Lamoureux *et al.* proposed this fast component of fluorescence represented early channel activation processes. Neither of these suggestions had been definitively proven, but the evidence taken as a whole from both studies seem to indicate a relation to the activation pathway. The signals produced by fluorophores in voltage clamp fluorescence experiments do not reflect quantitative distances travelled or gross movements of gating charge, but rather alterations in the quenching environment around the site of fluorophore incorporation. In our fluorescence experiments, alteration of the D411-K538 interaction dramatically reduced or eliminated the fast component of fluorescence, similarly to the fast component of gating charge (Fig. 3.5). This suggests that the fast component of fluorescence reports gating movements associated with Q_{fast} and is further evidence that the D411-K538 interaction stabilizes early closed states.

Also worth noting is the loss of the rate-limiting voltage-independent transition described previously (Goodchild *et al.*, 2015; Subbiah *et al.*, 2004; Wang *et al.*, 1997a). The rates of activation of D411N, K538Q, V535A, and D540A all exceed the rate previously determined by a voltage-independent transition for gating charge (Goodchild *et al.*, 2015). Should the voltage-independent transition be absent in mutant channels with the D411-K538 disruption, what does this mean for its place in the activation pathway? Typically, models of *hERG* gating have placed the voltage-independent transition as one of the last transitions a channel passes through before proceeding on to an open state (Clancy and Rudy, 2001; Mazhari *et al.*, 2001; Wang *et al.*, 1997a). The Piper *et al.* (2003) model, which was used here to illustrate the role of early closed states, places this transition as the C1-C2 transition prior to channel opening. Also worth considering is that in Goodchild *et al.* (2015), both gating charge and ionic current were shown to become rate-limited by a voltage-independent transition at extreme depolarizations, indicating that a voltage-independent transition precedes the majority of gating charge movement. These data suggest that a voltage-independent transition of *hERG* gating may occur earlier in the activation pathway than previously considered. An alternative possibility is that the loss of the D411-K538 interaction changes the activation pathway of the voltage sensor and the steric factors, which otherwise would have resulted in movements associated with the voltage-independent transition, are no longer relevant.

An alternative explanation to the loss of Q_{fast} is that perhaps the fast gating charge is not being eliminated at all, but rather being obscured by increases in the rate of slow activation gating charge. We believe this to be unlikely because of the findings of Fig. 3.3. Here we see that during depolarizations to -50 mV, the initial fast component of gating charge is apparent in

constructs that are similar to Control. In D411N and other constructs with a faster rate of gating charge activation, we do not see any movement of Q_{fast} at similar early depolarizations. This indicates that the fast charge movement is no longer relevant in these mutant constructs, despite some of these constructs also having a left-shifted voltage-dependence of gating charge activation.

3.4.3 Modelling the loss of Q_{fast} in *hERG* gating - The rate of activation for conventional VGKC is approximately ten times faster than the rate of activation for *hERG* channels (Bezanilla, 2000). This suggests that there may be unique constraints present in the *hERG* activation pathway that slow activation of the channel. D411 is unique to the *eag* family of channels, and is one of three extra charges in the voltage sensing domains of this family (Liu *et al.*, 2003). The interaction of D411 with the S4 is therefore also unique, if not solely to *hERG*, then to the *eag* family. The slow rate of activation also appears to correlate with a fast component of gating charge that is weakly voltage-dependent and suggested to reflect transitions through early closed states (Fig. 3.4D)(Goodchild and Fedida, 2014; Piper *et al.*, 2003; Wang *et al.*, 2013). It may be that the presence of these early closed states with weak voltage dependences (Fig. 3.1C) are the basis for the slow activation of overall *hERG* movement.

Through the use of variations of the Piper *et al.* model of *hERG* gating charge (Piper *et al.*, 2003), we have shown in a theoretical system the consequences of removing early, mildly voltage-dependent closed-state transitions (Fig. 3.7). Elimination of early closed states eliminates Q_{fast}, and substantially increases the rate of activation, and causes a left-shift of the voltage dependence of charge movement. Mutations that result in disruption to the D411-K538

interaction display very similar attributes, conceivably as a result of a destabilization of these early closed states. The D411-K538 interaction serves as an additional constraint in the *hERG* activation pathway that stabilizes early closed states of the channel, likely contributing to the rather slow activation of *hERG* channels.

Chapter 4: Investigating the molecular basis for *hERG* drug block using unnatural amino acid mutagenesis

4.1 Introduction

The *human ether-à-go-go related gene* (*hERG*) voltage-gated potassium channel is most well-known for its repolarizing role in the cardiac action potential as the rapid delayed rectifier potassium current, I_{Kr} (Sanguinetti *et al.*, 1995; Trudeau *et al.*, 1995). Compared to conventional voltage-gated potassium channels (VGKC), activation and deactivation of *hERG* are very slow and are paired with a fast and voltage-dependent inactivation and recovery from inactivation (Goodchild *et al.*, 2015; Sanguinetti *et al.*, 1995; Smith and Yellen, 2002; Spector *et al.*, 1996b). These kinetics result in little *hERG* current being passed throughout the plateau phase of the cardiac action potential as *hERG* channels slowly open and quickly inactivate. Upon repolarization, inactivation is quickly removed and, as deactivation gating is slow in *hERG*, a considerable amount of potassium current is passed before channels close. Instances in which *hERG* function is impaired, through either genetic mutation or drug block, reduce I_{Kr} and therefore increase the time needed to repolarize cardiomyocytes (Curran *et al.*, 1995; Splawski *et al.*, 2000). On an electrocardiogram, this would manifest as a prolongation of the QT interval and is referred to as long QT syndrome type 2 (LQT2) (Sanguinetti *et al.*, 1995; Sanguinetti and Tristani-Firouzi, 2006; Splawski *et al.*, 2000). LQT2 can have dire consequences such as ventricular tachycardia and sudden death (Sanguinetti and Tristani-Firouzi, 2006).

LQT2 as a result of *hERG* drug block (acquired LQT2) has received considerable attention over the past twenty years as *hERG* has been found to be uniquely susceptible to block by a wide

array of drugs across multiple pharmaceutical classes (Brown, 2004; Sanguinetti and Tristani-Firouzi, 2006). While many of these compounds have some similar chemical features, such as multiple phenyl rings and a basic amine group (Vandenberg *et al.*, 2012), that could allow for the creation of predictive tools such as QSARs, many drugs do not conform to these features, but also block the channel at therapeutically relevant concentrations, thereby hindering precise predictive tools (Braga *et al.*, 2014). Due to the susceptibility to and ramifications of drug block, as well as the imperfect predictive capabilities of current tools, pharmaceutical companies are required to screen their prospective compounds against *hERG* to assess potential for block at therapeutically relevant concentrations (Harmonisation, 2005; Kramer *et al.*, 2013).

As *hERG* channels bind a wide array of pharmaceuticals in an off-target manner, it is no surprise that many drug-induced arrhythmias stem from acquired LQT2 (Vandenberg *et al.*, 2012). The significance of this problem has yielded significant interest in understanding which structural features give rise to the widespread *hERG* channel blockade. In general, the structure of *hERG* is fairly typical of the family of voltage-gated potassium channels (Trudeau *et al.*, 1995; Warmke and Ganetzky, 1994). They are tetrameric proteins with each subunit consisting of six transmembrane-spanning segments and two cytosolically-located termini (Trudeau *et al.*, 1995). The first four transmembrane segments, the S1-S4, house several charged amino acids that are sensitive to the electric field across the cell membrane and are known as the voltage sensor of the channel (Bezanilla, 2000). Changes in membrane potential alter the repulsive or attractive forces experienced by these charged amino acids and as they move in response to these membrane potential changes, they initiate conformational changes in other regions of the protein (Bezanilla, 2000). Most notably, these conformational changes alter the open state probability of the pore

region, the S5 and S6, which also houses the selectivity filter of the channel (Long *et al.*, 2007). The pore region of *hERG* channels is thought to contain a large inner vestibule as a result of a lack of a PXP motif found in many K_v channels that introduces a kink in the S6 alpha helix, narrowing the pore region (Mitcheson *et al.*, 2000a; Thouta *et al.*, 2014). This larger inner vestibule may facilitate drug block of the channel as some drugs may be able to continue to reside in this space after the channel closes, becoming trapped in the pore region (Mitcheson *et al.*, 2000b). Many studies have noted the contributions to *hERG* block made by two aromatic residues at the bottom of the S6, Y652 and F656 (Du *et al.*, 2014; Dumont, 1972; Fernandez *et al.*, 2004; Ficker *et al.*, 2001; Kamiya *et al.*, 2006; Kamiya *et al.*, 2008; Melgari *et al.*, 2015a; Melgari *et al.*, 2015b; Mitcheson *et al.*, 2005; Mitcheson *et al.*, 2000a; Stansfeld *et al.*, 2006). In place of these aromatic residues, most K_v channels have the hydrophobic residues isoleucine or valine (Mitcheson *et al.*, 2000a). In *hERG*, mutation of either of these residues to an alanine drastically reduces the potency of most *hERG* blocking drugs (Mitcheson *et al.*, 2000a). Experimental and molecular dynamics studies have suggested that the aromaticity of these residues may underlie the basis of *hERG* drug block, through either cation- π (Fernandez *et al.*, 2004; Mitcheson, 2003; Pearlstein *et al.*, 2003; Perry *et al.*, 2004; Sanguinetti and Tristani-Firouzi, 2006) or π-stacking interactions (Boukharta *et al.*, 2011; Knape *et al.*, 2011; Melgari *et al.*, 2015b; Stansfeld *et al.*, 2007).

Means of investigating potential cation-π relationships in ion channels have been well established (Ahern *et al.*, 2006; Beene *et al.*, 2003; Pless *et al.*, 2011a; Pless *et al.*, 2011b). Incorporation of fluorinated aromatic amino acid analogues, such as fluorinated phenylalanines, through unnatural amino acid (UAA) mutagenesis can give the experimenter control over the π-

electron density of a specific aromatic residue (Dougherty, 1996; Zhong *et al.*, 1998). As a highly electronegative element, fluorine draws electron density towards itself, reducing π-electron density in the center of the phenyl ring. This technique allows one to reduce the ability of an aromatic amino acid to donate π-electrons in an interaction while imposing only subtle steric changes. Many past studies have been able to characterize cation-π relationships in ion channels using this technique (Ahern *et al.*, 2006; Pless *et al.*, 2011a; Pless *et al.*, 2011c). In this study, we have used fluorinated phenylalanine derivatives to assess whether cation-π interactions are involved in block of *hERG* by the well-studied *hERG* blockers terfenadine, quinidine, and dofetilide. Our data show that unnatural amino acids can be successfully incorporated into our sites of interest with minimal disruption of channel gating, and we demonstrate that cation-π interactions do not seem to make a significant contribution to *hERG* drug block at the aromatic residues Y652 and F656.

4.2 Materials and methods

4.2.1 Molecular biology - Incorporation of unnatural amino acids (UAA) through nonsense suppression was performed as described previously (Beene *et al.*, 2003). UAAs were coupled to nitroveratryloxycarbonyl as a protection group and activated as the cyanomethyl ester. This was then coupled to pdCpA (GE Healthcare/Dharmacon, Lafayette, CO), an aminoacyl dinucleotide, which was then ligated to a modified (G73) *Tetrahymena thermophile* tRNA. The amino-acylated tRNA-UAA was de-protected via ultraviolet irradiation immediately before oocyte injection.

Site-directed mutagenesis of WT *hERG* DNA in a pBluescript SK+ vector was used to make the Y652TAG and F656TAG constructs with the QuikChange II system (Stratagene). Mutations were confirmed by direct sequencing (Macrogen). DNA was linearized with *NotI* prior to RNA transcription using the mMessage mMachine T7 Ultra transcription kit (Ambion).

4.2.2 Oocyte preparation and injection - *Xenopus laevis* oocytes were used as a heterologous expression system for two electrode voltage clamp experiments. Mature female *Xenopus laevis* frogs (Boreal Science) were anaesthetized in a 2 g/L tricaine methanesulfonate solution at pH 7.4. Following anaesthetization, the animal was euthanized in accordance with University of British Columbia animal care protocols. The ovarian lobes were extracted and divided into sections of 10-20 eggs before undergoing follicular layer digestion for 1-2 hours in a 1 mg/mL collagenase A calcium free solution (82.5 mM NaCl, 2.5 mM KCl, 1 mM $MgCl_2$, 5 mM HEPES buffer, pH adjusted to 7.6). The digested eggs were then washed in the calcium free solution and stored in OR3 media (500 mL Liebovitz's L-15 medium, 15 mM HEPES, 1 mM glutamine, 500 μM gentamycin, filled to 1 L with distilled water and pH adjusted to 7.6). Stage IV and V oocytes were selected and stored at 18 ˚C prior to use. Selected oocytes were injected with roughly 80 ng of tRNA-UAA and 40 ng of mutant *hERG* cRNA in a 50 nL volume. In control experiments, the cRNA alone or the cRNA together with a tRNA coupled to pdCpA, but without an appended amino acid were injected.

4.2.3 Electrophysiology - Two electrode voltage clamp experiments were performed 1-3 days following injection. Experiments were performed using an Oocyte Clamp OC-725C (Warner Instruments) and an Axon Digidata 1440A (Molecular Devices) controlled by pClamp10

software (Molecular Devices). In experiments, oocytes were bathed in a continuous flow of ND96 media (96 mM NaCl, 3 mM KCl, 1 mM $MgCl_2$, 5 mM HEPES, 2 mM $CaCl_2$, pH adjusted to 7.4). All chemicals were obtained from Sigma-Aldrich Chemical Co. (St. Louis, MO). Microelectrodes of 0.2 to 1.0 MΩ resistances were made from borosilicate glass using a P-97 Flaming/Brown Micropipette Puller (Sutter Instruments) and were filled with 3 M KCl. Drugs were applied with a manual perfusion system. Stock solutions of 10 mM terfenadine, 10 mM dofetilide, and 100 mM quinidine in DMSO were stored at 4 ˚C and experimental solutions were obtained through dilutions of these stocks on the day of experiments. In control experiments in which a UAA-coupled tRNA was not co-injected, endogenous currents and non-selective incorporation at our site of interest were, at their largest, not found to exceed 0.2 μA tail currents at -50 mV following a prolonged depolarization. Recordings with initial tail currents of less than 0.5 μA at -50 mV following a prolonged activation were discarded. Currents were allowed to reach a stable level before beginning experimental recordings. The holding potential for all experiments was -110 mV. Recordings were performed at room temperature (20 - 22 ˚C).

4.2.4 Data analysis – Steady-state activation for all mutants was determined through conductance voltage relationships which were obtained through measuring tail currents at -110 mV following 5 s depolarizations to a range of potentials from -110 mV to +40 mV. Data points were normalized to their maximum values and then fit with a Boltzmann function of the form $G/G_{max} = 1/(1+\exp(-zF/RT(V-V_{0.5})))$, where $V_{0.5}$ is the potential of half-activation, and z is the equivalent charge.

Steady-state inactivation for all mutants was determined through a triple pulse protocol. The initial 900 ms pulse to +40 mV opens and inactivates nearly all channels present. The second pulse is a short, 30 ms pulse to a variety of potentials from -150 to +80. The aim of this pulse is to allow channels to, as the time constants of inactivation and recovery from inactivation are very rapid, settle into a steady state of inactivation at a particular potential with little contamination of the signal from channels entering a deactivated state. The third pulse is to 0 mV and the resulting instantaneous tail currents at the beginning of this pulse from each sweep can be normalized to the maximum value and then fit with a Boltzmann function of the form $G/G_{max} = 1/(1+\exp(-zF/RT(V-V_{0.5})))$, where $V_{0.5}$ is the potential of half-inactivation, and z is the equivalent charge. For the five most hyperpolarized second pulses it was found to be necessary to account for the deactivation that takes place over the 30 ms pulse. In a protocol run before measuring the steady state inactivation, we would obtain the time constants of deactivation by fully activating channels with a 900 ms +40 mV pulse, followed by hyperpolarizing pulses to potentials ranging from -150 mV to 0 mV. The kinetic data were fit with single exponential functions of the form $G = G_0 + A\, e^{-t/\tau}$ where G is the normalized response, A is the normalized amplitude, and τ is the time constant, or double exponential functions of the form $G = G_0 + A_1\, e^{-t/\tau 1} + A_2\, e^{-t/\tau 2}$, where $A_1$and A_2 are the normalized amplitudes of each component of the fit and $\tau 1$ and $\tau 2$ the associated time constants. These time constants of deactivation could be used to adjust for the amount of deactivation in the 30 ms of the second pulse of our triple pulse steady - state inactivation protocol.

Experiments detailing drug block were performed by a 5 s depolarization to 0 mV followed by a repolarization to -50 mV to remove inactivation and generate a larger signal from which to

assess current size. The holding potential used was -110 mV. Drugs were applied in increasing concentrations and allowed to reach a steady state before applying the next concentration. Half – maximal inhibition was estimated by fitting the normalized currents ($I_{drug}/I_{control}$) with a Hill equation of the form $y = A1 + ((A2-A1)/(1 + 10^{(\log K_A - [L])*h)})$, where K_A is the ligand concentration which results in half maximal block, A refers to asymptotic values, [L] refers to the concentration of drug, and h refers to the Hill coefficient.

Data are presented as mean ± standard error of the mean. F and R have their usual thermodynamic meanings and T = 293.15 K. Graphpad Prism was used to perform one-way analysis of variance with a Dunnett post-test to compare WT with mutant channel values with a significance level set at $P < 0.05$.

4.3 Results

4.3.1 Aromatic amino acids Y652 and F656 highlighted in past drug block studies - Fig. 4.1*A* depicts a cartoon of two of the four subunits of the *hERG* channel structure. Highlighted by yellow stars are the approximate locations of Y652 and F656, the two aromatic amino acids that many past studies have shown are fundamental to potent drug block of the *hERG* channel (Du *et al.*, 2014; Dumont, 1972; Fernandez *et al.*, 2004; Ficker *et al.*, 2001; Kamiya *et al.*, 2006; Kamiya *et al.*, 2008; Melgari *et al.*, 2015a; Melgari *et al.*, 2015b; Mitcheson *et al.*, 2005; Mitcheson *et al.*, 2000a; Stansfeld *et al.*, 2006). These sites are situated in the inner vestibule of the pore region which is thought to be larger than that of most K_v channels and as such can allow the pore to close around these drugs (Mitcheson *et al.*, 2000b; Thouta *et al.*, 2014). Fig. 4.1*B* gives a more detailed view of the pore region in the structure of the closely related *eag* channel.

The residues equivalent to Y652 and F656 are highlighted in pink. As can be seen in the model, residues Y652 and F656 are roughly one helical turn from one another and their aromatic side chains jut out into the pore lumen. The aromaticity of these residues has led to a suggestion that cation-π interactions may be an important factor leading to the non-selective drug block phenomenon seen in *hERG*. A cation-π interaction would be one in which a positively charged component of a drug, such as a protonated amine, interacts with the π electrons of a conjugated system, such as the π electrons of an aromatic ring.

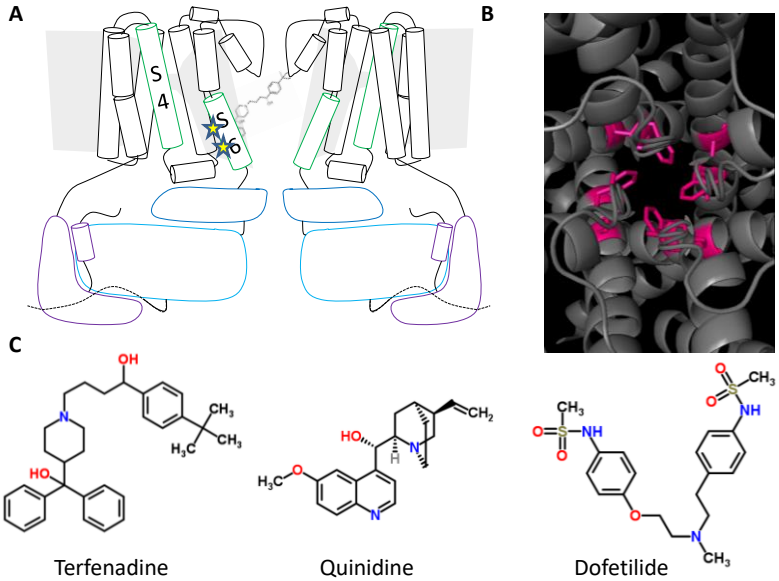

Figure 4.1 Aromatic residues Y652 and F656 in *hERG* have been shown to be important to blockade by a variety of pharmaceuticals.
(A) Cartoon schematic of approximate location of Y652 and F656 in *hERG* pore region. **(B)** Top-down view of the pore region of the closely related *eag* channel (5K7L). Residues homologous to Y652 and F656 (Y464 and F468) are highlighted in pink. **(C)** Structures hERG blocking drugs terfenadine, quinidine, and dofetilide.

4.3.2 Incorporation of unnatural amino acids into Kv 11.1 - Testing whether a cation-π relationship is occurring at an aromatic residue can be accomplished through incorporating a series of aromatic amino acid analogues, in this study phenylalanine analogues, that reduce the ability of the aromatic structure to donate their π electrons. Fluorine, as a highly electronegative

element, draws electron density towards itself. As such, incorporating it as a functional group onto a phenylalanine would reduce the ability of the aromatic ring to donate π electrons in a cation-π interaction, and would also polarize the ring and draw more electron density to the periphery. Successive fluorinations of an aromatic would yield incremental decreases in ability to donate π-electrons in a cation-π interaction (Dougherty, 1996). Through the use of nonsense suppression, we incorporated singly and doubly fluorinated phenylalanine derivatives at both Y652 and F656. These UAA also have the advantage of providing a sterically conservative means of studying the specific nature of interactions of individual residues. Should *hERG* drug interactions depend largely on cation-π binding interactions at sites Y652 and F656, then we would expect that successive fluorinations at these sites would decrease the potency for the drug in a linear manner (Dougherty, 1996). Several past studies have been able to successfully note cation–π relationships using this method (Ahern *et al.*, 2006; Lummis *et al.*, 2005; Pless *et al.*, 2011a; Pless *et al.*, 2011c). Incorporation of these unnatural amino acids was carried out through nonsense suppression, the basic steps of which are outlined in Section 4.2.1.

4.3.3 Fluorinated phenylalanine derivatives are well tolerated at Y652 and F656 - Fig. 4.2*A* shows representative traces from all mutants in two electrode voltage clamp experiments. The protocol used was a 5 s depolarization to 0 mV from a holding potential of -110 mV followed by a repolarization back to the holding potential of -110 mV. As can be seen, the unnatural amino acids are well tolerated in terms of maintaining a *hERG*-like phenotype. WT *hERG* and mutant currents elicited from this protocol exhibit little current throughout the breadth of the depolarization as channels that slowly open enter an inactivated state, but upon repolarization to – 110 mV, inactivation is relieved and a hooked tail current is observed for all of the mutant

channels. Expression varied considerably amongst the eggs injected with UAA. As such, we required that expression be able to reach a criterion of 0.5 μA tail current at -50 mV after activation. Drug block was assessed with a step to -50 mV after a prolonged activation. We assessed the parameters of steady state voltage dependence of activation and steady state voltage dependence of inactivation for each mutant construct. The unnaturally incorporated phenylalanine is termed as Y652F* or F656F*, the singly fluorinated phenylalanine incorporation is termed as Y652F1 or F656F1, and the doubly fluorinated phenylalanine incorporation is termed as Y652F2 or F656F2.

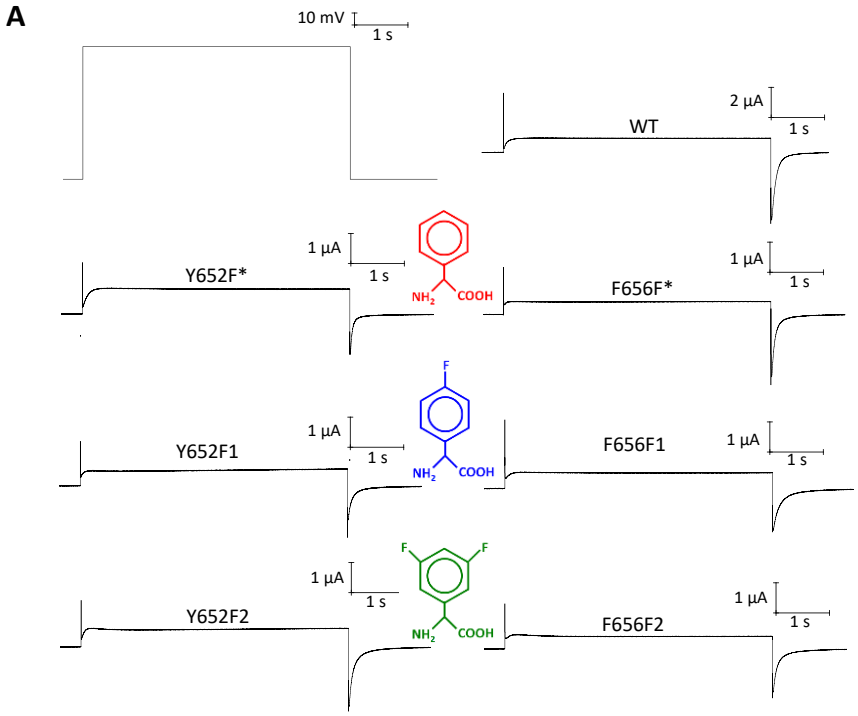

Figure 4.2 Incorporation of unnatural and natural amino acids through nonsense suppression is well tolerated at both Y652 and F656.
(A) A 5s depolarization to 0 mV from a holding potential of -110 mV was used to assess construct expression. All mutants were successfully expressed via nonsense suppression and representative traces are displayed here.

4.3.4 Voltage dependence of activation - Fig. 4.3*A* shows representative traces from WT, Y652F2, and F656F2 elicited from a protocol (inset) used to assess the voltage dependence of activation for all mutants. Initially, the lower depolarizing pulses do not activate any of the *hERG* channels and no tail currents result. Upon larger depolarization, channels activate slowly and inactivate quickly, leaving little current passing throughout the depolarization. Upon repolarization, recovery from inactivation is very fast and deactivation is slow so the very top of the resultant hooked tail current at -110 mV is a reliable indication of the proportion of channels that have reached the open state. With larger depolarizations, channels will activate more quickly and at the end of the 5 s more channels will be in an open state. Eventually, a maximal number channels will be open at the end of these depolarizations and a limit on the size of the tail current will be reached. The tail current at – 110 mV can be fit with a Boltzmann curve as a function of the depolarizing pulse that preceded it to give an idea of the voltage dependence of activation of the channel.

4.3.5 Voltage dependence of activation is unchanged amongst Y652 mutants - The phenylalanine mutation at position Y652 had little effect on the steady state voltage dependence of activation. Similarly, as can be seen in Fig. 4.3*B*, none of the fluorinated Y652 mutants resulted in a change in steady state voltage – dependence of activation. $V_{0.5}$ values obtained for all constructs were: WT *hERG* -25.5 ± 0.7 mV (n = 9); Y652F* -27.0 ± 0.6 mV (n = 15); Y652F1 -27.4 ± 0.7 mV (n = 8); Y652F2 -26.7 ± 1.0 mV (n = 11).

4.3.6 Voltage dependence of activation left-shifted upon increased phenylalanine fluorination at F656 - In Fig. 4.3*B* we see that upon increasing the level of fluorination seen at

F656, we see a corresponding slight left shift in voltage dependence of activation. $V_{0.5}$ values obtained for all constructs were: WT *hERG* -25.5 ± 0.7 mV (n = 9); F656F* -28.3 ± 1.8 mV (n = 10); F656F1 -32.8 ± 2.0 mV (n = 7); F656F2 -37.5 ± 1.9 mV (n = 9). While there was no statistical difference between fluorinated F656 constructs, Fig. 4.3*C* shows the Boltzmann curve fits for the F656 series of fluorinated phenylalanine mutants and their leftward shifts upon increased fluorination at F656. Table 4.1 displays $V_{0.5}$ and equivalent charge for all constructs.

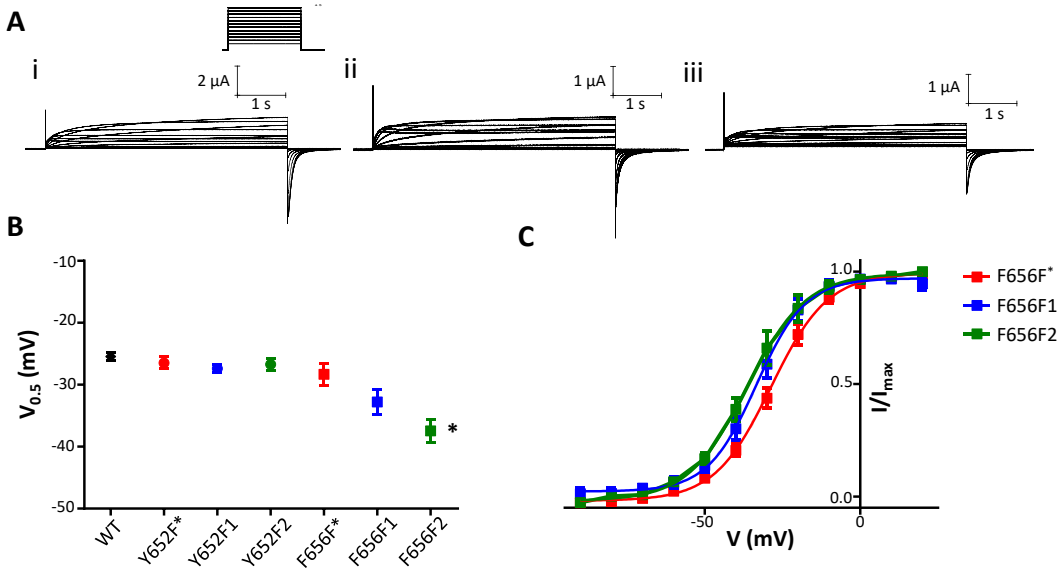

Figure 4.3 Voltage-dependent activation of Y652 fluorinated series unchanged, however increased fluorination of phenylalanine at position 656 results in increasing left shift in voltage dependence of activation.
(A) Ionic current from (i) WT (ii) Y652F2 and (iii) F656F2 mutant *hERG* channels recorded during (iii) 5 s depolarizations from -110 mV to 20 mV in 10 mV increments followed by repolarization to -110 mV (protocol inset in (i)). Pulses were applied every 7 s. **(B)** $GV_{0.5}$ and equivalent charge values for all constructs. GV_{act} fit parameters are shown in Table 4.1. **(C)** GV relationships of the UAA mutants at position 656 as measured from tail currents at -110 mV.

4.3.7 Voltage dependence of inactivation unchanged for all constructs - Several past studies have suggested that drugs that block *hERG* have a selective preference for binding to the inactivated state of the channel and so it was important to measure inactivation properties of the mutants. The steady-state voltage dependence of inactivation was assessed by a triple pulse protocol as shown in the inset of Fig. 4.4*A*, and more details are provided in Methods. As can be seen in Fig. 4.4*B*, the steady-state voltage dependence of inactivation did not vary considerably amongst mutant channels and no statistical differences were detected for any of the mutant channels when compared to WT with a Dunnett post – test. Table 4.1 shows $V_{0.5}$ and equivalent charge for all constructs.

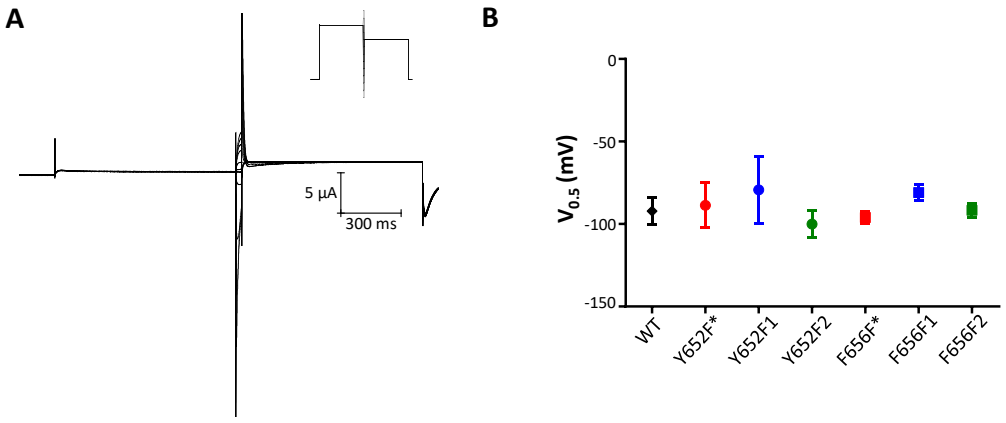

Figure 4.4 Voltage dependence of inactivation unchanged among mutant channels.
(A) Representative trace of WT *hERG* as assessed by the inactivation protocol inset. The protocol is described in further detail in Methods. **(B)** Voltage dependent inactivation V0.5 values of all constructs. GV_{inact} fit parameters are shown in Table 4.1.

	Activation			Inactivation		
Constructs	$V_{0.5}$ (mV)	z	n	$V_{0.5}$ (mV)	z	n
WT	-25.5 ± 0.7	3.8 ± 0.1	9	-92.3 ± 7.4	1.1 ± 0.2	3
Y652F*	-27.0 ± 0.6	3.2 ± 0.2	15	-88.7 ± 13.6	0.6 ± 0.1*	5
Y652F1	-27.4 ± 0.7	2.3 ± 0.1	8	-79.3 ± 20.5	0.6 ± 0.1*	4
Y652F2	-26.7 ± 1.0	3.1 ± 0.1	11	-100.1 ± 8.4	0.8 ± 0.0	5
F656F*	-28.3 ± 1.8	3.0 ± 0.2	10	-96.1 ± 3.7	1.1 ± 0.1	6
F656F1	-32.8 ± 2.0	3.2 ± 0.1	7	-81.0 ± 4.8	0.9 ± 0.1	4
F656F2	-37.5 ± 1.9 *	3.2 ± 0.2	9	-91.7 ± 4.2	1.2 ± 0.2	6

Table 4.1 Activation and inactivation parameters for WT and mutant constructs.

4.3.8 No evidence of a cation-π relationship detected for *hERG* terfenadine block at Y652 or F656 - Fig. 4.5*A* shows the protocol used to assess drug block. From a holding potential of -110 mV, a 5 s depolarization to 0 mV opens available channels as assessed by the GV relationships, and then a step is made to -50 mV where inactivation is largely removed and a large tail current appears, before the potential is returned to the holding potential. This protocol is repeated in successive sweeps as either control or drug containing solutions flow into the bath chamber and over the oocyte. A higher concentration of drug is not started until the last concentration of drug has reached a steady state level of block. Fig. 4.5*B* shows representative traces of constructs Y652F* and F656F* in solutions of no drug and in solutions with terfenadine concentrations of 10 nM, 30 nM, 100 nM, 300 nM, and 1 μM. Upon introduction of 10 nM terfenadine, minimal block is observed at -50 mV, but upon introduction of 30 nM terfenadine the amplitude of the current at -50 mV becomes observably reduced. This reduction in current due to terfenadine block of *hERG* increases with increasing concentration of terfenadine. The steady state current at -50 mV achieved at each drug concentration was normalized to the steady state current at -50 mV with no drug. From these normalized values, a concentration–response curve was generated and fit with a Hill equation. An IC_{50} and Hill coefficient (h) were generated from each Hill fit.

The IC_{50} for the F656 mutants remains unchanged upon increased fluorination of the phenylalanine. The IC_{50} of the Y652 mutants is greatly increased for the singly fluorinated mutant, but not the doubly fluorinated mutant. It is only when the C4 carbon of the phenylalanine is fluorinated that this reduced potency effect is seen. This is not what would be expected in a cation-π relationship. Fig. 4.5*D* shows the concentration response curves for the Y652 fluorinated phenylalanine mutants. The Y652F1 mutant is greatly left-shifted compared to the WT *hERG*, Y652F*, and Y652F2 constructs. Table 4.2 shows IC_{50} and Hill coefficients for all constructs.

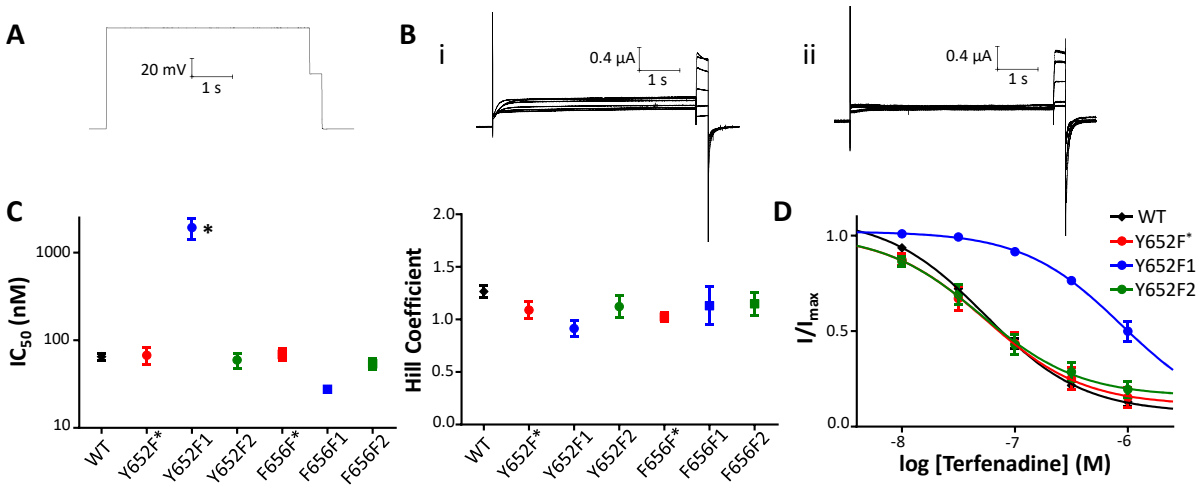

Figure 4.5 Fluorination of phenylalanine at residue 656 does not reduce terfenadine potency; however, fluorination of the phenylalanine at residue 652 at the C4 carbon of the phenyl ring results in a large reduction in terfenadine potency.
(A) Protocol used to evaluate drug block. From a holding potential of -110 mV, channels are depolarized to 0 mV for 5s and are then repolarized first to -50 mV for 300 ms and then back to -110 mV. **(B)** Currents from (i) Y652F and (ii) F656F* in response to terfenadine concentrations of 10, 30, 100, 300, 1000 nM. **(C)** Terfenadine IC_{50} and Hill Coefficients. IC_{50} and h fit parameters are found in Table 4.2. **(D)** Concentration response curve of WT and Y652F series.

4.3.9 No evidence of a cation-π relationship detected for *hERG* quinidine block at Y652 or F656 - Fig. 4.6*A* shows representative traces of constructs Y652F2 and F656F2 in solutions of no drug and in solutions with quinidine concentrations of 2 μM, 6 μM, 20 μM, 60 μM, and 200 μM. The steady state current at -50 mV achieved at each drug concentration was normalized to the steady state current at -50 mV with no drug. From these normalized values, a concentration – response curve was generated and fit with a Hill equation. An IC_{50} and cooperativity factor were generated from each Hill fit. Fluorination of the phenylalanine at both Y652 and F656 results in a decrease in drug potency and thereby an increased IC_{50}. At Y652, as seen with the terfenadine data, fluorination only reduced potency when the fluorine was incorporated in the C4 carbon position. The F2 mutant was again unaffected by fluorination as compared as compared to WT. Again, this is not consistent with what would be expected if cation-π interactions were a primary determinant of drug binding. The F656 fluorinated phenylalanine constructs all exhibited a decrease in potency to the same degree upon any level of fluorination. Fig. 4.6*C* shows the concentration response curves for both the Y652 and F656 families of fluorinated phenylalanine mutants. Table 4.2 shows IC_{50} and Hill coefficients for all constructs.

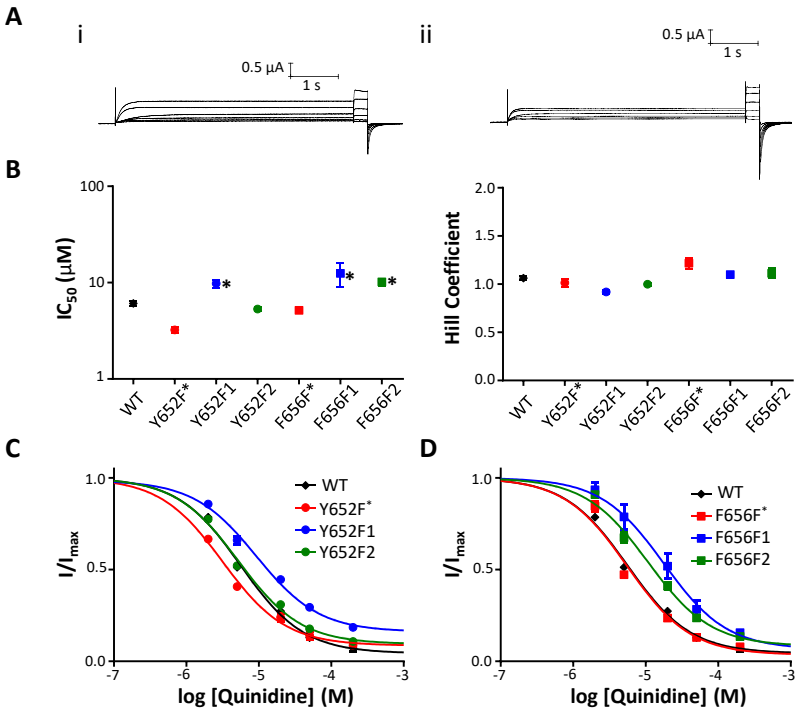

Figure 4.6 Fluorination of phenylalanine at residue 656 reduces quinidine potency; however, fluorination of the phenylalanine at residue 652 only results in reduced potency if fluorination occurs at the C4 carbon. **(A)** Currents from (i) Y652F2 and (ii) F656F2 elicited from the protocol shown in Fig. 4.5A in response to quinidine concentrations of 2, 6, 20, 60, 200 µM **(B)** Quinidine IC_{50} and Hill Coefficients. IC_{50} and h fit parameters are shown in Table 4.2. **(C)** Concentration response curves of Y652 fluorinated mutant series and WT **(D)** Concentration response curves of F656 fluorinated mutant series and WT.

4.3.10 No evidence of a cation-π relationship detected for *hERG* dofetilide block at Y652 or F656 - Fig. 4.7*A* shows representative traces of constructs Y652F1 and F656F1 in solutions of no drug and in solutions with dofetilide concentrations of 10 nM, 30 nM, 100 nM, 300 nM, and 1 µM. The steady state current at -50 mV achieved at each drug concentration was normalized to the steady state current at -50 mV with no drug. From these normalized values, a concentration-response curve was generated and fit with a Hill equation. An IC_{50} and cooperativity factor were generated from each Hill fit. Similar to what was seen with terfenadine, fluorination had little

effect on potency of dofetilide block at position F656. Also similar to what was seen with both terfenadine and quinidine, fluorination of the C4 carbon for the Y652 fluorinated phenylalanines reduced potency, but Y652F2 potency was unaffected (similar to WT and Y652F*). Table 4.2 shows IC_{50} and Hill coefficients for all constructs.

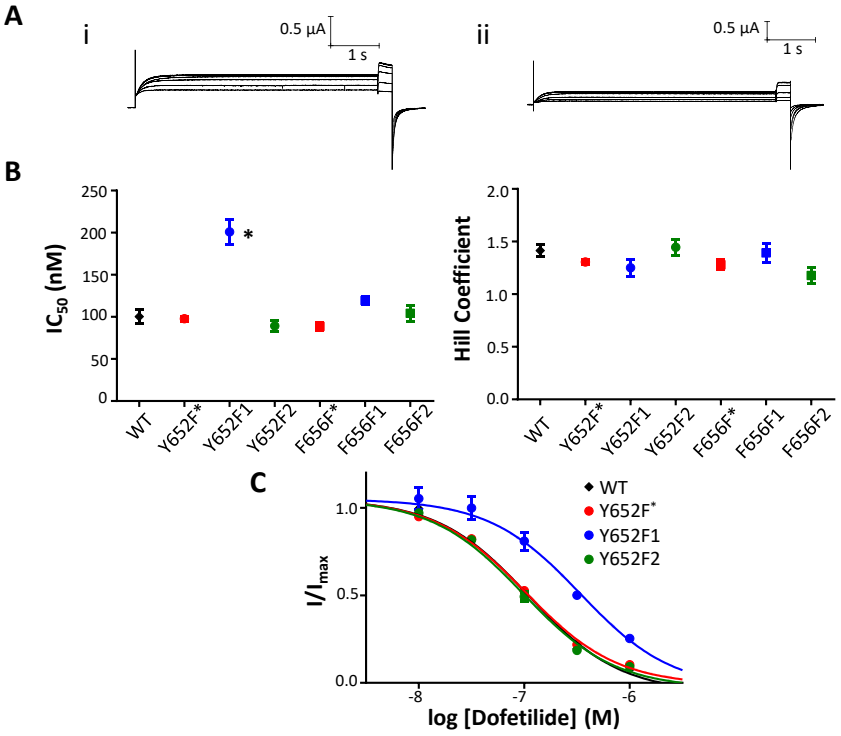

Figure 4.7 Fluorination of phenylalanine at residue 656 does not reduce dofetilide potency; however, fluorination of the phenylalanine at residue 652 at the C4 carbon of the phenyl ring results in a large reduction in dofetilide potency.
(A) Currents from (i) Y652F1 and (ii) F656F1 in response to dofetilide concentrations of 10, 30, 100, 300, 1000 nM. **(B)** Dofetilide IC_{50} and Hill Coefficients. IC_{50} and h fit parameters are shown in Table 4.2. **(C)** Concentration response curve of WT and Y652F series.

	Terfenadine			Quinidine			Dofetilide		
Constructs	IC_{50} (nM)	h	n	IC_{50} (μM)	h	n	IC_{50} (nM)	h	n
WT	65± 6	1.3± 0.1	7	6.1± 0.4	1.1± 0.0	4	100 ± 8	1.4 ± 0.1	5
Y652F*	67± 15	1.1± 0.1	7	3.2± 0.2	1.0± 0.0	6	98± 3	1.3± 0.1	4
Y652F1	1900± 700 *	0.9± 0.3	3	9.8± 0.9 *	0.9± 0.0	6	200± 15*	1.3± 0.1	6
Y652F2	59 ± 12	1.1± 0.1	8	5.3± 0.3	1.0± 0.0	8	90 ± 6	1.4± 0.1	4
F656F*	69 ± 11	1.0± 0.0	4	5.2± 0.2	1.3± 0.2	5	89 ± 5	1.3± 0.0	6
F656F1	28± 3	1.1± 0.2	4	16 ± 4.0*	1.1 ± 0.1	3	119± 5	1.4± 0.1	4
F656F2	54± 7	1.1± 0.1	4	10.2± 0.9*	1.1± 0.1	6	104± 10	1.2± 0.1	3
Cation – π behaviour?	No			No			No		

Table 4.2 Concentration of half maximal block and Hill coefficient for WT and all mutant constructs.

4.4 Discussion

The *hERG* channel is a major anti-target in the drug development process. The main determinants of drug interaction in *hERG* are two aromatic residues in the S6 transmembrane segment: Y652 and F656 (Kamiya *et al.*, 2008; Mitcheson *et al.*, 2000a; Vandenberg *et al.*, 2012). The aromaticity of these two residues has led to suggestion that the basis of this generalized drug interaction is due to molecular interactions specific to the π-electrons of aromatic systems (Boukharta *et al.*, 2011; Fernandez *et al.*, 2004; Knape *et al.*, 2011; Melgari *et al.*, 2015b; Mitcheson, 2003; Pearlstein *et al.*, 2003; Perry *et al.*, 2004; Sanguinetti and Tristani-Firouzi, 2006; Stansfeld *et al.*, 2007). Through two electrode voltage clamp experiments and unnatural amino acid mutagenesis, this study has attempted to determine the extent to which cation-π drug-protein interactions play a role in the molecular basis of *hERG* drug block at Y652 and F656. Our experiments have found no evidence indicating that cation-π interactions play a significant role in *hERG* drug block at either Y652 or F656.

4.4.1 State-dependence of *hERG* drug block - Several past studies have suggested that a variation of the modulated receptor hypothesis (Hille, 1977) may apply to the *hERG* channel (Lees-Miller *et al.*, 2000; Perrin *et al.*, 2008; Vandenberg *et al.*, 2012; Wang *et al.*, 1997b; Yang *et al.*, 2004). These studies have noted that some drugs that block the *hERG* channel seem to preferentially interact with the inactivated state(s) of the channel (Lees-Miller *et al.*, 2000; Perrin *et al.*, 2008; Wang *et al.*, 1997b; Yang *et al.*, 2004). The effect of inactivation gating on drug block is drug dependent and is not fully understood (Perrin *et al.*, 2008). All drugs investigated in our study have been shown by Yang *et al.* in 2004 to exhibit inactivation-dependent block (Yang *et al.*, 2004). The study found that by introducing the inactivation-deficient S631A mutation, the potency of dofetilide, terfenadine, and quinidine were all reduced. As such, we sought to assess whether the constructs used in our experiments affected the voltage dependence of inactivation as any large change in this parameter could have the effect of making interpretation of our later drug block data difficult.

Our data (Fig. 4.4) show no significant differences in the voltage dependence of inactivation. Therefore, any significant changes amongst constructs in drug potency are unlikely to be attributable to changes in inactivation state-dependence. We did not measure the kinetics of onset of inactivation and recovery from inactivation of our constructs. From comparing ionic current traces of WT with our mutant constructs, it seems evident that these processes are still fast enough that, should there have been any small changes in these parameters, it would not have affected our later drug block experiments as there would have been sufficient time for inactivation to reach steady state in all steps of that protocol.

We also determined the voltage dependence of activation for all of our constructs (Fig. 4.3). The fluorinated Y652 series of constructs showed no change in voltage dependence of activation. At F656 there was a small increasing left-shift of the GV curve upon increasing fluorination of the aromatic ring. The $V_{0.5}$ of activation shifted from -28.3 ± 1.8 mV for F656F* to -32.8 ± 2.0 mV for F656F1 to -37.5 ± 1.9 mV for F656 F2. The change in this parameter is unlikely to have an effect on our ability to accurately measure drug block of the channel as our voltage protocol to assess drug block involves an initial 5 s depolarization to 0 mV, which would be sufficient to bring all constructs to a near maximal state of conductance. We did not pursue this phenomenon further in this study as the purpose of this work was to investigate the molecular basis of drug block at Y652 and F656. More work would be needed to detail the basis of this left-shift in GV curve.

4.4.2 No evidence of cation-π activity at either Y652 or F656 - Our data show that cation-π interactions do not seem to play a role at either Y652 or F656 in the drug interaction of *hERG* with terfenadine, quinidine, or dofetilide (Figs. 4.5, 4.6, and 4.7). Should a cation-π interaction have been taking place at either site then upon further fluorination of the phenyl ring we would expect to see a further increase in IC_{50}, indicating a reduced potency of the drug for the binding site (Dougherty, 1996). Interestingly, the potencies of all drugs studied, as reflected by IC_{50} values, were initially decreased with single fluorination of the phenylalanine derivatives at Y652. However, upon doubly fluorinating the phenylalanine derivatives, the potency of the drug interaction remained unchanged as compared to the WT channel. As can be seen in Fig. 4.2*A*, the site of fluorine incorporation in the F1 and F2 phenylalanine derivatives are on different carbons of the phenyl ring. The F1 fluorine is incorporated at the C4 position, whereas the F2 fluorines

are incorporated at the C3 and C5 positions. The C4 position appears to be important to some sort of interaction that is weakened when the site is polarized, such as in an introduction of a fluorine to this position. However, in the WT channel the native tyrosine residue would have an alcohol group at the C4 position. This makes it seem unlikely that polarity of that specific region of the phenyl ring is important. The mutant channel Y652W also conserves the potency of drug block and can even reintroduce drug block in non-inactivating constructs (Fernandez *et al.*, 2004; Wu *et al.*, 2015). Many *in silico* molecular dynamics studies have studied the interactions taking place during *hERG* drug block and a common finding is that Y652 is involved in π-stacking interactions. Substituent effects on π-stacking interactions are still under debate and, as such, it is difficult to conclude much about this potential relationship of drugs with Y652. There is the potential that the fluorine incorporation at the C4 position introduces changes to the electrostatic potential of the phenyl ring in a way that disrupts the π-stacking relationship. Alternatively, should drug interactions at Y652 largely be coordinated through hydrophobic interactions, then polarization of the ring could potentially decrease drug potency. It would have to be a very site-specific hydrophobic interaction, though, as the doubly fluorinated phenylalanine derivative did not change drug potency.

Another possibility to consider is that the singly fluorinated UAA introduces a steric change in the orientation of the pore region that makes it less favourable for drug interaction. We think this to be unlikely because of the subtlety of the substitution. However, the increased polarization of the ring upon C4 fluorination would increase the hydrophilicity of the structure, but whether or not this would be enough to affect larger changes in pore structure can only be speculated upon.

All that can be said conclusively about our introductions of fluorinated phenylalanine derivatives at Y652 is that our results are not indicative of a cation-π interaction.

Drug potency in experiments involving fluorinated phenylalanine derivatives incorporated at F656 was not affected in terfenadine or dofetilide drug block. In experiments involving quinidine, potency was reduced upon any degree of fluorination. Neither of these behaviours are indicative of a cation-π interaction.

Should the interaction taking place at these aromatic residues of the *hERG* pore region not involve a cation-π interaction, what interaction is taking place? The data provided in this study are insufficient to specify a means of molecular interaction. However, one past study suggests that the aromaticity of residue 652 is important for the drug block effect to take place and that the residue at 656 needs only be a hydrophobic residue in order to be prone to drug block (Fernandez *et al.*, 2004). Our study indicates that at Y652, the aromaticity needs to be paired with an appropriate substituent on the C4 position of the phenyl ring to preserve WT-like levels of drug block. Recent structural studies investigating molecular dynamics of *hERG* drug block have suggested a π-stacking relationship at Y652 and hydrophobic interactions at F656 being the basis for the importance of these residues to *hERG* drug block (Boukharta *et al.*, 2011; Stansfeld *et al.*, 2007). Unfortunately, a crystal or cryo-EM structure of *hERG* is still lacking, and in order to understand how these two aromatic residues interact with drugs in the pore region, past studies have relied on structures of other potassium channels on which to base *hERG* homology models. However, MthK, KcsA, and Kv2.1/1.2 all lack substantial sequence identity with *hERG*, which

makes it difficult to definitively identify specific molecular interactions between drug and *hERG* pore residues.

Several past studies have been able to show significant cation-π relationships with respect to drug-protein interaction as well as protein-protein interaction (Ahern *et al.*, 2006; Lummis *et al.*, 2005; Pless *et al.*, 2011c; Pless *et al.*, 2008). In our study, neither of the aromatic residues of the S6, noted for their importance to drug block, exhibited increasingly reduced drug block upon increased fluorination at either site. At Y652, only upon fluorination of the C4 carbon was drug sensitivity significantly reduced. At F656, there was no appreciable effect for terfenadine or dofetilide block upon increased fluorination. For quinidine blockade, upon any degree of fluorination at F656, there was a reduction in potency to a similar extent. None of the potency-fluorination relationships are indicative of a cation-π relationship (Beene *et al.*, 2003; Dougherty, 1996).

In summary, this study shows that cation-π interactions do not appear to play a major role in *hERG* drug block at either Y652 or F656. This study contributes significantly to the understanding of *hERG* drug block as it provides experimental data in support of previous molecular dynamic drug docking studies that have argued against cation-π activity being largely responsible for *hERG* drug block.

Chapter 5: Conclusion

5.1 Scientific rationale for investigating *hERG* structure-function

Ion channels coordinate the complex electrical activity of life. These pore-forming membrane proteins, through their selectivity and gating differences, provide the means for phenomena such as the cardiac action potential and the impressively complicated workings of the nervous system. The functional differences among different ion channels can be attributed to permutations in the channel structure that change the tertiary and quaternary structure of the protein in ways that alter gating or selectivity. For example, a conventional voltage-gated sodium channel activates much more quickly than a conventional voltage-gated potassium channel. One study has suggested this to be a result of specific non-charged residues of the S2 and S4 segments, 'speed-control residues', as well as a beta-subunit interaction that speeds the activation gating of the sodium channel (Lacroix *et al.*, 2013). The faster activation of the sodium channel is physiologically relevant when you consider the respective roles for sodium and potassium ion channels. Identifying roles for specific amino acids or regions of the channel can also be informative as to the gating, pharmacology, temperature dependence, cofactor regulation, and tetramerization of the channel.

For many potassium channels, much is known about the functional roles of certain structural features. This can be largely attributed to the crystal structures of potassium channels that have been solved in the last two decades (Doyle *et al.*, 1998; Long *et al.*, 2005; Long *et al.*, 2007; Whicher and MacKinnon, 2016). While these structures give only a static description of a dynamic system, they have done much to inspire functional studies describing aspects of

channels that endow specific channels with specific properties. However, some voltage-gated potassium channels lack homology with the structures that have been solved. For the longest time, one such channel was *hERG* (a structure of the *eag* channel was recently solved with cryo-electron microscopy (Whicher and MacKinnon, 2016)). This lack of homology with channels with solved structures paired with the unusual gating and drug block susceptibility properties of *hERG* has inspired many studies aiming to identify structural bases for these attributes. Despite the efforts of many labs investigating *hERG* gating and drug block, a full understanding of the structural bases of these phenomena remains to be detailed. This thesis has sought to describe structural features of the *hERG* channel that endow it with its unique gating and drug block properties. Specifically targeted are the basis of slow *hERG* activation and deactivation, the role of the cytoplasmic domains in gating charge movement, and the molecular basis of *hERG* drug block at the aromatic amino acids Y652 and F656.

5.2 Basis of *hERG* slow activation

The first studies detailing the kinetics of *hERG* noted that activation of the channel was unusually slow for a VGKC (Sanguinetti *et al.*, 1995; Schonherr and Heinemann, 1996; Trudeau *et al.*, 1995; Wang *et al.*, 1997a). This could be due to slow movement of the voltage-sensing domain upon a change in membrane potential limiting the activation of ionic current or through a poor coupling of the voltage-sensing domain with the pore domain. The second chapter of this thesis has shown that, not only is the activation of gating charge much slower than one sees in a conventional VGKC, but the coupling of gating charge movement to the pore also bears responsibility in slowing the activation of ionic current at physiological potentials. This conclusion is in line with past works noting the slow activation of the voltage sensor (Piper *et al.*,

2003; Smith and Yellen, 2002), but strongly suggests that poor coupling of the VSD to the pore plays a considerable role as well. The much slower time constants of ionic activation as compared to those of gating indicate a slow coupling step of the gating charge to the pore domain (Fig. 2.2). This step would be one in which little gating charge is carried. Fluorophore incorporation at L520 has noted an FV relationship that overlays the GV relationship (Es-Salah-Lamoureux *et al.*, 2010; Smith and Yellen, 2002). This could be an indication of a late movement of the voltage sensing domain, possibly concerted, that is responsible for pore opening. Concerted transitions late in the activation pathway have been suggested for *Shaker* channels and have been suggested to be rate-limiting in pore activation (Ledwell and Aldrich, 1999). Alternatively, these fluorescence reports could be detailing movements of neighboring transmembrane segments moving in response to opening processes of the channel.

Experiments described in Chapter 3 have detailed the role of an intra-subunit interaction that slows activation by stabilizing early closed states of the channel. In this chapter, D411 in the S1 segment is shown to be a major determinant of the slow activation gating of *hERG*. Our double mutant cycle analysis experiments and past studies (Cheng *et al.*, 2013; Zhang *et al.*, 2005) suggest that D411 is likely involved in an electrostatic interaction with K538 and that residues near K538 in the S4 are important for correct positioning of K538. These interactions serve to stabilize a closed-state of the channel. The mutation D411N disrupts the interaction with K538 and significantly left-shifts the QV relationship. It also has the effect of increasing the rate of gating charge activation to faster time constants than the voltage-independent transition that we had observed in Chapter 2. Through interaction with the K538, D411, which is unique to the *eag*

family of VGKC, may be introducing an additional energetic barrier to channel activation not present in conventional VGKC.

5.3 Voltage dependence of activation

In Chapter 2, in experiments detailing the relationship of charge movement to the pore opening in activation of the channel, we found that the charge-voltage relationship was left-shifted to the opening of the pore by approximately 20 mV. A previous study by Piper *et al.* (2003) had a similar finding, and this phenomenon is also well-described in the *Shaker* potassium channel (Piper *et al.*, 2003; Stefani *et al.*, 1994). This left-shifted QV relative to the GV may be a reflection of pore opening requiring activation of all four voltage-sensors. For example, if one considers a single channel, should 3 out of 4 voltage sensors activate, the pore would not open, but three quarters of available charge would have moved, hence the left-shift in the QV relationship. Alternatively, this left-shift may indicate that the majority of charge movement is involved in conformational changes in the voltage sensing domain that occur prior to the opening of the pore region and that a subsequent movement of the VSD that does not involve much charge is responsible for pore opening. Hyperpolarized movements of gating charge were also reflected in fluorophore reports from the top of the S4 (Fig 3.5). These movements are likely to reflect early closed state transitions of the channel.

5.4 The role of the cytosolic domains in gating

The cytosolic domains of the *hERG* channel have been noted to play a unique role in the slow deactivation kinetics of the channel. Mutagenesis, cross-linking, and crystal structure studies have detailed interactions between the PAS domain of the N-terminus and the CNBHD domain

of the C-terminus (Gianulis *et al.*, 2013; Gustina and Trudeau, 2011, 2012; Haitin *et al.*, 2013; Morais-Cabral and Robertson, 2015; Morais Cabral *et al.*, 1998; Schonherr and Heinemann, 1996; Trudeau *et al.*, 1995; Wang *et al.*, 1998). This interaction serves to stabilize the open state of the channel. In Chapter 2, we investigated the role of the N-terminus in channel gating through gating current experiments using a cut open Vaseline gap voltage clamp apparatus. In order to study the role of these domains, we observed currents in WT, R56Q, R4AR5A, and an N-terminally truncated mutant. All mutants resulted in increased rates of deactivation gating, the ΔN mutant having the most increased rate of deactivation. The determination of the crystal structure of the *eag* channel cytosolic domains suggested that slowed deactivation was conferred on the channel through interaction of the cytosolic domains (Haitin *et al.*, 2013). Our experiments do not confirm or reject this study's finding, but only serve to show that mutations in the N-terminal domain can have significant effects on channel deactivation, primarily through destabilizing the open state of the channel.

The structure of the *eag* channel was recently determined by the Mackinnon lab using cryo-electron microscopy (Whicher and MacKinnon, 2016). The high homology of this closely related channel provides us an idea of what the general structure of *hERG* may look like. The structure suggests that the cytosolic domains play a novel role in the gating of the *eag* family. The authors of this study suggest that the S4 segment interacts directly with the C-linker of the C- terminus of the *hERG* channel to impose or relieve constraints of the bend of this segment that would lead to opening or closing of the pore region. Further functional work would need to be done to validate this finding.

5.5 *hERG* 1b involvement in vivo

Whether or not the gating role of the N-terminal domain is physiologically relevant is an issue that has come up recently in the literature. The studies of *hERG* presented in this thesis are all of homotetramers of the 1a transcript of the channel. Several studies have provided evidence that an alternate transcript, *hERG* 1b, is also present in significant levels and that it forms heterotetrameric proteins with the *hERG* 1a subunits (Jones *et al.*, 2004; Sale *et al.*, 2008). The *hERG* 1b transcript lacks the first 5 exons of the KCNH2 gene, which are the exons that code for the N-terminus. As a concatamer study had shown that slow deactivation is an all-or-none concerted process (Thomson *et al.*, 2014), heteromeric channels with just one *hERG* 1b subunit would not have the slow deactivation kinetics that the homomeric 1a channels display. Thus, the gating properties introduced by this large N-terminal domain in the homotetramers may have no real bearing in a physiological system should the majority of channels be heterotetramers. They would also display a greatly diminished mode shift of gating charge as indicated by our findings in Chapter 2. Future experiments could assess the validity of phenomena like the mode shift and N-terminal open-state stabilization through experiments involving *hERG* 1a/1b concatemers with N-terminal mutations in the *hERG* 1a subunits.

hERG 1a/1b heteromers are faster to activate than 1a homomers, but are still slower to activate than conventional K_v channels (Sale *et al.*, 2008). We suggest that the D411-S4 interaction described in Chapter 3 is likely still a factor influencing slow activation in the heteromeric channels. It would be of interest to show this interaction in a heteromeric system.

5.6 The voltage independent transition of *hERG* gating

The voltage independent transition of *hERG* gating was first proposed by Liu *et al.* in 1996 (Liu *et al.*, 1996). This study was done in ferret myocytes and suggested that *hERG* channel activation gating involved both voltage- dependent and independent transitions. A year later, in a study that extensively analyzed all *hERG* kinetic parameters, Wang *et al.* also described this voltage-independent transition. In this study, the group proposed a five state model of channel gating (Wang *et al.*, 1997a). In this model, the channel would transition through several closed states before opening, similar to that described for several K_v channels prior to that. This transition through several closed states can be noted in the different fluorescence signals that can be observed with fluorophore incorporation in different sites as well as the different movements of *hERG* gating charge (Es-Salah-Lamoureux *et al.*, 2010; Fougere *et al.*, 2011; Smith and Yellen, 2002; Tan *et al.*, 2012). The delay in ionic current activation time course also suggests the presence of movement through several closed states (Schoppa and Sigworth, 1998).

Chapter 2 details the voltage-independent step in activation gating as one being evident in both gating charge movement as well as ionic current activation of *hERG*. In this study, we detailed a convergence and stagnation of the activation kinetics of charge movement and pore opening at depolarized voltages. We attributed this to being either a result of the voltage-independent step being a transition that occurs upstream of the movement of the bulk of gating charge or, alternatively, a fundamental limit to the speed at which the voltage sensor can move across the pore. Interestingly, in Chapter 3, we found that upon disruption of the D411 interaction with the bottom of the S4 segment, the time constants of activation were increased and were much faster than time constants of activation determined at potentials at which the voltage-independent step

was rate limiting. This finding suggests that either the voltage-independent transition precedes the movement of the bulk of gating charge movement, or that the disruption of this interaction changes the activation pathway that increases the speed limit at which the voltage sensor can move through the pore as a means of sensing voltage change.

Several models of *hERG* gating have placed the voltage-independent transition later in the gating pathway, at a point after the bulk of gating charge has moved (Clancy and Rudy, 2001; Mazhari et al., 2001). Our data indicates that this is incorrect as the time constant of activation for gating charge movement and pore opening converge at high potentials. This indicates that the voltage-independent transition occurs at a time prior to the movement of the majority of gating charge.

5.7 The two components of *hERG* charge movement

Activation of the *hERG* gating charge, as observed in gating current experiments and fluorescence experiments, exhibits two phases of movement: Q_{fast} and Q_{slow} (Es-Salah-Lamoureux *et al.*, 2010; Goodchild *et al.*, 2015; Piper *et al.*, 2005; Piper *et al.*, 2003; Wang *et al.*, 2013). This was first detailed in *hERG* gating currents by Piper *et al.* in 2003 (Piper *et al.*, 2003). Gating currents from *hERG* in a mammalian expression system were later described in 2013 by the Fedida lab (Wang *et al.*, 2013). This system noted much faster rates of activation along with the two phases of charge movement. Both studies had suggested that Q_{fast} may reflect transitions between early closed states of the activation pathway. In *Shaker* channels, which also display this biphasic charge movement, it has been suggested that Q_{fast} is related to conformational changes that disrupt acidic residue interactions with the basic residues of the S4 (Perozo *et al.*, 1994). Our experiments in Chapters 2 and 3 confirmed the presence of this

biphasic movement of gating charge in the WT channel. In Chapter 3 we found that this biphasic nature of charge movement may result from an interaction between D411 of the S1 segment and the bottom of the S4. Disruption of this interaction results in both an elimination of Q_{fast} and an increase in the rate of activation of Q_{slow}. This result, along with the left-shift in voltage dependence of activation of constructs that had lost the fast-component of gating charge, indicates that this D411-bottom of the S4 interaction serves to stabilize an early closed state of the channel. The fast component of gating charge movement is only loosely voltage-dependent, and has its voltage dependence of activation right shifted by roughly 50 mV to that of the movement of the rest of gating charge, though this voltage dependence is extremely difficult to accurately measure as the proportion of fast-gating charge movement continues to increase well after the overall charge-voltage relationship has plateaued (Piper *et al.*, 2003). This loose voltage dependence seems to, as shown in Chapter 3, act as an overall rate limit to channel activation.

As we have placed the voltage-independent transition as one that occurs before the majority of gating charge movement, and it appears that the fast-gating charge movement of *hERG* also occurs before this larger charge movement, is it possible that these two are actually the same? The main argument against this would come from comparing the time constant of activation limit in gating charge movement and pore opening to that of the fast gating charge movement. The 15 ms time constant of activation limit is much slower than the 0.5 ms time constant of activation limit observed for the fast gating charge movement. Experiments from Chapters 2 and 3 suggest that both the fast gating charge movement and the voltage-independent transition are early, but distinct closed state transitions prior to the bulk of gating charge movement.

5.8 The mode shift of *hERG*

In several VGKC, the activation of gating charges upon depolarization requires less applied voltage than it does to return the activated gating charge from a high holding potential (Fedida *et al.*, 1996; Haddad and Blunck, 2011; Olcese *et al.*, 1997). As a result, the voltage dependence of gating charge activation is right-shifted to the voltage dependence of gating charge deactivation. This is now referred to as a mode shift (Haddad and Blunck, 2011). The data in Chapter 2 shows that an apparent stabilization of the open state of *hERG* onsets quite rapidly and would be relevant on the timescale of the cardiac action potential. We also found that the N-terminal domain appears to play a role in this open state stabilization. Several studies have described how the cytosolic domains of *hERG* stabilize the open state of the channel (de la Pena *et al.*, 2013; Gianulis *et al.*, 2013; Gustina and Trudeau, 2012; Haitin *et al.*, 2013; Morais Cabral *et al.*, 1998), and one previous study from the Vandenberg lab had described the mode shift of *hERG* gating through VCF experiments (Tan *et al.*, 2012). Their fluorescence records had noted that N-terminal disruption did not disrupt the mode shift of voltage sensor movement, but our gating current records show that the disruption of N- and C- terminal interactions attenuates this phenomenon. Their fluorescence experiments had also suggested that the time constants of voltage sensor deactivation in N-terminally disrupted mutants were similar to that of WT despite an increase in the time constant of deactivation of the ionic current. Our gating current experiments show that ionic deactivation is rate limiting in the deactivation pathway and that the time constants of gating charge deactivation for N-terminally disrupted mutants were faster. We suggest our findings to be correct as gating current experiments are a more robust measurement of the movement of gating charge as opposed to the quenching signal obtained from an S4-attached fluorophore.

A recent paper from the Claydon lab investigated the time dependence of the mode shift in *hERG* channels (Thouta *et al.*, 2017). It is difficult to approximate equilibrium in *hERG* channels as the activation and deactivation kinetics are so slow. Thus the use of shorter protocols, while descriptive of physiological events, may not accurately describe data such as the voltage dependence of activation at true equilibrium. The Claydon lab's data indicate that, at approximate equilibrium, the mode shift is much more significant in the activation and deactivation pathways of gating charge movement, not those of ionic current. Interestingly, this indicates that the stabilization of the activated state in the mode shift is predominantly one that affects the voltage sensing domain, not the pore domain. Perhaps this stabilization is one that would affect a post-pore closure transition in the deactivation pathway of the channel, but one prior to the movement of the majority of gating charge. This would mean that for voltage-sensors that have been activated for long periods of time, closure of the pore is no longer rate-limiting in the gating charge deactivation pathway, as we had shown in Chapter 2. This finding is also very different from mode shifts that had been described in Shaker, where the mode shift had been described as a stabilization of the open state of the channel which imposes a mechanical load on the voltage sensor, causing a conformational change of the voltage sensor (Haddad and Blunck, 2011).

The data from Thouta *et al.* (2017) are difficult to interpret. They show that the time constants of deactivation for ionic current are much slower, about two-fold, than those of gating charge. Should return of gating charge not occur until after the pore has closed, would pore closure not rate-limit the return of gating charge if this transition is slower to occur? Do these data suggest

that pore closure does not occur until the gating charge has been returned to baseline? It may be that differences in bath solution during gating current and ionic current recordings is the basis for these time constants of deactivation that are difficult to reconcile. However, we used very similar solutions in our gating and ionic experiments in Chapter 2 and found that deactivation rates of ionic and gating currents overlay one another, suggesting that pore closure rate-limits gating charge deactivation.

The mode shift of ionic current described in Chapter 2 is likely not a true mode shift, but rather a function of the slow kinetics of the *hERG* channel. The very slow deactivation kinetics would artificially left-shift the GV_{deact} curve, and the slow activation kinetics would artificially right-shift the GV_{act} curve should the protocols used be shorter than what would be necessary to reach equilibrium. This artificial mode shift is, however, one that would be relevant on a physiological timescale.

5.9 Modulated receptor hypothesis and *hERG*

The modulated receptor hypothesis as put forth by Hille in the 1970s suggested that local anaesthetics may preferentially interact with the inactivated state of the voltage-gated sodium channel (Hille, 1977). This theory provided a compelling explanation for the activity-dependent block seen in those channels. In *hERG* channels, block of the channel has also been suggested to interact preferably with the inactivated state of the channel (Vandenberg *et al.*, 2012; Wu *et al.*, 2015; Yang *et al.*, 2004). This is largely due to studies that have found that when you introduce a mutation that affects drug interaction with the channel, it often also has a large effect on the inactivation gating of the channel (Ficker *et al.*, 1998; Lees-Miller *et al.*, 2000; Perrin *et al.*,

2008). In Chapter 4, we sought to describe drug block at the aromatic amino acids of the *hERG* pore region and we wanted to ensure that the mutant channels we used in our study did not have drastically different inactivation properties to that of WT. We did not find a large change in the steady-state voltage dependence of inactivation in any of the constructs used in that study (Fig. 4.4).

Interestingly, in Chapter 4, we found that very slight permutations of Y652 could affect drug potency. Upon any fluorination of the C4 carbon at Y652, drug potency was reduced by 10x for terfenadine, and 2x for both quinidine and dofetilide. We interpreted this as either pinpointing a direct site of interaction of *hERG* with many of the drugs that block the channel or inducing a disruption of tertiary and quaternary structure by making a hydrophobic amino acid more hydrophilic through the charge polarization that comes with fluorination. In terms of how this relates to state-specific drug interaction, it is possible that the open and closed orientations of the pore region position this binding determinant and/or other binding determinants in positions that are less favourable for drug interaction than where it would be in an inactivated state. This would only need to be a very minor movement of the pore region. Some studies, in comparing the *eag* and *hERG* channels, have already shown that by just moving the aromatic residues in the *eag* channel one position over can introduce *hERG*- like drug block (Chen *et al.*, 2002).

5.10 Molecular basis of *hERG* block

Chapter 4 sought to determine the extent to which cation-π interactions played a role in the molecular basis of *hERG* drug block. Several drug block determinants have been noted in the *hERG* channel, the two most important being Y652 and F656 (Chen *et al.*, 2002; Mitcheson *et*

al., 2000a; Sanchez-Chapula *et al.*, 2002; Sanguinetti *et al.*, 2005; Vandenberg *et al.*, 2012). The aromaticity of these had led to suggestion that the nature of drug interaction may be specific to the aromaticity of the residues. One suggestion in particular was that cation-π interactions may play a role in drug interaction. In Chapter 4, we show that cation-π interactions do not appear to play a role in *hERG* drug block. Through incorporation of fluorinated phenylalanine derivatives at the two aromatic sites, we showed that increasing fluorination at these sites did not reduce the potency of terfenadine, quinidine, and dofetilide. Several cation-π interactions have already been successfully determined in ion channels (Ahern *et al.*, 2006; Beene *et al.*, 2003; Pless *et al.*, 2011a; Pless *et al.*, 2011b; Pless *et al.*, 2008; Santarelli *et al.*, 2007). As mentioned in the previous section, while we did not find a cation-π interaction to be taking place, we noted that fluorination of a particular carbon on the phenyl ring of Y652 resulted in reduced drug potency. The C4 carbon, which would typically house a hydroxyl group, when fluorinated, reduced potency for all drugs tested. The doubly fluorinated phenylalanine derivative, which was fluorinated at the C3 and C5 carbons, did not affect drug potency. This finding indicates that, at Y652, several drugs interact in a very site specific manner. Our findings are in general agreement with a study from the Sanguinetti lab that suggested that Y652 required an aromatic residue and F656 required a hydrophobic amino acid in order to maintain drug potency (Fernandez *et al.*, 2004).

5.11 Limitations of the thesis

The studies presented in this thesis have used a heterologous expression system to investigate biophysical and pharmacological phenomena of the *hERG* VGKC. Much of the interest in *hERG* stems from its role in the cardiac action potential where it is the alpha subunit that gives rise to

the I_{Kr} current that repolarizes cardiac myocytes. Since the parameters controlling I_{Kr} are what, on a physiological level, we wish to understand more clearly through our research with *hERG*, a potential limitation of our studies comes in the differences between *hERG* expressed in a *Xenopus* oocyte and I_{Kr} in vivo. The lipid membrane of a cardiac myocyte would be different than that of a *Xenopus* oocyte, and there is the potential that the lipid composition could have effects on gating and drug interaction of the channel. It is also a possibility that there may be other unknown cofactors that interact with the *hERG* alpha subunit to give rise to I_{Kr}. Also, as mentioned previously, the stoichiometry of the channel in vivo is not perfectly understood and the *hERG* 1a homotetramers have some different gating and drug interaction properties than the *hERG* 1a/1b heterotetramers (Abi-Gerges *et al.*, 2011; Jones *et al.*, 2014).

Temperature has been shown to significantly affect the gating of *hERG* (Vandenberg *et al.*, 2006). Higher temperatures result in increased rates of activation and deactivation. As such, in our experiments, the values defined as time constants of activation and values of half-maximal activation are not fully accurate to describe those parameters in the I_{Kr} current *in vivo* as they were determined *in vitro* at room temperature. However, the purpose of our experiments was to detail the structural bases that lead to the unique gating and pharmacological behaviour in *hERG*. We believe that our different expression system has not compromised this goal as similar structural interactions would likely still be in play.

5.12 Physiological and pharmaceutical relevance of findings

Chapters 2 and 3 have advanced our understanding of the structural interactions that lead to the unique gating behaviour of *hERG*. Chapter 2 describes the slow deactivation of the channel as

being partly related to cytosolic domain stabilization of the pore region. Chapter 3 describes the slow activation of the channel as being the result of an S1-S4 interaction that is unique to *eag* channels that works to stabilize an early closed state of the channel. These studies have detailed structural bases for the unique gating features crucial to proper I_{Kr} function.

Chapter 4 determined that cation-π interactions do not play a large role in the interaction with drugs blocking the *hERG* pore region. It also identified the C4 carbon of Y652 to be crucial to interactions of high potency. These findings should prove useful in the design of homology models used to detail *hERG* drug block.

5.13 Summary

VGKC are a diverse family of proteins that are expressed ubiquitously throughout the body. The many roles played by individual members of this family require different specific gating, pH dependence, temperature sensitivity, etc. The differences in response of channels to all of these stimuli are endowed to individual channels through their specific structures. The unique gating of the *hERG* VGKC allow it to provide a large repolarizing current that brings an end to cardiac systole. In this thesis, we have shown that the slow activation of the channel can be attributed to an interaction between the S1 and S4 subunits that stabilizes the closed state, N-terminal interactions contribute significantly to slow deactivation, and the mode shift occurs over a timescale that would be relevant in the cardiac action potential. Differences in protein structure, which have evolved over time to tailor proteins to specific roles, also influence cofactor and drug interaction. The *hERG* pore region is especially predisposed to drug interaction, largely through interaction of drugs with two aromatic amino acids in the pore, Y652 and F656. In this thesis, we

investigated whether the aromatic nature of these amino acids was responsible for drug interaction through cation-π interactions and showed that these interactions were not observable for three well-studied *hERG* blockers.

The findings in this thesis have added detail to our understanding of the gating and drug interaction of *hERG*. Hopefully, the experiments in these studies will kindle new ideas and experiments targeting how channel structure dictates function.

Bibliography

Abi-Gerges, N., Holkham, H., Jones, E.M., Pollard, C.E., Valentin, J.P., and Robertson, G.A. (2011). hERG subunit composition determines differential drug sensitivity. Br J Pharmacol *164*, 419-432.

Abraham, J.M., Saliba, W.I., Vekstein, C., Lawrence, D., Bhargava, M., Bassiouny, M., Janiszewski, D., Lindsay, B., Militello, M., Nissen, S.E., *et al.* (2015). Safety of oral dofetilide for rhythm control of atrial fibrillation and atrial flutter. Circ Arrhythm Electrophysiol *8*, 772-776.

Aggarwal, S.K., and MacKinnon, R. (1996). Contribution of the S4 segment to gating charge in the Shaker K+ channel. Neuron *16*, 1169-1177.

Ahern, C.A., Eastwood, A.L., Lester, H.A., Dougherty, D.A., and Horn, R. (2006). A cation-pi interaction between extracellular TEA and an aromatic residue in potassium channels. J Gen Physiol *128*, 649-657.

Al-Owais, M., Bracey, K., and Wray, D. (2009). Role of intracellular domains in the function of the herg potassium channel. Eur Biophys J *38*, 569-576.

Anderson, C.L., Delisle, B.P., Anson, B.D., Kilby, J.A., Will, M.L., Tester, D.J., Gong, Q., Zhou, Z., Ackerman, M.J., and January, C.T. (2006). Most LQT2 mutations reduce Kv11.1 (hERG) current by a class 2 (trafficking-deficient) mechanism. Circulation *113*, 365-373.

Anderson, C.L., Kuzmicki, C.E., Childs, R.R., Hintz, C.J., Delisle, B.P., and January, C.T. (2014). Large-scale mutational analysis of Kv11.1 reveals molecular insights into type 2 long QT syndrome. Nat Commun *5*, 5535.

Armstrong, C.M. (1966). Time course of TEA(+)-induced anomalous rectification in squid giant axons. J Gen Physiol *50*, 491-503.

Armstrong, C.M. (1969). Inactivation of the potassium conductance and related phenomena caused by quaternary ammonium ion injection in squid axons. J Gen Physiol *54*, 553-575.

Armstrong, C.M. (1971). Interaction of tetraethylammonium ion derivatives with the potassium channels of giant axons. J Gen Physiol *58*, 413-437.

Arrigoni, C., Schroeder, I., Romani, G., Van Etten, J.L., Thiel, G., and Moroni, A. (2013). The voltage-sensing domain of a phosphatase gates the pore of a potassium channel. J Gen Physiol *141*, 389-395.

Aydar, E., and Palmer, C. (2001). Functional characterization of the C-terminus of the human ether-a-go-go-related gene K(+) channel (HERG). J Physiol *534*, 1-14.

Beene, D.L., Dougherty, D.A., and Lester, H.A. (2003). Unnatural amino acid mutagenesis in mapping ion channel function. Curr Opin Neurobiol *13*, 264-270.

Bezanilla, F. (2000). The voltage sensor in voltage-dependent ion channels. Physiol Rev *80*, 555-592.

Bezanilla, F. (2008). How membrane proteins sense voltage. Nat Rev Mol Cell Biol *9*, 323-332.

Bezanilla, F., and Perozo, E. (2003). The voltage sensor and the gate in ion channels. Adv Protein Chem *63*, 211-241.

Bezanilla, F., Taylor, R.E., and Fernandez, J.M. (1982). Distribution and kinetics of membrane dielectric polarization. 1. Long-term inactivation of gating currents. J Gen Physiol *79*, 21-40.

Blunck, R., and Batulan, Z. (2012). Mechanism of electromechanical coupling in voltage-gated potassium channels. Front Pharmacol *3*, 166.

Borjesson, S.I., and Elinder, F. (2008). Structure, function, and modification of the voltage sensor in voltage-gated ion channels. Cell Biochem Biophys *52*, 149-174.
Boukharta, L., Keranen, H., Stary-Weinzinger, A., Wallin, G., de Groot, B.L., and Aqvist, J. (2011). Computer simulations of structure-activity relationships for HERG channel blockers. Biochemistry *50*, 6146-6156.
Braga, R.C., Alves, V.M., Silva, M.F., Muratov, E., Fourches, D., Tropsha, A., and Andrade, C.H. (2014). Tuning HERG out: antitarget QSAR models for drug development. Curr Top Med Chem *14*, 1399-1415.
Brelidze, T.I., Carlson, A.E., Sankaran, B., and Zagotta, W.N. (2012). Structure of the carboxy-terminal region of a KCNH channel. Nature *481*, 530-533.
Brelidze, T.I., Carlson, A.E., and Zagotta, W.N. (2009). Absence of direct cyclic nucleotide modulation of mEAG1 and hERG1 channels revealed with fluorescence and electrophysiological methods. J Biol Chem *284*, 27989-27997.
Brown, A.M. (2004). Drugs, hERG and sudden death. Cell Calcium *35*, 543-547.
Cha, A., Snyder, G.E., Selvin, P.R., and Bezanilla, F. (1999). Atomic scale movement of the voltage-sensing region in a potassium channel measured via spectroscopy. Nature *402*, 809-813.
Chanda, B., and Bezanilla, F. (2008). A common pathway for charge transport through voltage-sensing domains. Neuron *57*, 345-351.
Chen, F.S., Steele, D., and Fedida, D. (1997). Allosteric effects of permeating cations on gating currents during K+ channel deactivation. J Gen Physiol *110*, 87-100.
Chen, J., Seebohm, G., and Sanguinetti, M.C. (2002). Position of aromatic residues in the S6 domain, not inactivation, dictates cisapride sensitivity of HERG and eag potassium channels. Proc Natl Acad Sci U S A *99*, 12461-12466.
Chen, J., Zou, A., Splawski, I., Keating, M.T., and Sanguinetti, M.C. (1999). Long QT syndrome-associated mutations in the Per-Arnt-Sim (PAS) domain of HERG potassium channels accelerate channel deactivation. J Biol Chem *274*, 10113-10118.
Cheng Y. M., H.C.M., Niven C. M., Allard C. R., Claydon T. W. (2012). Molecular determinants of voltage-dependent gating in hERG potassium channels. Biophys J *102*.
Cheng, Y.M., and Claydon, T.W. (2012). Voltage-dependent gating of HERG potassium channels. Front Pharmacol *3*, 83.
Cheng, Y.M., Hull, C.M., Niven, C.M., Qi, J., Allard, C.R., and Claydon, T.W. (2013). Functional interactions of voltage sensor charges with an S2 hydrophobic plug in hERG channels. J Gen Physiol *142*, 289-303.
Clancy, C.E., and Rudy, Y. (2001). Cellular consequences of HERG mutations in the long QT syndrome: precursors to sudden cardiac death. Cardiovasc Res *50*, 301-313.
Curran, M.E., Splawski, I., Timothy, K.W., Vincent, G.M., Green, E.D., and Keating, M.T. (1995). A molecular basis for cardiac arrhythmia: HERG mutations cause long QT syndrome. Cell *80*, 795-803.
de la Pena, P., Alonso-Ron, C., Machin, A., Fernandez-Trillo, J., Carretero, L., Dominguez, P., and Barros, F. (2011). Demonstration of physical proximity between the N terminus and the S4-S5 linker of the human ether-a-go-go-related gene (hERG) potassium channel. J Biol Chem *286*, 19065-19075.
de la Pena, P., Machin, A., Fernandez-Trillo, J., Dominguez, P., and Barros, F. (2013). Mapping of interactions between the N- and C-termini and the channel core in HERG K+ channels. Biochem J *451*, 463-474.

Dempsey, C.E., Wright, D., Colenso, C.K., Sessions, R.B., and Hancox, J.C. (2014). Assessing hERG pore models as templates for drug docking using published experimental constraints: the inactivated state in the context of drug block. J Chem Inf Model *54*, 601-612.
Dou, Y., Goodchild, S.J., Velde, R.V., Wu, Y., and Fedida, D. (2013). The neutral, hydrophobic isoleucine at position I521 in the extracellular S4 domain of hERG contributes to channel gating equilibrium. Am J Physiol Cell Physiol *305*, C468-478.
Dougherty, D.A. (1996). Cation-pi interactions in chemistry and biology: a new view of benzene, Phe, Tyr, and Trp. Science *271*, 163-168.
Doyle, D.A., Morais Cabral, J., Pfuetzner, R.A., Kuo, A., Gulbis, J.M., Cohen, S.L., Chait, B.T., and MacKinnon, R. (1998). The structure of the potassium channel: molecular basis of K+ conduction and selectivity. Science *280*, 69-77.
Du, C., Zhang, Y., El Harchi, A., Dempsey, C.E., and Hancox, J.C. (2014). Ranolazine inhibition of hERG potassium channels: drug-pore interactions and reduced potency against inactivation mutants. J Mol Cell Cardiol *74*, 220-230.
Dumont, J.N. (1972). Oogenesis in Xenopus laevis (Daudin). I. Stages of oocyte development in laboratory maintained animals. J Morphol *136*, 153-179.
Duncan, R.S., Ridley, J.M., Dempsey, C.E., Leishman, D.J., Leaney, J.L., Hancox, J.C., and Witchel, H.J. (2006). Erythromycin block of the HERG K+ channel: accessibility to F656 and Y652. Biochem Biophys Res Commun *341*, 500-506.
Durdagi, S., Deshpande, S., Duff, H.J., and Noskov, S.Y. (2012). Modeling of open, closed, and open-inactivated states of the hERG1 channel: structural mechanisms of the state-dependent drug binding. J Chem Inf Model *52*, 2760-2774.
El Harchi, A., Zhang, Y.H., Hussein, L., Dempsey, C.E., and Hancox, J.C. (2012). Molecular determinants of hERG potassium channel inhibition by disopyramide. J Mol Cell Cardiol *52*, 185-195.
Eldstrom, J., and Fedida, D. (2011). The voltage-gated channel accessory protein KCNE2: multiple ion channel partners, multiple ways to long QT syndrome. Expert Rev Mol Med *13*, e38.
Elliott, D.J., Dondas, N.Y., Munsey, T.S., and Sivaprasadarao, A. (2009). Movement of the S4 segment in the hERG potassium channel during membrane depolarization. Mol Membr Biol *26*, 435-447.
Es-Salah-Lamoureux, Z., Fougere, R., Xiong, P.Y., Robertson, G.A., and Fedida, D. (2010). Fluorescence-tracking of activation gating in human ERG channels reveals rapid S4 movement and slow pore opening. Plos One *5*, e10876.
Fauchier, L., Babuty, D., Poret, P., Autret, M.L., Cosnay, P., and Fauchier, J.P. (1999). Effect of verapamil on QT interval dynamicity. Am J Cardiol *83*, 807-808, A810-801.
Fedida, D., Bouchard, R., and Chen, F.S. (1996). Slow gating charge immobilization in the human potassium channel Kv1.5 and its prevention by 4-aminopyridine. J Physiol *494 (Pt 2)*, 377-387.
Fernandez-Trillo, J., Barros, F., Machin, A., Carretero, L., Dominguez, P., and de la Pena, P. (2011). Molecular determinants of interactions between the N-terminal domain and the transmembrane core that modulate hERG K+ channel gating. Plos One *6*, e24674.
Fernandez, D., Ghanta, A., Kauffman, G.W., and Sanguinetti, M.C. (2004). Physicochemical features of the HERG channel drug binding site. J Biol Chem *279*, 10120-10127.

Ferrer, T., Rupp, J., Piper, D.R., and Tristani-Firouzi, M. (2006). The S4-S5 linker directly couples voltage sensor movement to the activation gate in the human ether-a'-go-go-related gene (hERG) K+ channel. J Biol Chem *281*, 12858-12864.
Ficker, E., Jarolimek, W., and Brown, A.M. (2001). Molecular determinants of inactivation and dofetilide block in ether a-go-go (EAG) channels and EAG-related K(+) channels. Mol Pharmacol *60*, 1343-1348.
Ficker, E., Jarolimek, W., Kiehn, J., Baumann, A., and Brown, A.M. (1998). Molecular determinants of dofetilide block of HERG K+ channels. Circ Res *82*, 386-395.
Fougere, R.R., Es-Salah-Lamoureux, Z., Rezazadeh, S., Eldstrom, J., and Fedida, D. (2011). Functional characterization of the LQT2-causing mutation R582C and the associated voltage-dependent fluorescence signal. Heart Rhythm *8*, 1273-1280.
French, R.J., and Finol-Urdaneta, R.K. (2012). Open-state stabilization in Kv channels: voltage-sensor relaxation and pore propping by a bound ion. J Gen Physiol *140*, 463-467.
Gianulis, E.C., Liu, Q., and Trudeau, M.C. (2013). Direct interaction of eag domains and cyclic nucleotide-binding homology domains regulate deactivation gating in hERG channels. J Gen Physiol *142*, 351-366.
Goodchild, S.J., and Fedida, D. (2012). Contributions of intracellular ions to kv channel voltage sensor dynamics. Front Pharmacol *3*, 114.
Goodchild, S.J., and Fedida, D. (2014). Gating charge movement precedes ionic current activation in hERG channels. Channels (Austin) *8*, 84-89.
Goodchild, S.J., Macdonald, L.C., and Fedida, D. (2015). Sequence of gating charge movement and pore gating in HERG activation and deactivation pathways. Biophys J *108*, 1435-1447.
Goodchild, S.J., Xu, H., Es-Salah-Lamoureux, Z., Ahern, C.A., and Fedida, D. (2012). Basis for allosteric open-state stabilization of voltage-gated potassium channels by intracellular cations. J Gen Physiol *140*, 495-511.
Gustina, A.S., and Trudeau, M.C. (2009). A recombinant N-terminal domain fully restores deactivation gating in N-truncated and long QT syndrome mutant hERG potassium channels. Proc Natl Acad Sci U S A *106*, 13082-13087.
Gustina, A.S., and Trudeau, M.C. (2011). hERG potassium channel gating is mediated by N- and C-terminal region interactions. J Gen Physiol *137*, 315-325.
Gustina, A.S., and Trudeau, M.C. (2012). HERG potassium channel regulation by the N-terminal eag domain. Cell Signal *24*, 1592-1598.
Gustina, A.S., and Trudeau, M.C. (2013). The eag domain regulates hERG channel inactivation gating via a direct interaction. J Gen Physiol *141*, 229-241.
Gutman, G.A., Chandy, K.G., Grissmer, S., Lazdunski, M., McKinnon, D., Pardo, L.A., Robertson, G.A., Rudy, B., Sanguinetti, M.C., Stuhmer, W., *et al.* (2005). International Union of Pharmacology. LIII. Nomenclature and molecular relationships of voltage-gated potassium channels. Pharmacol Rev *57*, 473-508.
Haddad, G.A., and Blunck, R. (2011). Mode shift of the voltage sensors in Shaker K+ channels is caused by energetic coupling to the pore domain. J Gen Physiol *137*, 455-472.
Haitin, Y., Carlson, A.E., and Zagotta, W.N. (2013). The structural mechanism of KCNH-channel regulation by the eag domain. Nature *501*, 444-448.
Hancox, J.C., McPate, M.J., El Harchi, A., and Zhang, Y.H. (2008). The hERG potassium channel and hERG screening for drug-induced torsades de pointes. Pharmacol Ther *119*, 118-132.

Harmonisation, I.C.o. (2005). International Conference on Harmonisation; guidance on S7B Nonclinical Evaluation of the Potential for Delayed Ventricular Repolarization (QT Interval Prolongation) by Human Pharmaceuticals; availability. Notice. Fed Regist *70*, 61133-61134.
Herzberg, I.M., Trudeau, M.C., and Robertson, G.A. (1998). Transfer of rapid inactivation and sensitivity to the class III antiarrhythmic drug E-4031 from HERG to M-eag channels. J Physiol *511 (Pt 1)*, 3-14.
Hill, A.P., Perrin, M.J., Heide, J., Campbell, T.J., Mann, S.A., and Vandenberg, J.I. (2014). Kinetics of drug interaction with the Kv11.1 potassium channel. Mol Pharmacol *85*, 769-776.
Hille, B. (1977). Local anesthetics: hydrophilic and hydrophobic pathways for the drug-receptor reaction. J Gen Physiol *69*, 497-515.
Hille, B. (2001). Ionic Channels of Excitable Membranes, 3rd edn (Sunderland, Sinauer Associates).
Horovitz, A. (1996). Double-mutant cycles: a powerful tool for analyzing protein structure and function. Fold Des *1*, R121-126.
Hoshi, T., Zagotta, W.N., and Aldrich, R.W. (1990). Biophysical and molecular mechanisms of Shaker potassium channel inactivation. Science *250*, 533-538.
Hoshi, T., Zagotta, W.N., and Aldrich, R.W. (1991). Two types of inactivation in Shaker K+ channels: effects of alterations in the carboxy-terminal region. Neuron *7*, 547-556.
Hull, C.M., Sokolov, S., Van Slyke, A.C., and Claydon, T.W. (2014). Regional flexibility in the S4-S5 linker regulates hERG channel closed-state stabilization. Pflugers Arch *466*, 1911-1919.
Imai, Y.N., Ryu, S., and Oiki, S. (2009). Docking model of drug binding to the human ether-a-go-go potassium channel guided by tandem dimer mutant patch-clamp data: a synergic approach. J Med Chem *52*, 1630-1638.
January, C.T., Gong, Q., and Zhou, Z. (2000). Long QT syndrome: cellular basis and arrhythmia mechanism in LQT2. J Cardiovasc Electrophysiol *11*, 1413-1418.
Jiang, Y., Lee, A., Chen, J., Cadene, M., Chait, B.T., and MacKinnon, R. (2002). Crystal structure and mechanism of a calcium-gated potassium channel. Nature *417*, 515-522.
Jones, D.K., Liu, F., Vaidyanathan, R., Eckhardt, L.L., Trudeau, M.C., and Robertson, G.A. (2014). hERG 1b is critical for human cardiac repolarization. Proc Natl Acad Sci U S A *111*, 18073-18077.
Jones, E.M., Roti Roti, E.C., Wang, J., Delfosse, S.A., and Robertson, G.A. (2004). Cardiac IKr channels minimally comprise hERG 1a and 1b subunits. J Biol Chem *279*, 44690-44694.
Ju, P., Pages, G., Riek, R.P., Chen, P.C., Torres, A.M., Bansal, P.S., Kuyucak, S., Kuchel, P.W., and Vandenberg, J.I. (2009). The pore domain outer helix contributes to both activation and inactivation of the HERG K+ channel. J Biol Chem *284*, 1000-1008.
Kamiya, K., Niwa, R., Mitcheson, J.S., and Sanguinetti, M.C. (2006). Molecular determinants of HERG channel block. Mol Pharmacol *69*, 1709-1716.
Kamiya, K., Niwa, R., Morishima, M., Honjo, H., and Sanguinetti, M.C. (2008). Molecular determinants of hERG channel block by terfenadine and cisapride. J Pharmacol Sci *108*, 301-307.
Kiehn, J., Lacerda, A.E., Wible, B., and Brown, A.M. (1996). Molecular physiology and pharmacology of HERG. Single-channel currents and block by dofetilide. Circulation *94*, 2572-2579.

Knape, K., Linder, T., Wolschann, P., Beyer, A., and Stary-Weinzinger, A. (2011). In silico Analysis of Conformational Changes Induced by Mutation of Aromatic Binding Residues: Consequences for Drug Binding in the hERG K+ Channel. Plos One *6*.
Kramer, J., Obejero-Paz, C.A., Myatt, G., Kuryshev, Y.A., Bruening-Wright, A., Verducci, J.S., and Brown, A.M. (2013). MICE models: superior to the HERG model in predicting Torsade de Pointes. Sci Rep *3*, 2100.
Lacroix, J.J., Campos, F.V., Frezza, L., and Bezanilla, F. (2013). Molecular bases for the asynchronous activation of sodium and potassium channels required for nerve impulse generation. Neuron *79*, 651-657.
Ledwell, J.L., and Aldrich, R.W. (1999). Mutations in the S4 region isolate the final voltage-dependent cooperative step in potassium channel activation. J Gen Physiol *113*, 389-414.
Lees-Miller, J.P., Duan, Y., Teng, G.Q., and Duff, H.J. (2000). Molecular determinant of high-affinity dofetilide binding to HERG1 expressed in Xenopus oocytes: involvement of S6 sites. Mol Pharmacol *57*, 367-374.
Li, Q., Gayen, S., Chen, A.S., Huang, Q., Raida, M., and Kang, C. (2010). NMR solution structure of the N-terminal domain of hERG and its interaction with the S4-S5 linker. Biochem Biophys Res Commun *403*, 126-132.
Li, Q., Ng, H.Q., Yoon, H.S., and Kang, C. (2014). Insight into the molecular interaction between the cyclic nucleotide-binding homology domain and the eag domain of the hERG channel. FEBS Lett *588*, 2782-2788.
Liu, J., Zhang, M., Jiang, M., and Tseng, G.N. (2003). Negative charges in the transmembrane domains of the HERG K channel are involved in the activation- and deactivation-gating processes. J Gen Physiol *121*, 599-614.
Liu, S., Rasmusson, R.L., Campbell, D.L., Wang, S., and Strauss, H.C. (1996). Activation and inactivation kinetics of an E-4031-sensitive current from single ferret atrial myocytes. Biophys J *70*, 2704-2715.
Long, S.B., Campbell, E.B., and Mackinnon, R. (2005). Voltage sensor of Kv1.2: structural basis of electromechanical coupling. Science *309*, 903-908.
Long, S.B., Tao, X., Campbell, E.B., and MacKinnon, R. (2007). Atomic structure of a voltage-dependent K+ channel in a lipid membrane-like environment. Nature *450*, 376-382.
Lorinczi, E., Gomez-Posada, J.C., de la Pena, P., Tomczak, A.P., Fernandez-Trillo, J., Leipscher, U., Stuhmer, W., Barros, F., and Pardo, L.A. (2015). Voltage-dependent gating of KCNH potassium channels lacking a covalent link between voltage-sensing and pore domains. Nat Commun *6*, 6672.
Lu, Y., Mahaut-Smith, M.P., Varghese, A., Huang, C.L., Kemp, P.R., and Vandenberg, J.I. (2001). Effects of premature stimulation on HERG K(+) channels. J Physiol *537*, 843-851.
Lummis, S.C., D, L.B., Harrison, N.J., Lester, H.A., and Dougherty, D.A. (2005). A cation-pi binding interaction with a tyrosine in the binding site of the GABAC receptor. Chem Biol *12*, 993-997.
MacKinnon, R. (1991). Determination of the subunit stoichiometry of a voltage-activated potassium channel. Nature *350*, 232-235.
Mazhari, R., Greenstein, J.L., Winslow, R.L., Marban, E., and Nuss, H.B. (2001). Molecular interactions between two long-QT syndrome gene products, HERG and KCNE2, rationalized by in vitro and in silico analysis. Circ Res *89*, 33-38.

Melgari, D., Brack, K.E., Zhang, C., Zhang, Y., El Harchi, A., Mitcheson, J.S., Dempsey, C.E., Ng, G.A., and Hancox, J.C. (2015a). hERG potassium channel blockade by the HCN channel inhibitor bradycardic agent ivabradine. J Am Heart Assoc *4*.
Melgari, D., Zhang, Y., El Harchi, A., Dempsey, C.E., and Hancox, J.C. (2015b). Molecular basis of hERG potassium channel blockade by the class Ic antiarrhythmic flecainide. J Mol Cell Cardiol *86*, 42-53.
Melishchuk, A., and Armstrong, C.M. (2001). Mechanism underlying slow kinetics of the OFF gating current in Shaker potassium channel. Biophys J *80*, 2167-2175.
Milnes, J.T., Witchel, H.J., Leaney, J.L., Leishman, D.J., and Hancox, J.C. (2006). hERG K+ channel blockade by the antipsychotic drug thioridazine: An obligatory role for the S6 helix residue F656. Biochem Biophys Res Commun *351*, 273-280.
Mitcheson, J., Perry, M., Stansfeld, P., Sanguinetti, M.C., Witchel, H., and Hancox, J. (2005). Structural determinants for high-affinity block of hERG potassium channels. Novartis Found Symp *266*, 136-150; discussion 150-138.
Mitcheson, J.S. (2003). Drug binding to HERG channels: evidence for a 'non-aromatic' binding site for fluvoxamine. Br J Pharmacol *139*, 883-884.
Mitcheson, J.S., Chen, J., Lin, M., Culberson, C., and Sanguinetti, M.C. (2000a). A structural basis for drug-induced long QT syndrome. Proc Natl Acad Sci U S A *97*, 12329-12333.
Mitcheson, J.S., Chen, J., and Sanguinetti, M.C. (2000b). Trapping of a methanesulfonanilide by closure of the HERG potassium channel activation gate. J Gen Physiol *115*, 229-240.
Morais-Cabral, J.H., and Robertson, G.A. (2015). The enigmatic cytoplasmic regions of KCNH channels. J Mol Biol *427*, 67-76.
Morais Cabral, J.H., Lee, A., Cohen, S.L., Chait, B.T., Li, M., and Mackinnon, R. (1998). Crystal structure and functional analysis of the HERG potassium channel N terminus: a eukaryotic PAS domain. Cell *95*, 649-655.
Muskett, F.W., Thouta, S., Thomson, S.J., Bowen, A., Stansfeld, P.J., and Mitcheson, J.S. (2011). Mechanistic insight into human ether-a-go-go-related gene (hERG) K+ channel deactivation gating from the solution structure of the EAG domain. J Biol Chem *286*, 6184-6191.
Ng, C.A., Gravel, A.E., Perry, M.D., Arnold, A.A., Marcotte, I., and Vandenberg, J.I. (2016). Tyrosine Residues from the S4-S5 Linker of Kv11.1 Channels Are Critical for Slow Deactivation. J Biol Chem *291*, 17293-17302.
Ng, C.A., Hunter, M.J., Perry, M.D., Mobli, M., Ke, Y., Kuchel, P.W., King, G.F., Stock, D., and Vandenberg, J.I. (2011). The N-terminal tail of hERG contains an amphipathic alpha-helix that regulates channel deactivation. Plos One *6*, e16191.
Ng, C.A., Perry, M.D., Tan, P.S., Hill, A.P., Kuchel, P.W., and Vandenberg, J.I. (2012). The S4-S5 linker acts as a signal integrator for HERG K+ channel activation and deactivation gating. Plos One *7*, e31640.
Ng, C.A., Phan, K., Hill, A.P., Vandenberg, J.I., and Perry, M.D. (2014). Multiple interactions between cytoplasmic domains regulate slow deactivation of Kv11.1 channels. J Biol Chem *289*, 25822-25832.
Noble, D., and Tsien, R.W. (1969). Outward membrane currents activated in the plateau range of potentials in cardiac Purkinje fibres. J Physiol *200*, 205-231.
Olcese, R., Latorre, R., Toro, L., Bezanilla, F., and Stefani, E. (1997). Correlation between charge movement and ionic current during slow inactivation in Shaker K+ channels. J Gen Physiol *110*, 579-589.

Pearlstein, R., Vaz, R., and Rampe, D. (2003). Understanding the structure-activity relationship of the human ether-a-go-go-related gene cardiac K+ channel. A model for bad behavior. J Med Chem *46*, 2017-2022.
Perozo, E., Papazian, D.M., Stefani, E., and Bezanilla, F. (1992). Gating currents in Shaker K+ channels. Implications for activation and inactivation models. Biophys J *62*, 160-168; discussion 169-171.
Perozo, E., Santacruz-Toloza, L., Stefani, E., Bezanilla, F., and Papazian, D.M. (1994). S4 mutations alter gating currents of Shaker K channels. Biophys J *66*, 345-354.
Perrin, M.J., Kuchel, P.W., Campbell, T.J., and Vandenberg, J.I. (2008). Drug binding to the inactivated state is necessary but not sufficient for high-affinity binding to human ether-a-go-go-related gene channels. Mol Pharmacol *74*, 1443-1452.
Perry, M., de Groot, M.J., Helliwell, R., Leishman, D., Tristani-Firouzi, M., Sanguinetti, M.C., and Mitcheson, J. (2004). Structural determinants of HERG channel block by clofilium and ibutilide. Mol Pharmacol *66*, 240-249.
Perry, M., Stansfeld, P.J., Leaney, J., Wood, C., de Groot, M.J., Leishman, D., Sutcliffe, M.J., and Mitcheson, J.S. (2006). Drug binding interactions in the inner cavity of HERG channels: molecular insights from structure-activity relationships of clofilium and ibutilide analogs. Mol Pharmacol *69*, 509-519.
Perry, M.D., Ng, C.A., Mann, S.A., Sadrieh, A., Imtiaz, M., Hill, A.P., and Vandenberg, J.I. (2015). Getting to the heart of hERG K(+) channel gating. J Physiol *593*, 2575-2585.
Perry, M.D., Ng, C.A., Phan, K., David, E., Steer, K., Hunter, M.J., Mann, S.A., Imtiaz, M., Hill, A.P., Ke, Y., *et al.* (2016). Rescue of protein expression defects may not be enough to abolish the pro-arrhythmic phenotype of long QT type 2 mutations. J Physiol *594*, 4031-4049.
Perry, M.D., Ng, C.A., and Vandenberg, J.I. (2013). Pore helices play a dynamic role as integrators of domain motion during Kv11.1 channel inactivation gating. J Biol Chem *288*, 11482-11491.
Piper, D.R., Hinz, W.A., Tallurri, C.K., Sanguinetti, M.C., and Tristani-Firouzi, M. (2005). Regional specificity of human ether-a'-go-go-related gene channel activation and inactivation gating. J Biol Chem *280*, 7206-7217.
Piper, D.R., Rupp, J., Sachse, F.B., Sanguinetti, M.C., and Tristani-Firouzi, M. (2008). Cooperative interactions between R531 and acidic residues in the voltage sensing module of hERG1 channels. Cell Physiol Biochem *21*, 37-46.
Piper, D.R., Varghese, A., Sanguinetti, M.C., and Tristani-Firouzi, M. (2003). Gating currents associated with intramembrane charge displacement in HERG potassium channels. Proc Natl Acad Sci U S A *100*, 10534-10539.
Pless, S.A., Galpin, J.D., Frankel, A., and Ahern, C.A. (2011a). Molecular basis for class Ib anti-arrhythmic inhibition of cardiac sodium channels. Nat Commun *2*, 351.
Pless, S.A., Galpin, J.D., Niciforovic, A.P., and Ahern, C.A. (2011b). Contributions of counter-charge in a potassium channel voltage-sensor domain. Nat Chem Biol *7*, 617-623.
Pless, S.A., Hanek, A.P., Price, K.L., Lynch, J.W., Lester, H.A., Dougherty, D.A., and Lummis, S.C. (2011c). A cation-pi interaction at a phenylalanine residue in the glycine receptor binding site is conserved for different agonists. Mol Pharmacol *79*, 742-748.
Pless, S.A., Millen, K.S., Hanek, A.P., Lynch, J.W., Lester, H.A., Lummis, S.C., and Dougherty, D.A. (2008). A cation-pi interaction in the binding site of the glycine receptor is mediated by a phenylalanine residue. J Neurosci *28*, 10937-10942.

Priest, M.F., Lacroix, J.J., Villalba-Galea, C.A., and Bezanilla, F. (2013). S3-S4 linker length modulates the relaxed state of a voltage-gated potassium channel. Biophys J *105*, 2312-2322.
Roden, D.M. (2004). Drug-induced prolongation of the QT interval. N Engl J Med *350*, 1013-1022.
Roden, D.M. (2016). Predicting drug-induced QT prolongation and torsades de pointes. J Physiol *594*, 2459-2468.
Roy, M., Dumaine, R., and Brown, A.M. (1996). HERG, a primary human ventricular target of the nonsedating antihistamine terfenadine. Circulation *94*, 817-823.
Sale, H., Wang, J., O'Hara, T.J., Tester, D.J., Phartiyal, P., He, J.Q., Rudy, Y., Ackerman, M.J., and Robertson, G.A. (2008). Physiological properties of hERG 1a/1b heteromeric currents and a hERG 1b-specific mutation associated with Long-QT syndrome. Circ Res *103*, e81-95.
Sanchez-Chapula, J.A., Navarro-Polanco, R.A., Culberson, C., Chen, J., and Sanguinetti, M.C. (2002). Molecular determinants of voltage-dependent human ether-a-go-go related gene (HERG) K+ channel block. J Biol Chem *277*, 23587-23595.
Sanguinetti, M.C., Chen, J., Fernandez, D., Kamiya, K., Mitcheson, J., and Sanchez-Chapula, J.A. (2005). Physicochemical basis for binding and voltage-dependent block of hERG channels by structurally diverse drugs. Novartis Found Symp *266*, 159-166; discussion 166-170.
Sanguinetti, M.C., Curran, M.E., Zou, A., Shen, J., Spector, P.S., Atkinson, D.L., and Keating, M.T. (1996). Coassembly of K(V)LQT1 and minK (IsK) proteins to form cardiac I(Ks) potassium channel. Nature *384*, 80-83.
Sanguinetti, M.C., Jiang, C., Curran, M.E., and Keating, M.T. (1995). A mechanistic link between an inherited and an acquired cardiac arrhythmia: HERG encodes the IKr potassium channel. Cell *81*, 299-307.
Sanguinetti, M.C., and Jurkiewicz, N.K. (1990). Two components of cardiac delayed rectifier K+ current. Differential sensitivity to block by class III antiarrhythmic agents. J Gen Physiol *96*, 195-215.
Sanguinetti, M.C., and Jurkiewicz, N.K. (1991). Delayed rectifier outward K+ current is composed of two currents in guinea pig atrial cells. Am J Physiol *260*, H393-399.
Sanguinetti, M.C., and Tristani-Firouzi, M. (2006). hERG potassium channels and cardiac arrhythmia. Nature *440*, 463-469.
Sanguinetti, M.C., and Xu, Q.P. (1999). Mutations of the S4-S5 linker alter activation properties of HERG potassium channels expressed in Xenopus oocytes. J Physiol *514 (Pt 3)*, 667-675.
Santarelli, V.P., Eastwood, A.L., Dougherty, D.A., Horn, R., and Ahern, C.A. (2007). A cation-pi interaction discriminates among sodium channels that are either sensitive or resistant to tetrodotoxin block. J Biol Chem *282*, 8044-8051.
Santiago-Castillo, J.A., Covarrubias, M., Sanchez-Rodriguez, J.E., Perez-Cornejo, P., and Arreola, J. (2010). Simulating complex ion channel kinetics with IonChannelLab. Channels (Austin) *4*, 422-428.
Saxena, P., Zangerl-Plessl, E.M., Linder, T., Windisch, A., Hohaus, A., Timin, E., Hering, S., and Stary-Weinzinger, A. (2016). New potential binding determinant for hERG channel inhibitors. Sci Rep *6*, 24182.
Schonherr, R., and Heinemann, S.H. (1996). Molecular determinants for activation and inactivation of HERG, a human inward rectifier potassium channel. J Physiol *493 (Pt 3)*, 635-642.

Schonherr, R., Rosati, B., Hehl, S., Rao, V.G., Arcangeli, A., Olivotto, M., Heinemann, S.H., and Wanke, E. (1999). Functional role of the slow activation property of ERG K+ channels. Eur J Neurosci *11*, 753-760.
Schoppa, N.E., McCormack, K., Tanouye, M.A., and Sigworth, F.J. (1992). The size of gating charge in wild-type and mutant Shaker potassium channels. Science *255*, 1712-1715.
Schoppa, N.E., and Sigworth, F.J. (1998). Activation of shaker potassium channels. I. Characterization of voltage-dependent transitions. J Gen Physiol *111*, 271-294.
Seoh, S.A., Sigg, D., Papazian, D.M., and Bezanilla, F. (1996). Voltage-sensing residues in the S2 and S4 segments of the Shaker K+ channel. Neuron *16*, 1159-1167.
Shibasaki, T. (1987). Conductance and kinetics of delayed rectifier potassium channels in nodal cells of the rabbit heart. J Physiol *387*, 227-250.
Sine, S.M., Wang, H.L., and Bren, N. (2002). Lysine scanning mutagenesis delineates structural model of the nicotinic receptor ligand binding domain. J Biol Chem *277*, 29210-29223.
Smith, P.L., Baukrowitz, T., and Yellen, G. (1996). The inward rectification mechanism of the HERG cardiac potassium channel. Nature *379*, 833-836.
Smith, P.L., and Yellen, G. (2002). Fast and slow voltage sensor movements in HERG potassium channels. J Gen Physiol *119*, 275-293.
Snyders, D.J., and Chaudhary, A. (1996). High affinity open channel block by dofetilide of HERG expressed in a human cell line. Mol Pharmacol *49*, 949-955.
Spector, P.S., Curran, M.E., Keating, M.T., and Sanguinetti, M.C. (1996a). Class III antiarrhythmic drugs block HERG, a human cardiac delayed rectifier K+ channel. Open-channel block by methanesulfonanilides. Circ Res *78*, 499-503.
Spector, P.S., Curran, M.E., Zou, A., Keating, M.T., and Sanguinetti, M.C. (1996b). Fast inactivation causes rectification of the IKr channel. J Gen Physiol *107*, 611-619.
Splawski, I., Shen, J., Timothy, K.W., Lehmann, M.H., Priori, S., Robinson, J.L., Moss, A.J., Schwartz, P.J., Towbin, J.A., Vincent, G.M., *et al.* (2000). Spectrum of mutations in long-QT syndrome genes. KVLQT1, HERG, SCN5A, KCNE1, and KCNE2. Circulation *102*, 1178-1185.
Stansfeld, P.J., Gedeck, P., Gosling, M., Cox, B., Mitcheson, J.S., and Sutcliffe, M.J. (2007). Drug block of the hERG potassium channel: insight from modeling. Proteins *68*, 568-580.
Stansfeld, P.J., Sutcliffe, M.J., and Mitcheson, J.S. (2006). Molecular mechanisms for drug interactions with hERG that cause long QT syndrome. Expert Opin Drug Metab Toxicol *2*, 81-94.
Stary, A., Wacker, S.J., Boukharta, L., Zachariae, U., Karimi-Nejad, Y., Aqvist, J., Vriend, G., and de Groot, B.L. (2010). Toward a consensus model of the HERG potassium channel. ChemMedChem *5*, 455-467.
Stefani, E., and Bezanilla, F. (1998). Cut-open oocyte voltage-clamp technique. Methods Enzymol *293*, 300-318.
Stefani, E., Toro, L., Perozo, E., and Bezanilla, F. (1994). Gating of Shaker K+ channels: I. Ionic and gating currents. Biophys J *66*, 996-1010.
Subbiah, R.N., Clarke, C.E., Smith, D.J., Zhao, J., Campbell, T.J., and Vandenberg, J.I. (2004). Molecular basis of slow activation of the human ether-a-go-go related gene potassium channel. J Physiol *558*, 417-431.
Subbiah, R.N., Kondo, M., Campbell, T.J., and Vandenberg, J.I. (2005). Tryptophan scanning mutagenesis of the HERG K+ channel: the S4 domain is loosely packed and likely to be lipid exposed. J Physiol *569*, 367-379.

Tan, P.S., Perry, M.D., Ng, C.A., Vandenberg, J.I., and Hill, A.P. (2012). Voltage-sensing domain mode shift is coupled to the activation gate by the N-terminal tail of hERG channels. J Gen Physiol *140*, 293-306.
Tao, X., Lee, A., Limapichat, W., Dougherty, D.A., and MacKinnon, R. (2010). A gating charge transfer center in voltage sensors. Science *328*, 67-73.
Taylor, B.L., and Zhulin, I.B. (1999). PAS domains: internal sensors of oxygen, redox potential, and light. Microbiol Mol Biol Rev *63*, 479-506.
Thomson, S.J., Hansen, A., and Sanguinetti, M.C. (2014). Concerted all-or-none subunit interactions mediate slow deactivation of human ether-a-go-go-related gene K+ channels. J Biol Chem *289*, 23428-23436.
Thouta, S., Hull, C.M., Shi, Y.P., Sergeev, V., Young, J., Cheng, Y.M., and Claydon, T.W. (2017). Stabilization of the Activated hERG Channel Voltage Sensor by Depolarization Involves the S4-S5 Linker. Biophys J *112*, 300-312.
Thouta, S., Sokolov, S., Abe, Y., Clark, S.J., Cheng, Y.M., and Claydon, T.W. (2014). Proline scan of the HERG channel S6 helix reveals the location of the intracellular pore gate. Biophys J *106*, 1057-1069.
Tiwari-Woodruff, S.K., Lin, M.A., Schulteis, C.T., and Papazian, D.M. (2000). Voltage-dependent structural interactions in the Shaker K(+) channel. J Gen Physiol *115*, 123-138.
Tristani-Firouzi, M., Chen, J., and Sanguinetti, M.C. (2002). Interactions between S4-S5 linker and S6 transmembrane domain modulate gating of HERG K+ channels. J Biol Chem *277*, 18994-19000.
Tristani-Firouzi, M., and Sanguinetti, M.C. (2003). Structural determinants and biophysical properties of HERG and KCNQ1 channel gating. J Mol Cell Cardiol *35*, 27-35.
Trudeau, M.C., Warmke, J.W., Ganetzky, B., and Robertson, G.A. (1995). HERG, a human inward rectifier in the voltage-gated potassium channel family. Science *269*, 92-95.
Van Slyke, A.C., Rezazadeh, S., Snopkowski, M., Shi, P., Allard, C.R., and Claydon, T.W. (2010). Mutations within the S4-S5 linker alter voltage sensor constraints in hERG K+ channels. Biophys J *99*, 2841-2852.
Vandenberg, J.I., Perry, M.D., Perrin, M.J., Mann, S.A., Ke, Y., and Hill, A.P. (2012). hERG K(+) channels: structure, function, and clinical significance. Physiol Rev *92*, 1393-1478.
Vandenberg, J.I., Varghese, A., Lu, Y., Bursill, J.A., Mahaut-Smith, M.P., and Huang, C.L. (2006). Temperature dependence of human ether-a-go-go-related gene K+ currents. Am J Physiol Cell Physiol *291*, C165-175.
VanDongen, A.M., Frech, G.C., Drewe, J.A., Joho, R.H., and Brown, A.M. (1990). Alteration and restoration of K+ channel function by deletions at the N- and C-termini. Neuron *5*, 433-443.
Varga, Z., Rayner, M.D., and Starkus, J.G. (2002). Cations affect the rate of gating charge recovery in wild-type and W434F Shaker channels through a variety of mechanisms. J Gen Physiol *119*, 467-485.
Villalba-Galea, C.A., Sandtner, W., Starace, D.M., and Bezanilla, F. (2008). S4-based voltage sensors have three major conformations. Proc Natl Acad Sci U S A *105*, 17600-17607.
Wang, D.T., Hill, A.P., Mann, S.A., Tan, P.S., and Vandenberg, J.I. (2011). Mapping the sequence of conformational changes underlying selectivity filter gating in the K(v)11.1 potassium channel. Nat Struct Mol Biol *18*, 35-41.
Wang, J., Myers, C.D., and Robertson, G.A. (2000). Dynamic control of deactivation gating by a soluble amino-terminal domain in HERG K(+) channels. J Gen Physiol *115*, 749-758.

Wang, J., Trudeau, M.C., Zappia, A.M., and Robertson, G.A. (1998). Regulation of deactivation by an amino terminal domain in human ether-a-go-go-related gene potassium channels. J Gen Physiol *112*, 637-647.
Wang, S., Liu, S., Morales, M.J., Strauss, H.C., and Rasmusson, R.L. (1997a). A quantitative analysis of the activation and inactivation kinetics of HERG expressed in Xenopus oocytes. J Physiol *502 (Pt 1)*, 45-60.
Wang, S., Morales, M.J., Liu, S., Strauss, H.C., and Rasmusson, R.L. (1997b). Modulation of HERG affinity for E-4031 by [K+]o and C-type inactivation. FEBS Lett *417*, 43-47.
Wang, Z., Dou, Y., Goodchild, S.J., Es-Salah-Lamoureux, Z., and Fedida, D. (2013). Components of gating charge movement and S4 voltage-sensor exposure during activation of hERG channels. J Gen Physiol *141*, 431-443.
Warmke, J.W., and Ganetzky, B. (1994). A family of potassium channel genes related to eag in Drosophila and mammals. Proc Natl Acad Sci U S A *91*, 3438-3442.
Whicher, J.R., and MacKinnon, R. (2016). Structure of the voltage-gated K(+) channel Eag1 reveals an alternative voltage sensing mechanism. Science *353*, 664-669.
Wicks, N.L., Chan, K.S., Madden, Z., Santoro, B., and Young, E.C. (2009). Sensitivity of HCN channel deactivation to cAMP is amplified by an S4 mutation combined with activation mode shift. Pflugers Arch *458*, 877-889.
Wu, W., Gardner, A., and Sanguinetti, M.C. (2014). Cooperative subunit interactions mediate fast C-type inactivation of hERG1 K+ channels. J Physiol *592*, 4465-4480.
Wu, W., Gardner, A., and Sanguinetti, M.C. (2015). The Link between Inactivation and High-Affinity Block of hERG1 Channels. Mol Pharmacol *87*, 1042-1050.
Wu, W., and Sanguinetti, M.C. (2016). Molecular Basis of Cardiac Delayed Rectifier Potassium Channel Function and Pharmacology. Card Electrophysiol Clin *8*, 275-284.
Wymore, R.S., Gintant, G.A., Wymore, R.T., Dixon, J.E., McKinnon, D., and Cohen, I.S. (1997). Tissue and species distribution of mRNA for the IKr-like K+ channel, erg. Circ Res *80*, 261-268.
Yang, B.F., Xu, D.H., Xu, C.Q., Li, Z., Du, Z.M., Wang, H.Z., and Dong, D.L. (2004). Inactivation gating determines drug potency: a common mechanism for drug blockade of HERG channels. Acta Pharmacol Sin *25*, 554-560.
Yang, P., Kanki, H., Drolet, B., Yang, T., Wei, J., Viswanathan, P.C., Hohnloser, S.H., Shimizu, W., Schwartz, P.J., Stanton, M., *et al.* (2002). Allelic variants in long-QT disease genes in patients with drug-associated torsades de pointes. Circulation *105*, 1943-1948.
Yellen, G. (2002). The voltage-gated potassium channels and their relatives. Nature *419*, 35-42.
Yifrach, O., and MacKinnon, R. (2002). Energetics of pore opening in a voltage-gated K(+) channel. Cell *111*, 231-239.
Zagotta, W.N., Olivier, N.B., Black, K.D., Young, E.C., Olson, R., and Gouaux, E. (2003). Structural basis for modulation and agonist specificity of HCN pacemaker channels. Nature *425*, 200-205.
Zhang, M., Liu, J., Jiang, M., Wu, D.M., Sonawane, K., Guy, H.R., and Tseng, G.N. (2005). Interactions between charged residues in the transmembrane segments of the voltage-sensing domain in the hERG channel. J Membr Biol *207*, 169-181.
Zhang, M., Liu, J., and Tseng, G.N. (2004). Gating charges in the activation and inactivation processes of the HERG channel. J Gen Physiol *124*, 703-718.

Zhang, T., Moss, A., Cong, P., Pan, M., Chang, B., Zheng, L., Fang, Q., Zareba, W., Robinson, J., Lin, C., *et al.* (2010). LQTS gene LOVD database. Hum Mutat *31*, E1801-1810.
Zhong, W., Gallivan, J.P., Zhang, Y., Li, L., Lester, H.A., and Dougherty, D.A. (1998). From ab initio quantum mechanics to molecular neurobiology: a cation-pi binding site in the nicotinic receptor. Proc Natl Acad Sci U S A *95*, 12088-12093.
Zhou, Y., Morais-Cabral, J.H., Kaufman, A., and MacKinnon, R. (2001). Chemistry of ion coordination and hydration revealed by a K+ channel-Fab complex at 2.0 A resolution. Nature *414*, 43-48.

Appendix A: Supplemental Material for Chapter 3

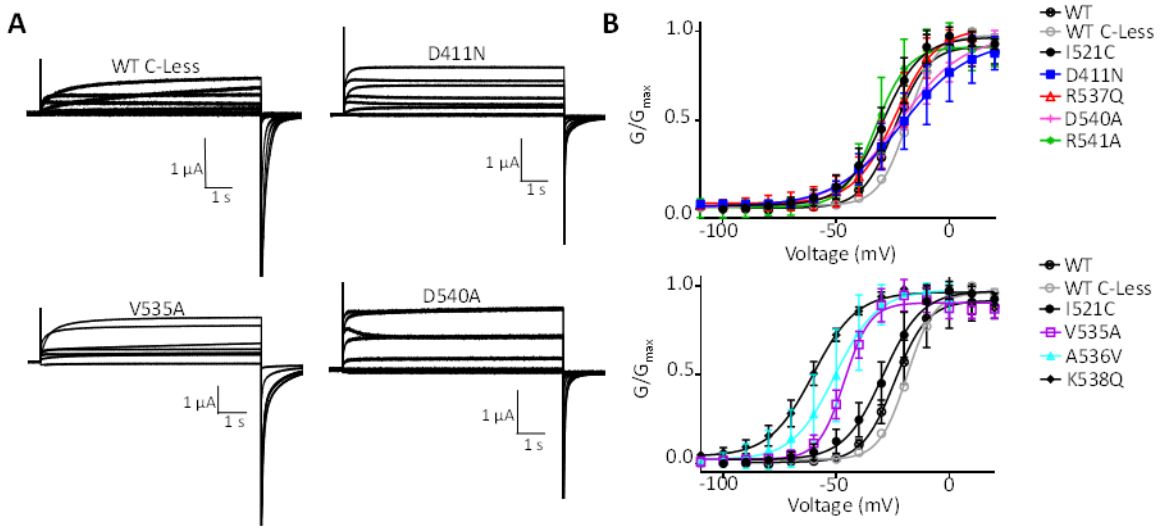

Supplemental Figure 1 Conductance-voltage relationships of constructs studied.
(A) Representative traces of WT C-Less, D411N, V535A, and D540A recorded during 8 s depolarizing steps to potentials from -90 mV to +50 mV in 20 mV steps from a holding potential of – 110 mV. **(B)** Conductance-voltage relationships from 8 s depolarizations from -110 mV to +50 mV in 10 mV steps from a holding potential of – 110 mV. $V_{0.5}$ and z values for each construct are as follows: WT $V_{0.5}$ = -20.3 ± 1.7 mV, z = 3.4 ± 0.1 (n = 6); WT C-Less $V_{0.5}$ = -18.5 ± 0.3 mV, z = 3.4 ± 0.2 (n = 3); I521C $V_{0.5}$ = -29.4 ± 0.6 mV, z = 3.0 ± 0.2 (n = 14); D411N $V_{0.5}$ = -20.8 ± 1.6 mV, z = 1.7 ± 0.2 (n = 7); V535A $V_{0.5}$ = -46.4 ± 0.8 mV, z = 4.4 ± 0.5 (n = 3); A536V $V_{0.5}$ = -50.5 ± 2.3 mV, z = 2.7 ± 0.6 (n = 3); R537Q $V_{0.5}$ = -23.9 ± 1.2 mV, z = 2.8 ± 0.3 (n = 6); K538Q $V_{0.5}$ = -60.3 ± 0.7 mV, z = 2.6 ± 0.2 (n = 3); D540A $V_{0.5}$ = -21.9 ± 0.9 mV, z = 1.8 ± 0.1(n = 4); R541A $V_{0.5}$ = -32.6 ± 1.3 mV, z = 3.5 ± 0.5(n = 3).

Construct	-70 mV $Q_{fast}/Q_{total\ max}$	-60 mV $Q_{fast}/Q_{total\ max}$	-50 mV $Q_{fast}/Q_{total\ max}$	-40 mV $Q_{fast}/Q_{total\ max}$	-30 mV $Q_{fast}/Q_{total\ max}$	-20 mV $Q_{fast}/Q_{total\ max}$	-10 mV $Q_{fast}/Q_{total\ max}$	0 mV $Q_{fast}/Q_{total\ max}$	10 mV $Q_{fast}/Q_{total\ max}$	20 mV $Q_{fast}/Q_{total\ max}$	30 mV $Q_{fast}/Q_{total\ max}$	n
Control (I521C)	0.0008 ± 0.0004	0.0015 ± 0.0009	0.0024 ± 0.0002	0.0044 ± 0.0008	0.0083 ± 0.0013	0.0126 ± 0.0015	0.0179 ± 0.0021	0.00225 ± 0.0023	0.0281 ± 0.0028	0.0335 ± 0.0031	0.0398 ± 0.0030	3
D411N	-0.0007 ± 0.0022	0.0003 ± 0.0047	0.0024 ± 0.0015	0.0013 ± 0.0014	0.0014 ± 0.0015	0.0022 ± 0.0027 *	0.0030 ± 0.0004 *	0.0046 ± 0.0023 *	0.0057 ± 0.0061 *	0.0038 ± 0.0030 *	0.0021 ± 0.0058 *	3
V535A	0.0016 ± 0.0001	0.0024 ± 0.0020	0.0027 ± 0.0013	0.0025 ± 0.0014	0.0035 ± 0.0014	0.0040 ± 0.0027	0.0029 ± 0.0008 *	0.0039 ± 0.0020 *	0.0029 ± 0.0013 *	0.0018 ± 0.0026 *	0.0039 ± 0.0035 *	3
A536V	0.0010 ± 0.0010	0.0020 ± 0.0020	0.0030 ± 0.0020	0.006 ± 0.0020	0.0090 ± 0.003	0.013 ± 0.002	0.017 ± 0.004	0.022 ± 0.005	0.026 ± 0.006	0.028 ± 0.004	0.035 ± 0.011	3
R537Q	0.0014 ± 0.003	-0.0009 ± 0.003	0.0036 ± 0.002	0.0048 ± 0.004	0.0068 ± 0.004	0.0107 ± 0.006	0.0140 ± 0.006	0.0192 ± 0.007	0.0253 ± 0.008	0.0309 ± 0.007	0.0384 ± 0.017	3
K538Q	0.0010 ± 0.0002	0.0013 ± 0.0003	0.0015 ± 0.0001	0.00307 ± 0.0003	0.00375 ± 0.0015	0.0054 ± 0.0010	0.0052 ± 0.0012 *	0.0066 ± 0.0013 *	0.0076 ± 0.0020 *	0.0092 ± 0.0007 *	0.0086 ± 0.0026 *	3
L539A (C-less)	0.001 ± 0.0006	0.002 ± 0.0009	0.003 ± 0.0007	0.005 ± 0.0006	0.009 ± 0.0007	0.011 ± 0.0011	0.015 ± 0.0019	0.020 ± 0.0026	0.025 ± 0.0034	0.030 ± 0.0044	0.035 ± 0.0053	4
D540A (C-Less)	0.0031 ± 0.002	0.0069 ± 0.003	0.0063 ± 0.003	0.0082 ± 0.006	0.0096 ± 0.007	0.0054 ± 0.004	0.0055 ± 0.001 *	-0.0002 ± 0.004 *	0.0058 ± 0.005 *	0.0037 ± 0.020 *	0.0068 ± 0.011 *	3
R541A	-0.0005 ± 0.0003	0.0001 ± 0.0008	0.0009 ± 0.0002	0.0035 ± 0.0009	0.0051 ± 0.0018	0.0095 ± 0.0021	0.0129 ± 0.0026	0.0153 ± 0.0034	0.0205 ± 0.0030	0.0230 ± 0.0059	0.0287 ± 0.0062 *	3

Supplemental Table 1 $Q_{fast}/Q_{totalmax}$ of 300 ms depolarizations from a holding potential of -110 mV. Values for D540A are from 100 ms depolarizations.

Construct	-40 mV τ (ms)	-20 mV τ (ms)	0 mV τ (ms)	+20 mV τ (ms)	+40 mV τ (ms)	+60 mV τ (ms)
Control (n = 3-5)	-	157 ± 61	81 ± 5	60 ± 11	37 ± 5	29 ± 3
D411N (n = 3)	46 ± 11	27 ± 4	15 ± 1	7 ± 0	5 ± 0	-
V535A (n = 2-3)	-	76 ±	35 ±	14 ±	10 ± 2	10 ± 2
A536V (n = 2-4)	203 ±	82 ±	45 ± 5	23 ± 2	17 ± 2	-
R537Q (n = 3)	-	-	95 ± 22	61 ± 11	31 ± 6	20 ± 2
K538Q (n = 1-5)	96 ±	45 ± 8	23 ± 2	12 ± 1	6 ± 1	5 ± 2
L539A (C-less) (n = 2-4)	-	137 ± 25	58 ± 3	60 ± 12	29 ± 5	24 ±
D540A (n = 2-3)	9 ±	7 ± 1	4 ± 0	3 ± 0	3 ± 0	-
R541A (n = 2-3)	-	133 ±	62 ± 4	36 ± 2	25 ± 3	25 ± 3

Supplemental Table 2 Time constants of activation at -40, -20, 0 , +20, +40, and +60 mV for Control, D411N, V535A, A536V, R537Q, K538Q, L539A (C-Less), D540A, and R541A.

Transition	α_0 (ms^{-1})	β_0 (ms^{-1})	z_α (e_0)	z_β (e_0)	Cooperativity
S0S1	1	1.5	0.2	0.04	1
S1S2	0.15	0.28	0.15	0.05	1.5
S2C1	1	3.49E-04	0.971	1.062	-
C1C2	0.024	0.16	0	0	-
C2O1	0.03	1.70E-04	1	1.2	-
O1O2	0.2	0.02	0.1	0.8209	-
C2I0	0.025	0.00085	1.57	1.84	-
O1I1	0.2	0.005	0.4	0.8209	-
O2I2	1	0.05	0.4	0.2	-
I0I1	0.24	0.001	0.0109	0	-
I1I2	2.5	0.5	0.3	0	-

Transition	α_0 (ms^{-1})	β_0 (ms^{-1})	z_α (e_0)	z_β (e_0)	Cooperativity
S0S1	-	-	-	-	-
S1S2	0.075*	0.28	0.15	0.05	1.5
S2C1	1	3.49E-04	0.971	1.062	-
C1C2	1*	0.16	0	0	-
C2O1	0.03	1.70E-04	1	1.2	-
O1O2	0.2	0.02	0.1	0.8209	-
C2I0	0.025	0.00085	1.57	1.84	-
O1I1	0.2	0.005	0.4	0.8209	-
O2I2	1	0.05	0.4	0.2	-
I0I1	0.24	0.001	0.0109	0	-
I1I2	2.5	0.5	0.3	0	-

Supplemental Table 3 Markov model parameter values for Piper Model (left) and the modified Piper model with no S0 state (right). Altered parameters are marked with an asterisk.

Transition	α_0 (ms^{-1})	β_0 (ms^{-1})	z_α (e_0)	z_β (e_0)	Cooperativity
S0S1	1	1.5	0.2	0.04	1
S1S2	0.15	0.28	0.15	0.05	1.5
S2C1	1	3.49E-04	0.971	1.062	-
C1C2	0.024	0.16	0	0	-
C2O1	0.03	1.70E-04	1	1.2	-
O1O2	0.2	0.02	0.1	0.8209	-
C2I0	0.025	0.00085	1.57	1.84	-
O1I1	0.2	0.005	0.4	0.8209	-
O2I2	1	0.05	0.4	0.2	-
I0I1	0.24	0.001	0.0109	0	-
I1I2	2.5	0.5	0.3	0	-

Transition	α_0 (ms^{-1})	β_0 (ms^{-1})	z_α (e_0)	z_β (e_0)	Cooperativity
S0S1	-	-	-	-	-
S1S2	-	-	-	-	-
S2C1	1	0.01*	1.3*	1.062	-
C1C2	1*	0.16	0	0	-
C2O1	0.03	1.70E-04	1	1.2	-
O1O2	0.2	0.02	0.1	0.8209	-
C2I0	0.025	0.00085	1.57	1.84	-
O1I1	0.2	0.005	0.4	0.8209	-
O2I2	1	0.05	0.4	0.2	-
I0I1	0.24	0.001	0.0109	0	-
I1I2	2.5	0.5	0.3	0	-

Supplemental Table 4 Markov model parameter values for Piper Model (left) and the modified Piper model with no S0 or S1 state (right). Altered parameters are marked with an asterisk.